الجمهورية الجزائرية الديمقراطية الشعبية

PEOPLE'S DEMOCRATIC REPUBLIC OF ALGERIA

وزارة التعليم العالي والبحث العلمي

MINISTRY OF HIGHER EDUCATION

AND SCIENTIFIC RESEARCH



MOHAMED SEDDIK BENYAHIA JIJEL UNIVERSITY

Faculty of Science and Technology

Department of Electrical Engineering

N° ……/2026

# MASTER THESIS

**DOMAINE: Science and Technology**

**FILIERE: Electromechanics**

**SPECIALITY: Electromechanics**

## Theme

# Projectile Search Algorithm-Based MPPT Control for Solar Water Pumping System

**Presented by: Zakaria BOUTERRA** **Supervisor: Mounir HADEF**

**Abdelali BOUNNAH**

**Defended on: 21/06/2026**

**In front of the jury**

| | | |
|---|---|---|
| **President: I. HAFSAOUI** | **Grade …MCA….** | **Univ MSB jijel** |
| **Supervisor: M. HADEF** | **Grade …Prof…** | **Univ MSB jijel** |
| **Examiner: M. BOUKHNAF** | **Grade …MCB….** | **Univ MSB jijel** |

**Academic Year: 2025 /2026**


بسم الله الرحمن الرحيم

# Dedication

First and foremost, we express our deepest gratitude to Allah, who granted us the strength, determination, and health to complete this work.

We have always been grateful in our lives to people who hold a special place in our hearts. Today, the opportunity has come to express our appreciation and dedicate this work to them as a token of gratitude for all the efforts they made just to see us succeed.

We dedicate this work:

To our dear parents, for all their sacrifices, love, tenderness, support, and heartfelt prayers throughout our academic journey. We wish them a life filled with happiness and good health.

To our brothers and sisters, for their constant support and encouragement.

To all our family members without exception.

To my teachers, who shared their knowledge with me and guided me throughout my studies.

And to our friends who stood by us during difficult times.

# ACKNOWLEDGMENTS

﴿ وَإِذْ تَأَذَّنَ رَبُّكُمْ لَئِن شَكَرْتُمْ لَأَزِيدَنَّكُمْ ۖ وَلَئِن كَفَرْتُمْ إِنَّ عَذَابِي لَشَدِيدٌ ﴾

[ إبراهيم: 7]

ABOVE ALL, WE EXPRESS OUR DEEP GRATITUDE TO ALLAH, WHO HAS GRANTED US THE PATIENCE, STRENGTH, AND DETERMINATION NEEDED TO BRING THIS PROJECT TO FRUITION.

WE EXTEND OUR SINCERE GRATITUDE TO OUR SUPERVISOR, MR. MOUNIR HADEF, FOR HIS VALUABLE ASSISTANCE AND ADVICE THROUGHOUT THIS PROJECT. WE ALSO THANK THE MEMBERS OF THE JURY FOR HONORING US BY AGREEING TO JUDGE OUR WORK. WE ALSO EXTEND OUR SINCERE THANKS TO OUR FRIENDS, BROTHERS, AND SISTERS WHO ACCOMPANIED US THROUGHOUT OUR JOURNEY, AND TO EVERYONE WHO CONTRIBUTED, DIRECTLY OR INDIRECTLY, TO THE COMPLETION OF THIS PROJECT. AND FINALLY, OUR DEEPEST GRATITUDE—AFTER GOD—GOES TO OUR PARENTS, WHO HAVE BEEN THERE FOR US THROUGH THICK AND THIN SINCE WE WERE LITTLE.

## Summary:

I. General Introduction ..... 1

**Chapter I Overview of Photovoltaic Systems:**

I.1 Introduction ..... 3
I.2 Renewable Energy ..... 3
I.2.1 Hydro power ..... 3
I.2.1.1 Advantages of hydroelectric power ..... 4
I.3 Solar radiation: ..... 7
I.3.1 Types of solar radiation ..... 8
I.3.1.1 Depending on the form in which it reaches the Earth: ..... 8
I.3.1.2 Depending on the types of light: ..... 8
I.4 Challenges of Photovoltaic Technology ..... 8
I.4.1 Efficiency of the PV Cell ..... 8
I.4.2 Stability of PV generation ..... 8
I.4.3 Partial shading condition ..... 9
I.4.4 Mismatch of PV load ..... 9
I.4.5 Lifespan of an installed PV module ..... 9
I.5 The photovoltaic cell ..... 9
I.5.1 Definition ..... 9
I.5.2 PV cell types ..... 10
I.5.2.1 Mono-crystalline (single crystalline) cells: ..... 10
I.5.2.2 Poly-crystalline (multi-crystalline) cells: ..... 10
I.5.2.3 Amorphous cells: ..... 11
I.5.2.4 Comparison of the different PV cell technologies ..... 11
I.7 Water pumping systems ..... 13
I.7.1 PV generator ..... 13
I.7.2 Power converters ..... 13
I.7.2.1 Buck converter ..... 13
I.7.2.2 Boost converter ..... 14
I.7.2.3 Buck-Boost converter ..... 14
I.7.3 Photovoltaic Water pumps and motors ..... 15
I.7.4 Pumping methods ..... 15
I.7.4.1 Pumping as the sun moves across the sky ..... 16

I.7.4.2 Pumped storage using electrochemical storage (batteries) ..... 16
I.8 Conclusion ..... 17

**Chapter II: Modeling of the photovoltaic pumping system**

II.1 Introduction: ..... 18
II.2 Modeling of the photovoltaic cell ..... 18
II.2.1 PV cell model ..... 18
II.2.2 Photovoltaic generator (GPV) ..... 19
II.2.3 Current-voltage (I-V) characteristic of the photovoltaic cell: ..... 19
II.2.3.1 Open circuit voltage $V_{OC}$: ..... 19
II.2.3.2 Short-circuit current $I_{SC}$: ..... 19
II.2.3.3 maximum power $P_m$ ..... 20
II.2.3.5 Maximum energy efficiency ηm ..... 21
II.3 PV Module ..... 21
II.3.1 Types of Associations ..... 22
II.3.1.1 Series Associations ..... 22
II.3.1.2 Parallel Association ..... 23
II.3.1.3 Series-parallel associations (mixed or hybrid association) ..... 24
II.4 Modeling the DC-DC Converter: ..... 26
II.4.1 DC-DC boost converter ..... 26
II.4.2 Parameters of DC-DC boost converter ..... 26
II.4.2.1 Duty cycle D ..... 26
II.4.2.2 Inductor and capacitor of the boost converter ..... 26
II.4.2.3 The input capacitor $C_{in}$ ($C_{pv}$) ..... 27
II.5 Maximum Power Point Tracking Techniques (MPPT) ..... 27
II.5.1 MPPT classification for PV systems ..... 28
II.5.2 Performance specifications of MPPT control algorithm ..... 28
II.5.2.1 Dynamic response ..... 28
II.5.2.2 Steady-state error ..... 29
II.5.2.3 Tracking efficiency ..... 29
II.5.3 Examples of two most common methods of MPPT: ..... 29
II.5.3.1 Perturb and Observe (P&O) method of MPPT ..... 29
II.5.3.2 Incremental Conductance method of MPPT ..... 31
II.6 Modeling the voltage inverter (DC/AC) ..... 33

II.7 Direct Torque Control (DTC)..... 34
II.7.1 Principle of DTC Control..... 35
II.7.1.1 Stator Flux Estimation..... 36
II.7.1.2 Torque Calculation.....36
II.7.1.3 Hysteresis Comparators..... 36
II.7.1.4 Switching Table (Look-Up Table).....36
II.8 Permanent Magnet Synchronous Motor (PMSM)..... 37
II.8.1 Modeling of a permanent-magnet synchronous motor in the park plane.....38
II.9 Centrifugal Pump Performance and Characteristics..... 39
II-9.1 Definition..... 39
II.9.2 Flow Rate (Q).....40
II.9.3 Head (H).....40
II.9.4 Performance Curves..... 41
II.9.4.1 The pump's flow-head Q(H) characteristic:.....41
II.9.4.2 Efficiency-Flow Curve ($\eta$-Q).....42
II.9.4.3 Power-Flow Curve (P-Q).....43
II.9.5 Power calculation:..... 43
II.9.6 The pump's torque-speed characteristic (ω):..... 43
II.9.7 efficiency calculation:.....43
II.10 Conclusion…….....44

**Chapter III: Simulation of PSA-based MPPT control for a solar PV water pumping system**

III.1 Introduction.....45
III.2 Projectile model:.....45
III.3 Modeling of Projectile search algorithm PSA.....46
III.4 Simulation of solar water pumping system based on PSA-MPPT control.....48
III.4.1 Description of the Simulink Model.....48
III.4.2 Parameters of Photovoltaic Panel and Boost Converter used in Simulation.....49
III.4.3 Analysis of environmental impacts.....50
III.4.3.1 Partial Shading.....50
III.4.3.2 Rapid irradiance fluctuation..... 53
III.4.3.3 Temperature-induced non-linearities.....53
III.4.4 Performance indicators.....53

III.4.4.1 Tracking Response Time.....53
III.4.4.2 Electromagnetic Torque Ripple $\sigma Te$.....53
III.4.4.3 Total Harmonic Distortion THD (%).....54
III.4.4.4 Steady-State Power RMSE.....54
III.4.4.5 System Efficiency.....54
III.5 Simulation Results and Discussion.....55
III.5.1 Simulation Environment and Scenarios.....55
III.5.2 Discussion of Simulation Results:.....60
III.5.2.1 Electromagnetic Torque.....60
III.5.2.2 Rotor Speed.....60
III.5.2.3 Stator Currents $I_{abc}$.....61
III.5.2.4 Pump Flow Rate Q.....61
III.5.2.5 Pump Head H.....62
III.5.2.6 Pump Power $P_{pump}$.....62
III.5.3 Overall Comparison Between PSA and P&O.....62
III.5.3.1 performances metrics.....62
III.5.4 Discussion of performances metric results.....66
III.5.5 Simulation of the 4S × 2P PV Array under Partial Shading.....67
III.5.5.1 Comparative Performance Results between PSA and P&O.....69
III.6.Conclusion……..…..……69

# List of figures

## Chapter I Overview of Photovoltaic Systems:

Figure I-1: hydropower

Figure I-2: Basic system of wind power

Figure I-3: Parabolic trough systems using mirrors

Figure I-4: PV panels to generate electricity directly from the sunlight

Figure I-5: The equivalent electrical circuit model of a solar cell

Figure I-6: mono crystalline

Figure I-7: polycrystalline

Figure I-8: Amorphous cells

Figure I-9: the Algerian solar map

Figure I-10: Step-down Buck converter.

Figure I-11: Step-up boost converter

Figure I-12: Buck-boost converter.

Figure I-13: Pumping system as the sun moves across the sky

Figure I-14: Pumping system storage using electrochemical storage.

## Chapter II Modeling of the photovoltaic pumping system

Figure II-1: Equivalent circuit of photovoltaic cells

Figure II-2: Overview of a solar cell, a solar panel, and a solar array

Figure II-3: mains parameters of a solar panel array type BP Solar SX3195W

Figure II-4: curve representing the main parameters of a solar panel array type BP Solar SX3195W

Figure II-5: IV curve of series connected solar cells

Figure II-6: Representing series association of 4 PV array

Figure II-7: IV curve of parallel connected solar cells

Figure II-8: Representing Parallel association of 3 PV array

Figure II-9: Association hybrid

Figure II-10: Representing Series-Parallel association of 4 Series PV array & 2 parallel PV array

Figure II-11: Design of the DC/DC boost converter.

Figure II-12: Basic photovoltaic conversion chain

Figure II-13: Basic classification of tracking techniques

Figure II-14: P&O Algorithm

Figure II-15: Flow chart of IC method

Figure II-16: Schematic diagram of a two-level three-phase inverter

Figure II-17: Block diagram of the DTC

Figure II-18: Stator flux trajectory according to the voltage vector command under DTC using LUT (lookup table).

Figure II-19: Exploded view diagram of PMSM

Figure II-20: Equivalent circuit of a PMSM in the (d,q) coordinate system

Figure II-21: Centrifugal pump components

Figure II-22: Pump characteristic curve H(Q)

Figure II-23: Pump Efficiency

Figure II-24: Pump Shaft Power curve

## Chapter III Simulation of PSA-based MPPT for a solar PV water pumping system

Figure III-1: The projectile moving path

Figure III-2: The enveloping parabola path

Figure III-3: Model of a solar pumping system based on projectile search algorithm-MPPT on MATLAB-Simulink

Figure III-4: Partially shaded Solar panel

Figure III-5: Partial shading of a PV module

Figure III-6: P–V & I-V Characteristics Under different partial shadow patterns

Figure III-7: the irradiation and temperature profiles used in simulation

Figure III-8: Electromagnetic torque output used P&O and PSA techniques

Figure III-9: Rotor speed output used P&O and PSA techniques

Figure III-10: (1) Stator currents $I_{abc}$ output used PSA method (2) Zoomed Output current.

Figure III-11: (1) Stator currents $I_{abc}$ output used P&O method (2) Zoomed Output current.

Figure III-12: Pump flow rate Q output used P&O and PSA techniques

Figure III-13: Pump Head H output used P&O and PSA techniques

Figure III-14: Pump Power $P_{pump}$ output used P&O and PSA techniques

Figure III-15: average centrifugal pump power of PSA and P&O Methods

Figure III-16: global system efficiencies and MPPT efficiencies of PSA and P&O Methods

Figure III-17: Tracking response time of PSA and P&O Methods

Figure III-18: Electromagnetic Torque Ripple $\sigma_{Ce}$ (N.m) of PSA and P&O Methods

Figure III-19: Stator Current Total Harmonic Distortion THD of PSA and P&O Methods

Figure III-20: Steady-State Power RMSE of PSA and P&O Methods

Figure III-21: Representing Series-Parallel association of 2 Series PV array & 2 parallel PV array

Figure III-22 Performance metrics under a partial shading condition. (1): RMSE, THD & $\sigma_{Ce}$ . (2): $P_{pump}$, $\eta$ & $t_r$

# List of tables:

## Chapter I Overview of Photovoltaic Systems:

Table I-1: Types of photovoltaic cells

## Chapter II Modeling of the photovoltaic pumping system

Table II -1: LUT (lookup table) used for conventional DTC control.

Table II -2: Types of head

## Chapter III Simulation of PSA-based MPPT for a solar PV water pumping system

Table III -1: Technical Specifications of BP Solar SX3190 Solar Panel

Table III -2: Technical Parameters of the Boost Converter Implemented

Table III -3: Technical Parameters of the Projectile search algorithm

Table III -4: comparison table between PSA and P&O Performances metrics

Table III -5: Different patterns of shading on each of the four solar panels modules.

Table III -6: comparison table between PSA and P&O Performances metrics for Scenario of simulation under a partial shading condition

# List of abbreviations:

| | |
|---|---|
| PV | Photovoltaic |
| PV cell | Photovoltaic cell |
| GPV | Photovoltaic generator |
| MPP | Maximum power point |
| MPPT | Maximum power point tracking |
| PSO | Particle Swarm Optimization |
| PSA | Projectile Search Algorithm |
| P&O | Perturb and Observe |
| INC | Incremental Conductance |
| PTS | Projectile Target Search |
| DC-DC | Direct current to direct current |
| AC | Alternating current |
| CCM | Continuous conduction mode |
| DTC | Direct torque control |
| LUT | Look-up table |
| PMSM | Permanent magnet synchronous motor |
| THD | Total Harmonic Distortion |
| TR | Load/resistant torque |
| $R_{load}$ | Load Resistance |
| BEP | Best efficiency point |
| RMSE | Root Mean Square Error |
| ANN | Artificial Neural Network |
| MPC | Model Predictive Control |
| GA | Genetic Algorithm |
| $P_{pump}$ | Pump Power / Average Centrifugal Pump Power |
| $P_{max}$ | Maximum Power |
| $N_{cell}$ | Number of Cells |
| I-V | Current-voltage |

| | |
|---|---|
| $V_{mp}$ | Voltage at Maximum Power |
| $V_{oc}$ | Open-circuit voltage |
| $I_{sc}$ | Short-circuit current |
| $I_{cc}$ | Short-circuit current notation |
| $I_{abc}$ | Stator currents |
| $F_f$ | Form factor |
| $I_c$ | Incremental Conductance |
| D | Duty cycle |
| $C_{in}$ | Input capacitor |
| $C_{pv}$ | PV-side capacitor / input capacitor notation |
| $f_{sw}$ | Switching frequency |
| $I_l$ | Inductor current ripple |
| $V_0$ | Output voltage ripple |
| $V_{pv}$ | PV voltage |
| $V_{dc}$ | DC-link voltage |
| $V_{si}$ | Voltage source inverter |
| $T_e$ | Electromagnetic torque |
| J | Moment of inertia |
| f | Friction coefficient |
| $L_d$ | d-axis inductance |
| $L_q$ | q-axis inductance |
| $I_d$ | d-axis current |
| $I_q$ | q-axis current |
| sf | Permanent magnet flux linkage |
| d-q | Direct-quadrature axis |
| Q | Flow rate |
| H | Head |
| $H_S$ | Static head |
| $H_D$ | Dynamic head |

| | |
|---|---|
| NPSH | Net positive suction head |
| NPSH'r | Net positive suction head required |
| NPSHa | Net positive suction head available |
| $P_h$ | Hydraulic power |
| $P_m$ | Mechanical power |
| p | Pump efficiency symbol |
| m | Maximum efficiency symbol in text |
| Pi | Incident solar power |
| $P_{out}$ | discharge pressure |
| $P_{in}$ | suction pressure |
| $\rho$ | fluid density |
| $g$ | gravitational acceleration |
| $V_t$ | Total volume |
| $U_{ab}$, $U_{bc}$, $U_{ca}$ | Line-to-line inverter voltages |
| $V_{an}$, $V_{bn}$, $V_{cn}$ | Phase voltages |
| $V_{an0}$, $V_{bn0}$, $V_{cn0}$ | Phase voltages relative to reference point n0 |
| Sa, Sb, Sc | Switch states of inverter legs |
| $n_0$ | Load neutral reference point |
| $I_{ph}$ | Current generated by the photovoltaic effect |
| $I_d$ | Diode Current |
| $I_{sh}$ | Shunt Current |
| $I_{pv}$ | photovoltaic current |
| $I_s$ | Saturation current due to the diffusion mechanism |
| $N_p$ | number of modules connected in parallel |
| $N_s$ | number of modules connected in series |
| $R_s$ | series resistance |
| $R_{sh}$ | shunt resistance |
| $V_{mpp}$ | Maximum Power Point Voltage |
| $I_{mpp}$ | Maximum Power Point Current |

| | |
|---|---|
| $I_{mp}$ | Current at Maximum Power |
| $P_{obt}$ | obtained power |
| $\eta_m$ | Maximum energy efficiency |
| $P_m$ | maximum power |
| $P_i$ | incident solar power |
| S | Surface area of the solar cell |
| $V_m$ | voltage at the maximum power point |
| $I_m$ | the current at maximum power point |
| $L_{boost}$ | boost converter inductor |
| $C_{boost}$ | boost converter capacitor |
| $I_{dc}$ | direct-current output current |
| $\Delta I_L$ | estimated maximum amplitude of the current ripple |
| $\Delta V_{pv}$ | ripple of the output voltage |
| PSC's | partially shaded conditions |
| $\eta_{mpp}$ | maximum power point efficiency |
| $\sigma_{Ce}$ | Electromagnetic Torque Ripple |
| $\eta_{system}$ | System Efficiency |
| $P_{actual}$ | *i*th sample of real measured power |
| $P_{max}$ | *i*th sample of true maximum power |
| $C_{out}$ | Output capacitor |
| $\psi_{\alpha,\beta,s}$ | estimated flux |
| q | Elementary electron charge |
| k | Boltzmann constant |
| T | Absolute temperature of the PV cell |
| n | Diode ideality factor. |
| A | Diode quality factor |
| E | Incident solar irradiance |
| S | Active surface area of the PV cell or module |
| $C_{O2}$ | Carbon dioxide |

# General introduction

# General Introduction

The global energy landscape is undergoing a pivotal transition. Driven by rapid population growth, intense industrialization, and the urgent need to mitigate climate change, the demand for clean, sustainable energy has never been higher. Among the various renewable energy options, photovoltaic (PV) technology has emerged as one of the most promising solutions due to its abundance, low operating costs, and minimal environmental footprint

In remote or rural regions isolated from the main electrical grid, securing a reliable energy and water supply remains a critical challenge. Photovoltaic-powered pumping systems (PVPS) offer a sustainable alternative to fossil-fueled generators, providing decentralized, clean water for agriculture, livestock, and domestic use.

Despite their environmental advantages, PV systems suffer from two primary limitations: high initial capital costs and relatively low energy conversion efficiency. Because a solar panel's output is highly non-linear and depends directly on environmental parameters (such as irradiance and temperature), it must be continuously managed to operate at its highest possible efficiency. This process is known as Maximum Power Point Tracking (MPPT).

This technical challenge is significantly exacerbated under Partial Shading Conditions (PSC), which occur when clouds, trees, nearby structures, or dust unevenly block sunlight across the PV array. Under uniform irradiance, the Power-Voltage (P-V) curve features a single peak. Under PSC, however, the activation of bypass diodes introduces a complex, multi-peaked P-V curve consisting of several Local Maximum Power Points (LMPPs) and a single true Global Maximum Power Point (GMPP).

The core problem is that classic MPPT techniques—such as Perturb & Observe (P&O) and Incremental Conductance (INC)—are deterministic. While simple and effective under uniform irradiance, they easily get trapped in the first local peak they encounter during partial shading. This causes severe power loss, reduces water pumping throughput, and compromises the overall economic viability of the installation.

To overcome the limitations of conventional methods, modern research has shifted toward metaheuristic optimization algorithms capable of searching the entire operating space without getting trapped in local maxima.

The primary objective of this Master’s thesis is to study, simulate, and evaluate a novel metaheuristic-based optimization technique: the Projectile Search Algorithm (PSA), applied specifically to MPPT within a solar water pumping system under partial shading. Inspired by the physical mechanics of projectile motion, the PSA sweeps across the search space via parabolic trajectories, allowing it to "leap" over local maxima and isolate the true GMPP..

To validate its viability, this work provides a rigorous performance comparison between the proposed PSA-MPPT and conventional tracking methods. This comparative analysis evaluates key engineering performance metrics:

- Tracking Response Time (s)
- Total Harmonic Distortion of the stator current THD (%)

- Steady-State Power RMSE (W)
- Electromagnetic Torque Ripple $\sigma_{Ce}$ (N.m)
- System Efficiency $\eta_{system}$ (%)
- Average Centrifugal Pump Power $P_p$ (W)

The first chapter provides an overview of photovoltaic systems. The second chapter is dedicated to the modeling of photovoltaic pumping system, such as, PV generator, DC-DC boost, inverter, DTC control, Permanent Magnet Synchronous Motor and centrifugal pump. Afterwards, we give a brief overview of the conventional based MPPT techniques as Perturb & Observe (P&O), and Incremental Conductance (INC). Chapter three describes the projectile model motion and modeling our projectile search algorithm used for extracting the power in solar PV system. After that we present our simulation Simulink-MATLAB model with every parameter and described the environmental impact (shading conditions). Our simulation results evaluate the performance of the proposed PSA-MPPT method against the conventional P&O-MPPT algorithm, where we compare its metric, hydraulic and electrical performances results in different shading conditions.

# Chapter I

Overview of Photovoltaic Systems

## I.1 Introduction

Global energy demand is still predominantly met by non-renewable energy sources. Since these resources, particularly fossil fuels, are finite and subject to depletion, various energy strategies have been developed to improve the efficiency of electrical systems, reduce energy waste, and promote the adoption of renewable energy sources such as wind power, solar photovoltaic and thermal energy, biomass, and geothermal energy.

This chapter provides a general overview of the fundamental concepts necessary for understanding photovoltaic systems, including the different types of photovoltaic installations and their main fields of application like solar pumping systems.

## I.2 Renewable Energy

Since the Industrial Revolution, energy consumption has kept increasing, as did the demand for energy resources. Today, conventional resources such as coal, natural gas, and oil, as well as radioactive elements like uranium meet the majority of global energy demand. Thus far, the uncontrollable burning of fossil fuels by humanity has driven a dramatic rise in atmospheric $CO_2$, increasing from a pre-industrial historical level of approximately 280 ppm to over 430 ppm today. The focus nowadays consists in using alternative renewable energy sources, in order to lower the greenhouse gas emissions for avoiding irreversible climate changes. Another concern that drives the motivation for the ongoing research in renewable resources is that conventional energy sources are limited in the long run and are depleting faster than anticipated with the increasing energy and demographic demand [Tan20].

Among the sectors that contribute to global energy use, the building sector accounts for around 40% worldwide. This highlights the necessity of reducing energy consumption for heating and cooling, as people increasingly yearn for thermal comfort, especially in private households. This provides an ongoing problem that engineers and researchers face today, namely methods to reduce the energy consumption and increase the thermal comfort at the same time. Therefore, the use of renewable energy sources such as solar energy, geothermal energy, air energy, water energy and even biofuel represent the main renewable energy sources for heating, cooling and ventilation systems for which the research is concentrated today. [Bul22]

### I.2.1 Hydro power

The process of generating electricity from the potential energy of water stored in dams and waterfalls is known as a hydropower system. This system uses water turbines to generate the power as shown in Figure I-1. It shows another way, which is putting water wheels that are linked to turbines in fast flowing rivers to generate electricity without building water reservoirs or dams. [Car11]

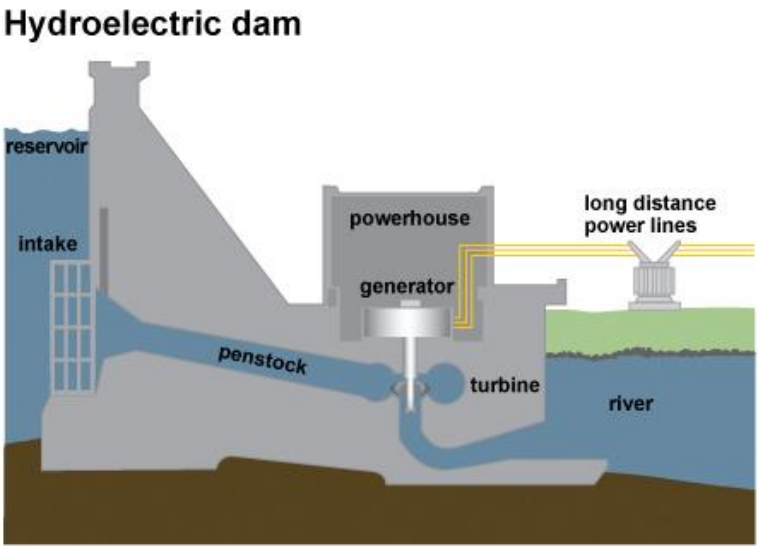


Figure I- 1: hydropower [Car11]

**I.2.1.1 Advantages of hydroelectric power** [Bel25]

- These systems offer high durability and low maintenance costs, while providing a clean and renewable source of energy
- High production capacity
- Furthermore, hydropower systems enable energy storage through pumped-storage power stations and offer high generation flexibility to meet fluctuating demand

**I.2.1.2 Disadvantages of hydroelectric power** [Bel25]

- These systems can cause a significant environmental impact on local ecosystems and lead to the displacement of populations.
- They exhibit a high dependence on climatic conditions, such as rainfall and droughts.
- Risk of natural disasters Habitat fragmentation
- High initial cost

**I.2.2 Wind power**

Wind power can be defined as the energy available in airflows that can be harnessed by using wind turbines. These days, large wind turbines generally range between 600 kW and 7.5 MW in capacity. Wind turbine power increases according to an increase of the cubic of wind speed. Therefore, wind turbines are always setup on tall towers to face the wind that operates the generators. Figure 1.2 shows a basic system of wind power. [Bur01]

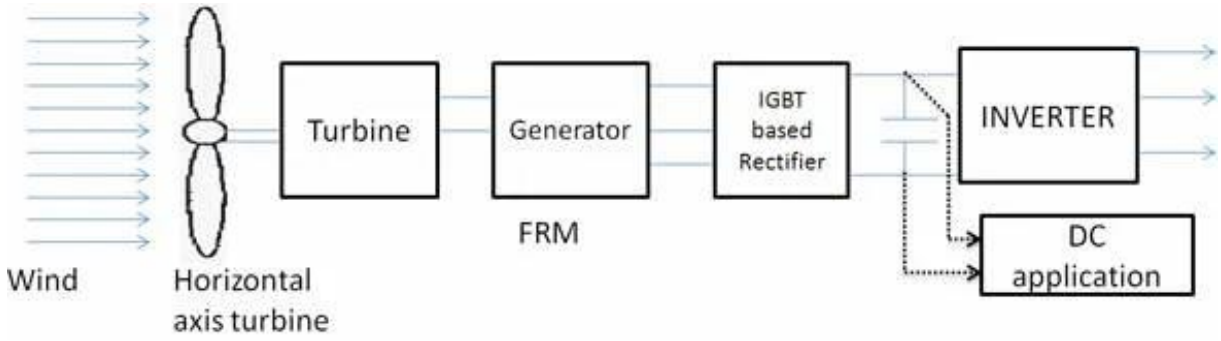


Figure I-2: Basic system of wind power [Bur01]

**I.2.2.1 Advantages of Wind power** [Bel25]

- Clean and renewable energy.
- An inexhaustible resource.
- Low production costs.
- Decentralized energy.
- Job creation.
- Low land footprint.

**I.2.2.2 Disadvantages of Wind power** [Bel25]

- Intermittency and variability
- Impact on the landscape and ecosystems
- Noise and disturbance to local wildlife
- High initial cost
- Problems with recycling wind turbines

**I.2.3 Solar energy**

Solar power is energy from the sun that is converted into thermal or electrical energy. Solar energy is the cleanest and most abundant renewable energy source available. Solar technologies can harness this energy for a variety of uses, including generating electricity, providing light or a comfortable interior environment, and heating water for domestic, commercial, or industrial use. [Sol26] The advantage of solar power can be taken by two main ways, the first way is to collect the sun heat by using curved mirrors and concentrate it on pipes to exchange the solar heat with a certain fluid and then it can be used to produce electricity, Figure I-3 demonstrates this method of solar power. The second way is a generating electricity directly from the falling sunlight by using photovoltaic cells as shown in Figure I-4. [Kal13]

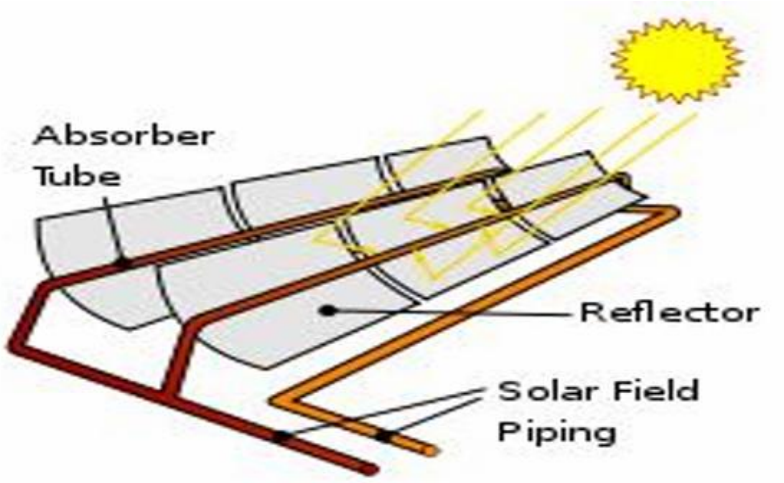


Figure I-3: Parabolic trough systems using mirrors [Kal13]



Figure I-4: PV panels to generate electricity directly from the sunlight [Goe05]

### I.2.3.1 Differences between Solar technologies

#### I.2.3.1.1 Thermodynamic concentrated solar power [Dee24]

Concentrated Solar Power (CSP) technology is proving a feasible option in the quest to produce affordable renewable energy worldwide. CSP plants produce electricity from the heat produced by the sun. These systems mainly operate by tracking the focus of the sun's rays on a receiver through a focus reflector mirror or lens. Concentrated solar energy is employed to produce high-temperature heat, which is then used to produce electricity in a conventional ranking cycle, most often a steam turbine.

#### I.2.3.1.2 Solar thermal:

Solar thermal collectors (STCs) convert solar radiation into thermal energy, which is then transferred to a storage system for later use. They commonly produce hot water or heat a room, but they can also be used for other purposes. A distinction is made between two types of STC: unconcentrated and concentrated. Unconcentrated solar collectors are devices designed to capture solar radiation without tracking the sun's position because they are installed in a fixed orientation. [Ela24]

#### I.2.3.1.3 Photovoltaic solar power

Solar PV energy is an integral part of our energy use and a vital component of renewable energy networks. With the rapid advancement of technology, PV module prices are declining and PV panels become more efficient. National economies are making ambitious investments in off-grid PV systems and grid-connected PV networks. PV electricity is volatile, relies on solar irradiation and other meteorological influences, such as temperature, humidity, precipitation, wind direction, and cloud coverage, unlike conventional energy production systems. The photovoltaic system consists of interconnected components designed in a way to achieve the specific target of delivering the desired electricity from a small device to the load. Photovoltaic systems are categorized by the main categories of grid connected, stand-alone systems and hybrid system which comprises different sources of energy such as PV arrays, diesel generators and wind generators. In the grid connected and the stand-alone systems, storage elements such as batteries or super capacitors may be adopted to store the energy during the day time when there is enough sunshine. Hybrid and stand-alone systems are used increasingly in rural areas. [Elt10]

## I.3 Solar radiation:

Solar radiation is the energy emitted by the Sun, propagating in all directions through space as electromagnetic waves. Emitted by the surface of the Sun, this energy influences atmospheric and climatological processes. It is also, directly and indirectly, responsible for common phenomena, such as plant photosynthesis, keeping the planet at a temperature. The Sun emits energy in the form of short-wave radiation, which is weakened in the atmosphere by the presence of clouds and absorbed by gas molecules or suspended particles. After passing through the atmosphere, solar radiation reaches the oceanic and continental land surface and is reflected or absorbed. Finally, the surface returns it to outer space in the form of long-wave radiation. [Ibe26]

Solar radiation is measured on a horizontal surface by means of a radiation sensor or pyranometer, which is placed in a south-facing, shadow-free location. Data are collected in units of power, watts per square meter ($W/m^2$), at all weather stations and tend to be taken at ten-minute or 24-hour intervals to establish averages. To convert solar radiation from power density ($W/m^2$) to cumulative energy ($J/m^2$), the power value must be multiplied by the time interval in seconds.

For instance, multiplying by 600 or 86,400 yields the total energy per square meter over a ten-minute or a 24-hour period, respectively." [Ibe26]

### I.3.1 Types of solar radiation [Ibe26]

#### I.3.1.1 Depending on the form in which it reaches the Earth:

- *Direct solar radiation*: This type of radiation penetrates the atmosphere and reaches the Earth's surface without dispersing at all on the way.
- *Diffuse solar radiation*: This is the radiation that reaches the Earth's surface after having undergone multiple deviations in its trajectory, for example by gases in the atmosphere.
- *Reflected solar radiation*: This is the fraction of solar radiation that is reflected by the earth's surface itself, in a phenomenon known as the albedo effect.

#### I.3.1.2 Depending on the types of light:

- *Infrared rays (IR):* Longer wavelength than visible light, they emit heat and are given off by anybody whose temperature is greater than 0º Kelvin.
- *Visible rays (VI):* They emit light and are those that the human eye perceives in the form of colors (red, orange, yellow, green, cyan, blue and violet).
- *Ultraviolet (UV) rays:* They are invisible to the human eye and have the most serious impact on the skin (burns, spots, wrinkles)

## I.4 Challenges of Photovoltaic Technology

### I.4.1 Efficiency of the PV Cell

The output power of a PV cell changes according to the weather conditions surrounding the PV cell. Basically, the generating power of the PV array increases as the irradiance increases owing to high numbers of photon-voltage hitting the electron-hole of the cell, thus resulting in increased PV output current. Conversely, this decreases at a high operating temperature, because the open circuit voltage of PV cell will drop as temperature increases due to the extension of the band gap of the PV semiconductor. During this time, the movement of PV electrons becomes less valent when input irradiation is absorbed, resulting in a decreasing loss of energy. However, there is a unique operation point for the PV cell, which is called the maximum power point (MPP) and this point shifts according to the weather conditions. [Alm20]

### I.4.2 Stability of PV generation

The fluctuation of PV output power due to passing clouds is considered a major issue for designing a grid-connected PV system. Several issues can affect the operation of the PV system,

such as a voltage rise and voltage oscillation. That is, the stability and reliability of PV power generation can be severely affected by fluctuating atmospheric conditions, especially in large-scale installations. [Alm20]

### I.4.3 Partial shading condition

In normal conditions, a PV array exhibits a single unique maximum power point (MPP) in relation to the input solar irradiance and temperature operation. However, the PV array will generate several MPPs when there is a shading, which can be caused by trees or dust, i.e. on part of the PV array. This is because each PV module will produce its MPP and as a result, several PV power values will be generated in same time. Hence, the global PV power generation will be decreasing. In this case, a hotspot on the PV module may occur owing to a large change in PV voltage when the operation point shafts rapidly, thus leading to damage in the PV system. [Ish13]

### I.4.4 Mismatch of PV load

The voltage operation of a PV array also depends upon the value of the load. When the output power generation of a PV array is lower or higher than the power load, the PV voltage operation will drop or rise to a new operating point and consequently, the efficiency of PV generation will drop. In addition, the equipment of a grid-connected PV system may be damaged in case of a large-scale PV plant when it disconnects due to the fault. [Alm20]

### I.4.5 Lifespan of an installed PV module

Most PV manufacturing companies assert that the lifespan of a PV module is typically 20 years, with its output remaining at least 80% of the rated power. [Hai11]. However, several studies have indicated that the weather operating conditions of an installed PV system play an important role in degrading its lifespan by about 0.2% per year. This is due to large changes in PV voltage that accrue when the weather conditions change rapidly. [Bra11]

## I.5 The photovoltaic cell

### I.5.1 Definition

Solar PV cells are semiconductor devices that turns sunlight into electrical energy. The efficiency of a solar cell depends on the strength of the sunlight, the temperature, and the cell materials basic properties. It must then be an actual load to be transformed into an equivalent circuit to approximate the measurement. The equivalent electrical circuit of a PV cell is shown in Figure I-5. Therefore, it needs to build a PV cell simulation model to permit the solar panels maximum power point to perform their photoelectric conversion efficiency by influencing the solar panels production capacity by their light intensity and the outside temperature. It can better consider the effect on its production capacity of the external climate. [Roy21]

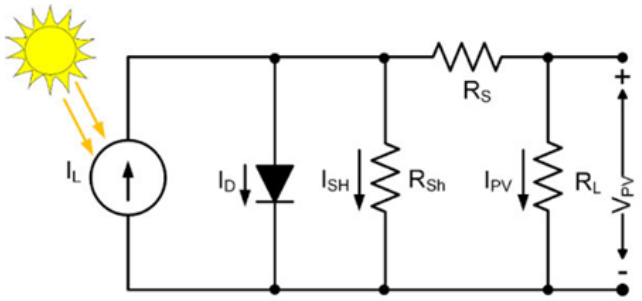


Figure I-5: The equivalent electrical circuit model of a solar cell [Mis21]

### I.5.2 PV cell types:

Photovoltaic cells are produced in a variety of types, each of which has different benefits. Below is a list of the most common forms of PVs. [Goe05]

#### I.5.2.1 Mono-crystalline (single crystalline) cells:

As shown in Figure I-6 these types of cells derive from a single crystal of silicon and are quite smooth in texture. Although they are the most efficient of the PV cells, mono-crystalline cells are also the most costly to manufacture. [Sas17]



Figure I-6: Mono crystalline [Goe05]

#### I.5.2.2 Poly-crystalline (multi-crystalline) cells:

As their name implies, polycrystalline cells are several crystals combined. As shown in Figure I-7, they are cut from a block of silicon. Although PV solar panels made from poly-crystalline cells types are less efficient than mono-crystalline cells, they are less expensive [Sas17].



Figure I-7: Polycrystalline [Goe05]

### I.5.2.3 Amorphous cells:

As shown in Figure I-8, amorphous cells are produced by setting a thin film of non-crystalline (i.e., amorphous) silicon on top of different surfaces. Amorphous cells provide the least efficient type of photovoltaic solar panels, but they are also the least expensive to produce and have the characteristic of making PV panes flexible [Sas17].

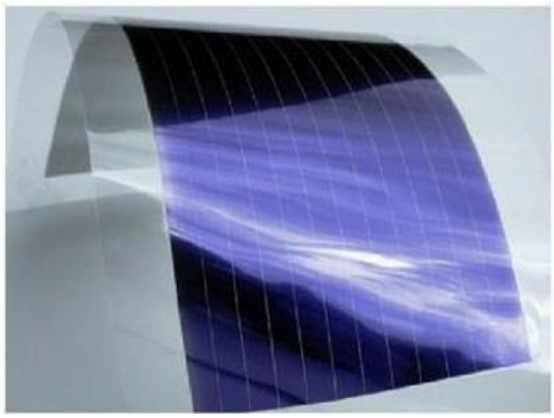

Figure I-8: Amorphous cells [Goe05]

### I.5.2.4 Comparison of the different PV cell technologies

Table I.1 shows the types of photovoltaic cells. [Lou08]

Table I-1: Types of photovoltaic cells

| **Types** | **Monocrystalline silicon** | **Polycrystalline silicon** | **Amorphous silicon** |
|---|---|---|---|
| |  |  |  |
| **Yield** | 15% to 19% | | 7% to 10% |
| **Service life** | 35 years | 35 years | ≤10 years |
| **Advantages** | Good efficiency in direct sunlight | Good efficiency in direct sunlight (less than monocrystalline but more than amorphous) | Flexibility<br>Lower price than crystalline panels<br>Good efficiency in diffuse light |
| **Disadvantage** | Poor performance in diffused sunlight (cloudy weather, etc.)<br>High price. | Poor performance in diffused sunlight (cloudy weather, etc.)<br>High price | Poor performance in direct sunlight. |

## I.6 Development of solar PV in Algeria

The exceptional solar irradiance in Algeria, alongside major state-led utility-scale solar projects and the technological expertise of New Energy of Algeria (NEAL), are critical factors that will undoubtedly position the country as a key player in the deployment of photovoltaic energy across the MENA region ( Figure I-9) .

This includes the ability to supply enough energy to meet the population's needs and even the potential to export such projects to other European countries. The population distribution in Algeria also indicates a large potential market for renewable energies, among which solar energy stands out due to its consistent presence across the entire region. The amount of solar radiation in Algeria suggests that solar energy could be considered a viable energy source for various applications, in the form of individual solar panels or photovoltaic systems. Photovoltaic solar energy in Algeria is

primarily developed for six applications: household use, water pumping, refrigeration, village electrification, lighting, and telecommunications [Man24].

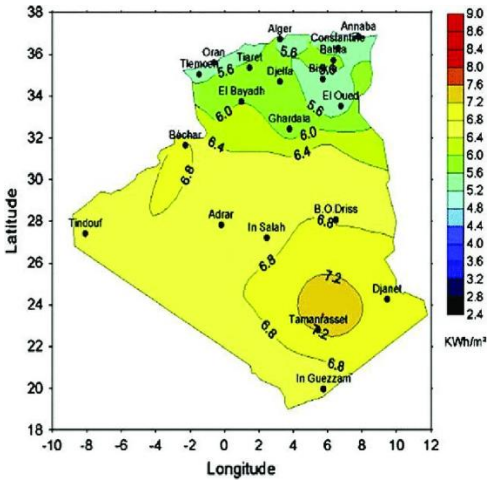


Figure I-9: the Algerian solar map [Res25]

## I.7 Water pumping systems

A solar pumping system consists of several key components that work together to ensure it operates at its best. These components include, in particular: photovoltaic generator, converters, inverters, motors and pumps.

### I.7.1 PV generator

The PV field or PV generator (PVG) or solar generator is composed of some combination of series and parallel PV modules and known by its nominal output power. the voltage output of the solar generator depends on the PV modules connected in series. the current output of the PV generator depends on the PV modules connected in parallel, which means the PV modules can be wired in series to increase voltage, and in parallel to increase current [Bou12]

### I.7.2 Power converters

#### I.7.2.1 Buck converter

In this type of DC-DC converter, the average output voltage Vo produced is always lower than the DC input voltage. The buck converter is used for voltage step-down in PV applications, such as for charging batteries and in water pumping systems. The basic circuit of the step-down converter as illustrated bellow in Figure I-10. The diode (d) is used to enhance the output filtering effect and prevent the switch from absorbing or dissipating the inductive energy because this would

lead to overheating the switch. In addition to that, there is an inductor and capacitor at the output of the converter which forms a low-pass filter to attenuate the output voltage fluctuation. [Moh07]

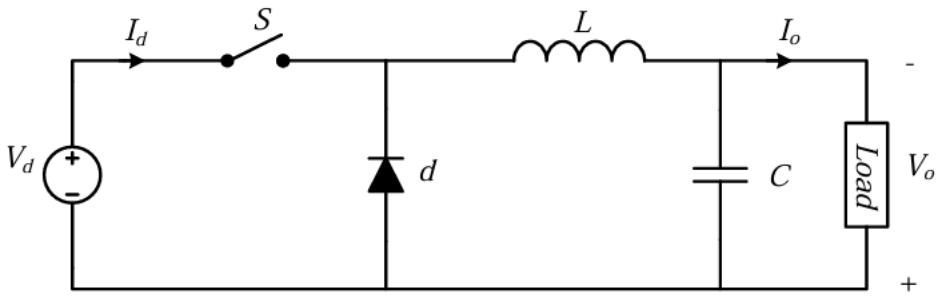


Figure I-10: Step-down Buck converter. [Moh07]

### I.7.2.2 Boost converter

In this type of converter, the output voltage is always greater than the input voltage. Therefore, the step-up converter can be applied to MPPT systems where the output voltage needs to be greater than the input voltage. Such as in a grid-connected system where the boost converter maintains a high output voltage even if the PV array voltage falls to low values. The circuit topology of the step-up converter as illustrated in Figure I-11. [Moh07]

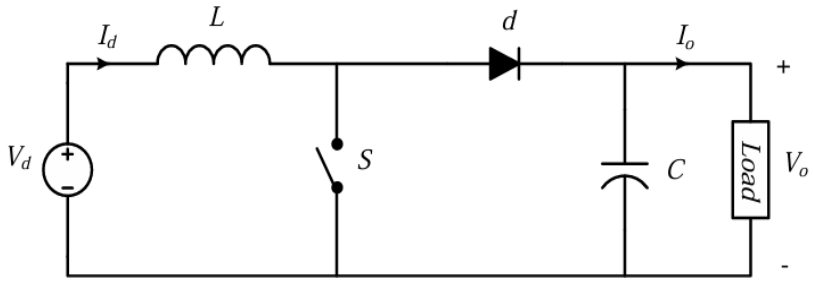


Figure I-11: Step-up boost converter [Aas15]

### I.7.2.3 Buck-Boost converter

A Buck-Boost converter is cascade connection of two basic converters, the buck converter and boost converter. The Buck-Boost converter provides an output voltage can be higher or lower than the input voltage. Also, this type of converter produces a negative polarity output with respect to the common terminal of the input voltage. The main application of Buck-boost converter is in regulated DC power supplies. Figure I-12 shows the circuit topology of Buck-Boost converter. [Aas15]

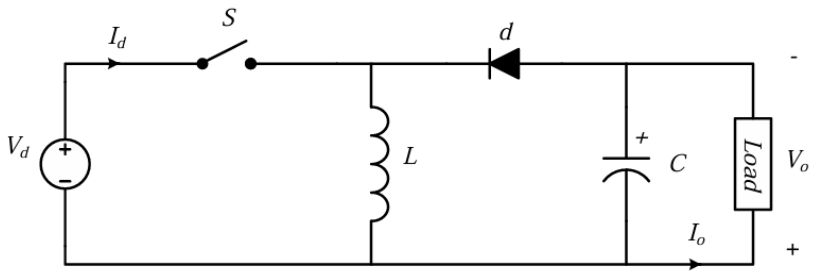


Figure I-12: Buck-boost converter**.** [Aas15]

### I.7.3 Photovoltaic Water pumps and motors

The stand-alone photovoltaic (PV) water pumping system has received increasing attention in the last 20 years because of the significant, on-going cost reductions achieved in manufacturing PV arrays. Past studies of PV energized water pumping systems have previously considered a number of suitable pumps and motors [Aas15] . Two types of pumps are widely employed in PV systems: the centrifugal pump and volumetric pump. The centrifugal pump is capable of pumping a high volume of water and operating at relatively high efficiency. These pumps are used to pump the water from boreholes and from surface water reservoir and they are ideally suitable for medium to high water demands.

As the maximum energy available from solar panels is in the form of slowly changing DC, the pumps are usually driven by DC motors to minimize system complexity since they can be directly connected to the PV panel or array. Separately-excited and permanent magnet (PM) brushed DC motors are often recommended for PV pumping system. The permanent magnet types however, are more popular than the separately-excited types, because the rotation of the motor is caused by the brushed commutator without inducing the surrounding magnetic field electrically. Hence there is no power consumed in field windings, which increases the efficiency and reduces the size of the PV array of the system.

AC motors have attractive features such as high efficiency, brushless configuration, simpler geometry and rugged construction; and initial cost can be lower in the case of the cage induction motor. However, a detailed analysis of DC and AC motors used in PV pumping has been carried out [Aas15] in and it was concluded that the efficiency and dynamic performance of permanent magnet DC motor is better than an AC single phase induction motor. Additionally, if AC motor is used an inverter is required to convert the DC output of the PV array to AC power to drive the motor. Consequently, the cost and complexity of the overall system significantly increase. [Aas15]

### I.7.4 Pumping methods

Many people in isolated areas such as rural and remote regions suffer from water shortages, particularly in desert areas, and even where wells are used to pump water, there is the problem of

electricity supply for places not connected to the mains grid; to resolve this issue, is one of the best solutions, as it employs a relatively simple principle involving the generation of electricity via photovoltaic panels using solar radiation to power the pump [Abi23]. There are two basic types:

### I.7.4.1 Pumping as the sun moves across the sky

Storage is achieved hydraulically, with water being pumped, when there is sufficient sunlight, into an aboveground tank. It is then distributed by gravity as required. Pumping as the sun moves across the sky allows for a simpler photovoltaic system, as shown in Figure I-13. [Deh14]

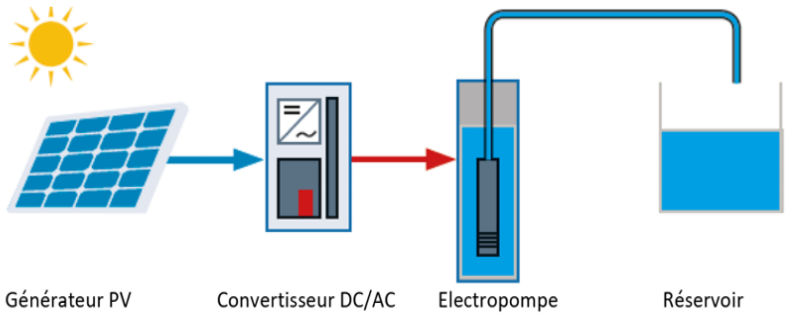


Figure I-13: Pumping system as the sun moves across the sky [Ben14]

The operating principle of such a system is relatively straightforward: photovoltaic panels power a pump (either surface-mounted or submersible), assisted by a controller (which may be integrated into the pump, depending on the manufacturer), to supply water when the panels are exposed to sunlight. Sun-powered pumping uses a tank to store water until it is needed. This solution is less expensive, but these pumps do not have a constant flow rate and do not operate below a certain level of sunlight (at the start and end of the day), as their efficiency is lower outside the nominal operating power range. Depending on the type of actuator, the main components of these systems are: - With a DC motor: a PV generator, a DC-DC converter (chopper), a DC motor and a pump. - With an AC motor: a PV generator, a DC-DC converter (chopper), a DC-AC converter (inverter), a synchronous or asynchronous motor and a pump.

### I.7.4.2 Pumped storage using electrochemical storage (batteries)

This technique is based on energy storage via batteries. These batteries store the energy generated by the PV panels during periods of sunshine so that they can release this energy to pump water when required. Water can be pumped on demand, whenever users need it. Pumping using solar energy should always be prioritized, given the cost of batteries and the weak link they represent in a PV system due to their limited lifespan. Nevertheless, it has certain drawbacks that should not be overlooked when making a choice. [Roy98]

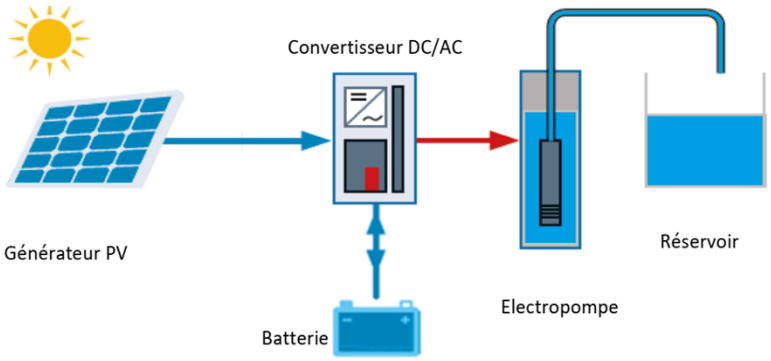


Figure I-14: Pumping system storage using electrochemical storage. [Roy98]

## I.8 Conclusion

In conclusion, this chapter provided a general overview of renewable energy sources, such as solar energy, photovoltaic energy, and wind power. It explored the core principles of solar energy by defining the structural differences between solar technologies. While photovoltaic technology faces critical grid-integration and environmental challenges, its strategic development in Algeria capitalizes on exceptional regional irradiance to drive modern energy infrastructure. Ultimately, these principles culminate in the optimization of decentralized water pumping systems, where the seamless integration of the photovoltaic generator, converters, inverters, motors, and pumps offers sustainable socio-economic solutions.

# Chapter II

## Modeling of the photovoltaic pumping system

## II.1 Introduction:

Solar photovoltaic (PV) systems have emerged as a clean, inexhaustible, and low-maintenance source of energy. PV technology is currently recognized as one of the most innovative and economically viable electrical energy sources available to meet these rising global power needs. [Ham25]. A typical solar pumping system is a multi-stage architecture consisting of a PV generator, a DC-DC converter equipped with a Maximum Power Point Tracking (MPPT) controller, and an electric motor coupled to a centrifugal pump. Modeling these systems is essential because, unlike simple resistive loads, solar pumps introduce complex nonlinear electromechanical dynamics between the motor and the pump. Precise mathematical modeling allows researchers to simulate electrical and mechanical behavior under diverse climatic conditions, enabling the validation of control strategies and ensuring maximum energy extraction before hardware implementation. This chapter is devoted to the modeling of the photovoltaic pumping system.

## II.2 Modeling of the photovoltaic cell

### II.2.1 PV cell model

Modeling photovoltaic (PV) cells often involves using mathematical formulas to describe their electrical behavior. [Khe25]

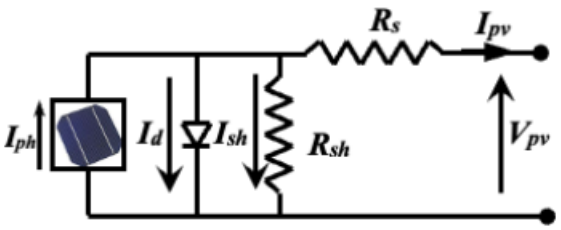


Figure II- 1 – Equivalent circuit of photovoltaic cells [Khe25]

One commonly used model is the single-diode model, which represents a PV cell with a simple equivalent circuit, as shown in Figure II- 1. The current-voltage (I-V) characteristics of a solar cell are described by:

$$I_{PV} = I_{PH} - I_D - I_{SH} \tag{II.1}$$

$$I_{PV} = I_{PH} - I_S\left[exp\left(\frac{R_S I_{PV}+V_{PV}}{V_t}\right) - 1\right] - \left(\frac{R_S I_{PV}+V_{PV}}{R_{Sh}}\right) \tag{II.2}$$

$$V_t = \frac{N_s nkT}{q} \tag{II.3}$$

$$\begin{cases} I_D = I_S\left[exp\left(\frac{R_S I_{PV}+V_{PV}}{V_t}\right) - 1\right] \\ I_{Sh} = \left(\frac{R_S I_{PV}+V_{PV}}{R_{Sh}}\right) \end{cases} \tag{II.4}$$

$$I_{Ph} = N_P I_{Ph-cell}, \quad I_S = N_P I_{S-cell} \tag{II.5}$$

### II.2.2 Photovoltaic generator (GPV)

A photovoltaic generator (GPV) is an assembly consisting of PV cells, connections, protective components, and mounting brackets, etc. Thus, any PV device (solar cells, modules, panels, etc.) can be referred to as a "PV generator." In practice, a PV solar cell produces only a very small amount of electrical power, typically 1 to 3 W with a voltage of 0.5 to 1.5 V depending on the technologies used [Dem22].

To achieve higher power output, PV cells are typically connected in series and encapsulated under glass to form a module. Modules are connected in series and/or in parallel to form a panel. Several panels grouped together at a single site form a PV array Figure II-2. [Abi23]

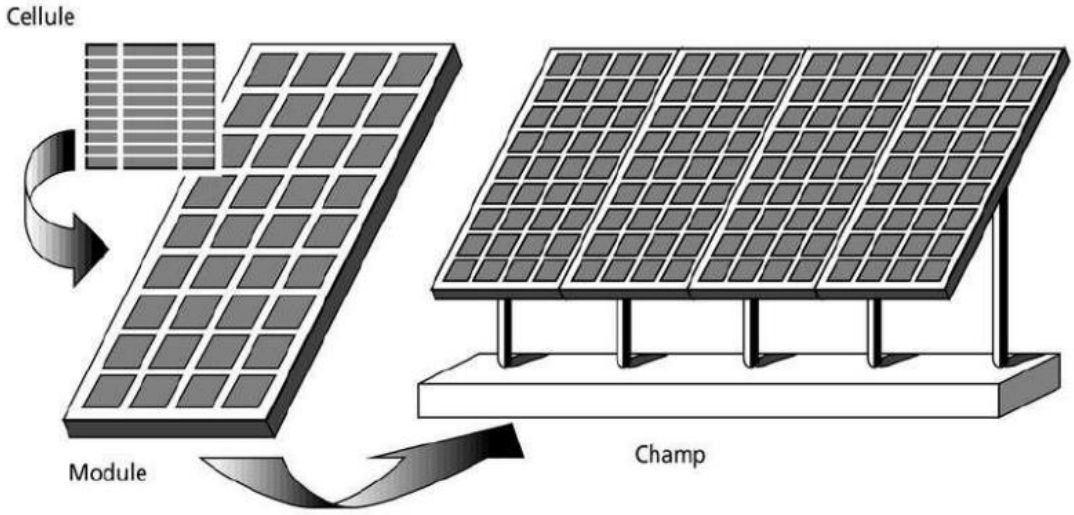


Figure II-2 : Overview of a solar cell, a solar panel, and a solar array [Roy98].

### II.2.3 Current-voltage (I-V) characteristic of the photovoltaic cell:

The characteristics of a photovoltaic solar cell are defined by a number of parameters derived from the current-voltage curve: [Zer25]

#### II.2.3.1 Open circuit voltage $V_{OC}$:

The open-circuit voltage is obtained when the current flowing through the cell is zero. It depends on the energy barrier and the shunt resistance. It decreases with temperature and varies little with light intensity. [Abi23]

We can write:

$$V_{oc} = AU_T \, ln(\frac{I_{PH}}{I_S} + 1) \tag{II.6}$$

#### II.2.3.2 Short-circuit current $I_{SC}$:

This is the current produced by a PV cell when exposed to light, with its terminals directly connected to each other and no external load. This current is denoted as $I_{sc}$ and is a key value

for determining the cell's ability to generate current under specific irradiance conditions [Bab25]. In a short circuit, V = 0 Hence: $I_{cc} = I_{PH}$ (in the ideal case). The approximate expression for the short-circuit current is:

$$I_{SC} = \frac{I_{PH}}{1+\frac{R_S}{R_{SH}}} \quad \text{(II.7)}$$

### II.2.3.3 maximum power $P_m$

It's the product between Voltage and Current at maximum power point ($V_{mpp}$ & $I_{mpp}$), we can write:

$$P_M = V_{mpp} \times I_{mpp} \quad \text{(II.8)}$$

### II.2.3.4 Form factor $F_F$

The form factor ($F_F$) is defined as the ratio between the maximum power that a PV cell can deliver and the theoretically maximum power that can be obtained. It is used to quantify the efficiency of a PV cell in terms of converting solar energy into electricity. [Bab25]

We can define it as:

$$F_F = \frac{P_M}{P_{Obt}} = \frac{V_{mpp} \times I_{mpp}}{V_{OC} \times I_{SC}} \quad \text{(II.9)}$$

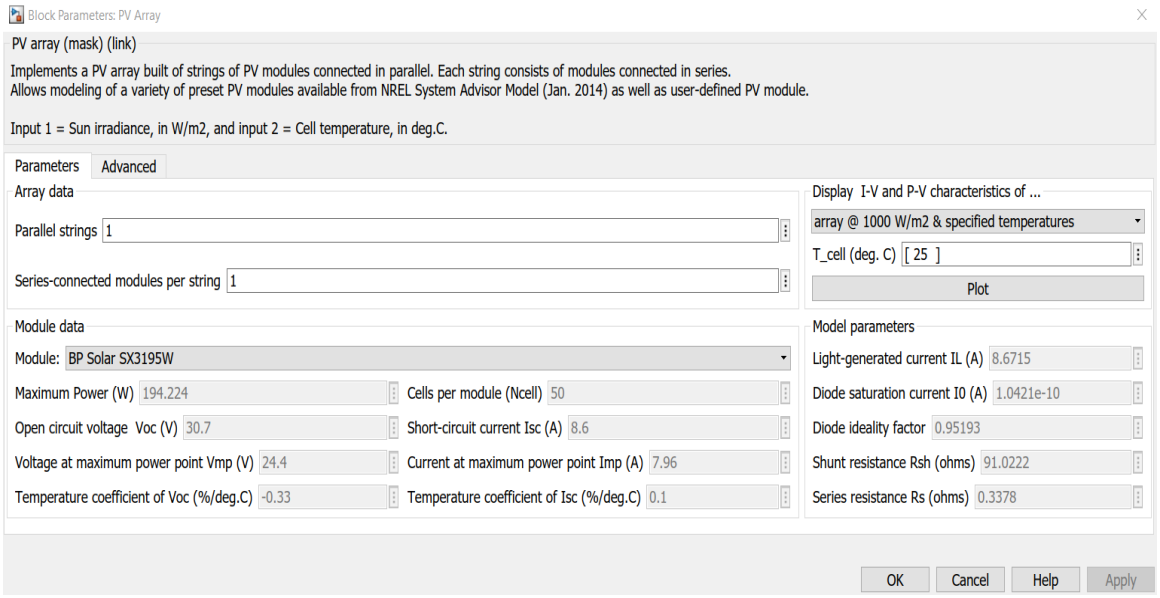


Figure II-3: mains parameters of a solar panel array type BP Solar SX3195W

Figure II-4 shows the P-V & I-V characteristics of a solar panel array type BP Solar SX3195W.

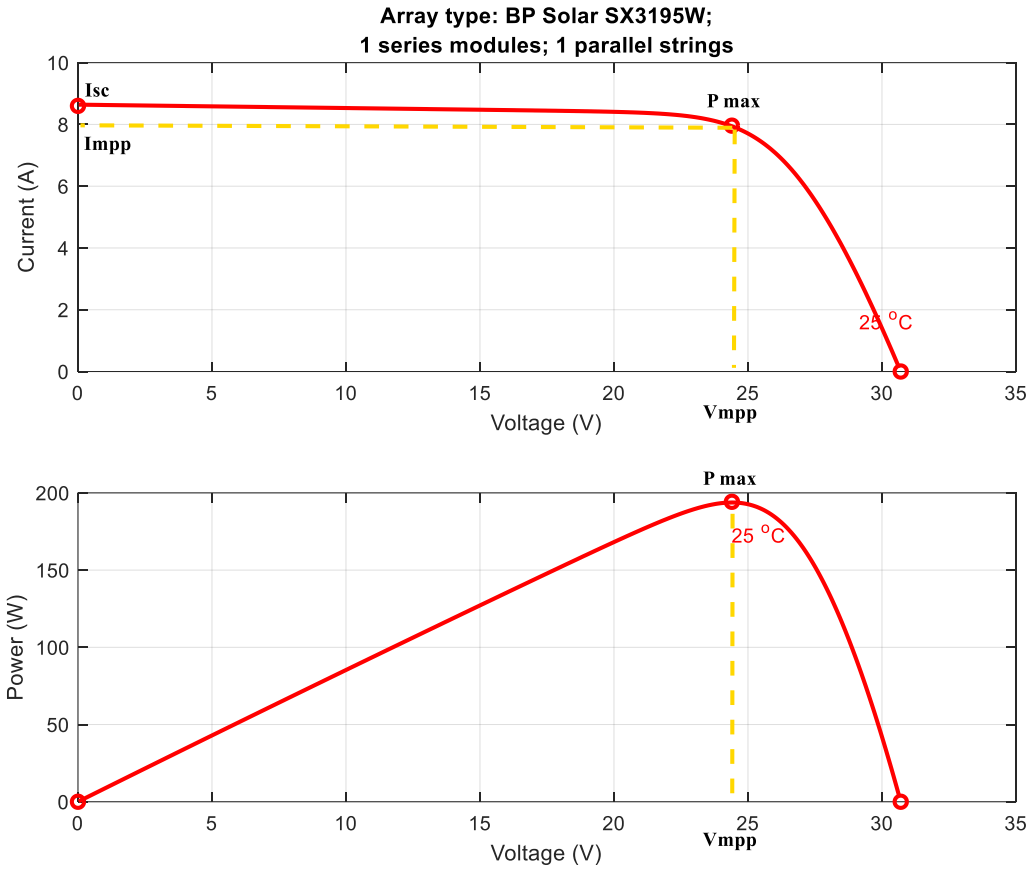


Figure II-4: curve representing the main parameters of a solar panel array type BP Solar SX3195W

### II.2.3.5 Maximum energy efficiency ηm

Maximum energy efficiency is the ratio of the maximum power output ($P_M$) to the incident solar radiation power ($P_i$). [Bab25]

We can define it as :

$$\eta_{m(Cell)} = \frac{P_m}{P_i} = \frac{V_{mpp} \times I_{mpp}}{E \times S} \quad \text{(II.10)}$$

Where:

S: Surface area of the solar cell.

E: Incident flux.

## II.3 PV Module

A PV module consists of several solar cells interconnected to form a circuit capable of generating electricity when exposed to a light source, such as sunlight. To increase the output voltage, the cells are generally connected in series, while a parallel connection increases the current. Furthermore, a PV module can be structured into several subassemblies called

submodules, which are themselves connected in series or in parallel, depending on the system's performance requirements [Ben17].

### II.3.1 Types of Associations

#### II.3.1.1 Series Associations

In most cases, solar panels are formed by solar cells connected in series, as the voltage produced by a single cell is too low for many applications.. The number of interconnected solar cells depends on the amount of power desired to be generated. Figure II-5 shows the IV behavior of the solar cells connected in series. To distinguish the different curves, a nomenclature is employed in which, the first term corresponds to the number of solar cells connected in series followed by an S (series) and finally SC (solar cell). For example, two solar cells connected in series are represented by 2S SC. [Rod15]

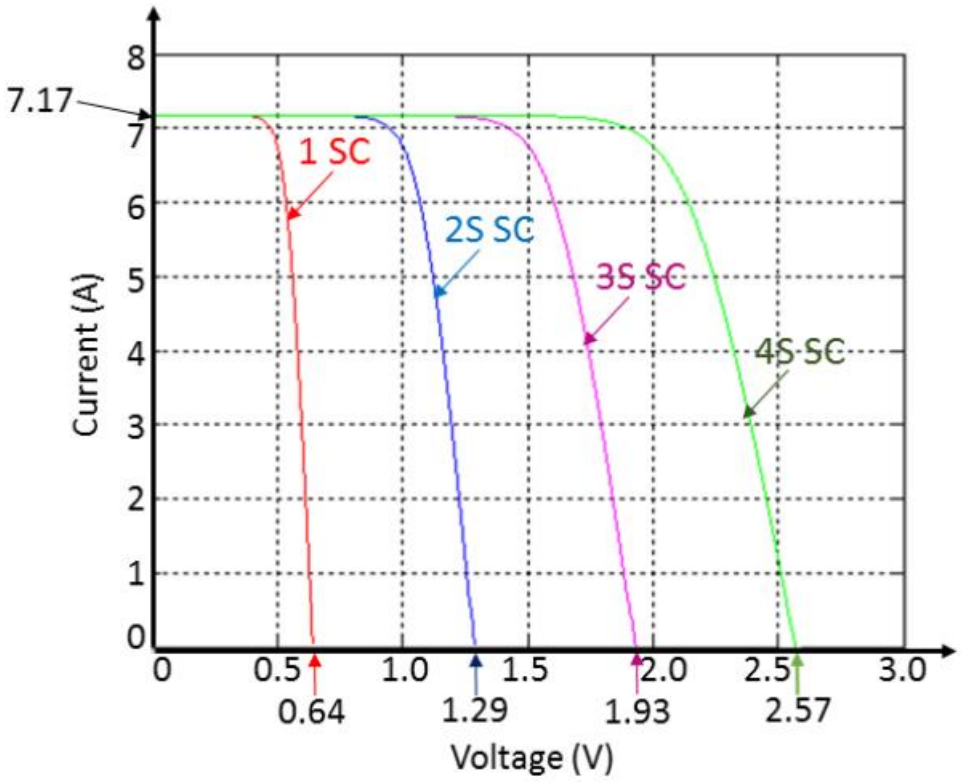


Figure II-5 : IV curve of series connected solar cells [Rod15]

$$V_{OC} = \sum_1^n V_n = V_1 + V_2 + V_3 + \ldots\ldots + V_n \qquad I \geq 0 \tag{II.11}$$

$$\text{Where } V_{OC} == NsV_{OC1} = NsV_{OC2} = NsV_{OC3} = \ldots\ldots = NsV_{OCn} \tag{II.12}$$

$N_s$ is the number of the solar cells connected on series

To find Number of modules in series (Fig. II-6) we can use:

$$N_s = \frac{V_{mpp}}{V_m} \tag{II.13}$$

where $V_{MPP}$ and $V_m$ are the MPP voltage of solar array and module.

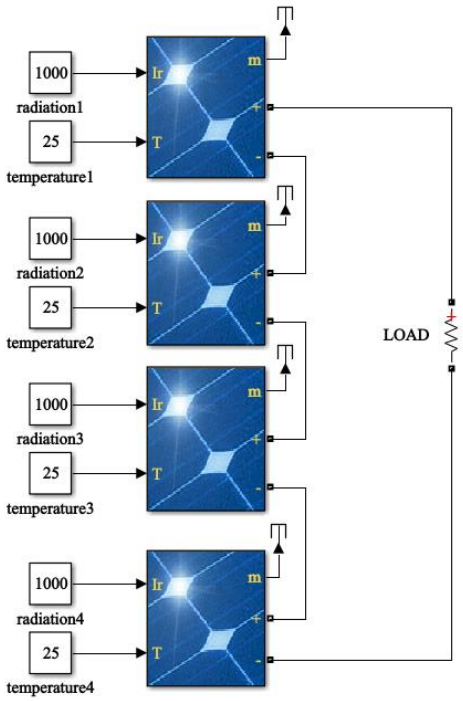


Figure II-6: Representing series association of 4 PV array

### II.3.1.2 Parallel Association

Connecting cells in parallel generates an increase in the current of the total system, as shown in Figure II-7. For the employed nomenclature, the first term corresponds to the number of solar cells connected in parallel followed by a P (parallel) and finally SC (solar cell). For example, three solar cells connected in parallel are represented by 3P SC.

The $V_{OC}$ has a constant value, equal to the one of a single solar cell, regardless of the number of cells in parallel.

The number of cells connected in parallel determines the increase in the short-circuit current (Isc) of the entire system. For example, three solar cells in parallel provide a short circuit current three times higher than the one of one solar cell. [Rod15]

$$I_{sc} = \sum_1^n I_n = I_1 + I_2 + I_3 + \ldots\ldots + I_n \qquad I \geq 0 \tag{II.14}$$

$$\text{Where :} \quad V_{OC} == V_1 = V_2 = V_3 = \ldots\ldots = V_n \tag{II.15}$$

To find Number of modules in parallel (Fig. II-8) we can use:

$$N_p = \frac{I_{mpp}}{I_m} \tag{II.16}$$

where $I_{mpp}$ and $I_m$ are the MPP current of a solar array and module.

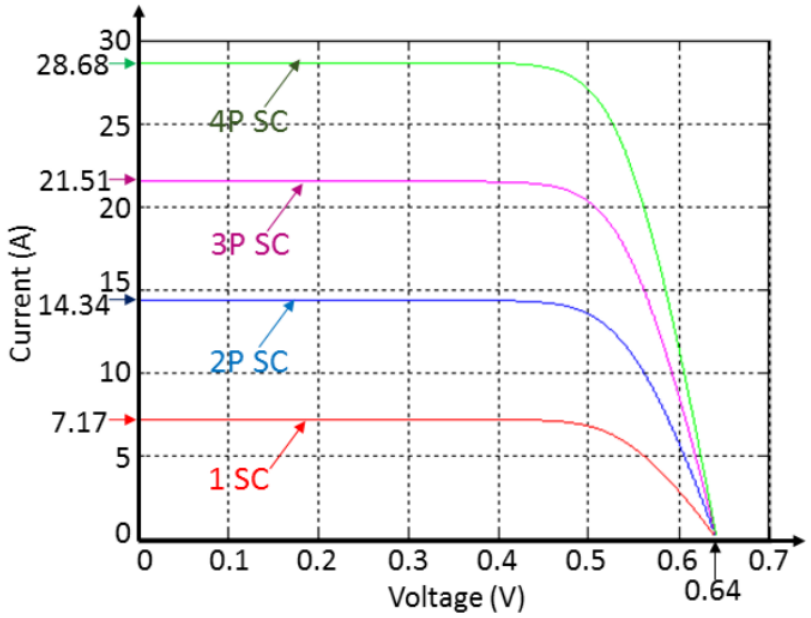


Figure II-7: IV curve of parallel connected solar cells [Rod15]

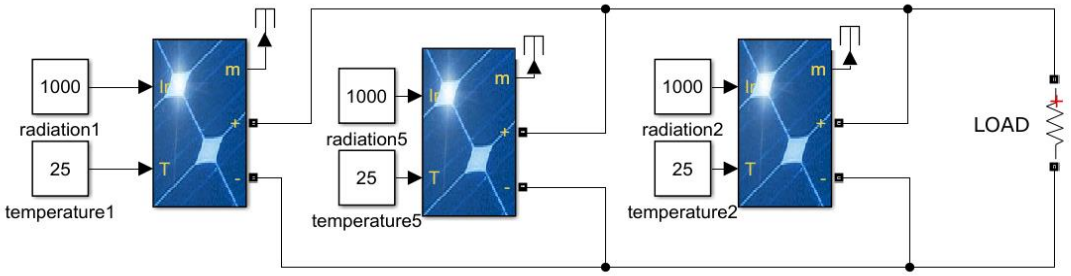


Figure II-8: Representing Parallel association of 3 PV array

### II.3.1.3 Series-parallel associations (mixed or hybrid association)

The hybrid series-parallel configuration of PV modules involves combining multiple PV modules in a way that leverages the benefits of both series and parallel wiring. This type of configuration increases both the system's output voltage and current, while optimizing the use of available space. Furthermore, it offers better tolerance to partial shading, as part of the system can continue to operate even if another part is partially shaded. In addition, this architecture reduces the amount of wiring required and improves the system's overall energy efficiency (Figs. II-9 and II-10) [Ben11].

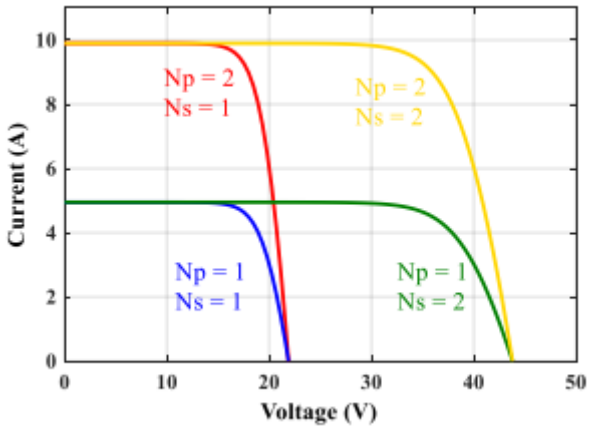


Figure II-9: Association hybrid [Ben11]

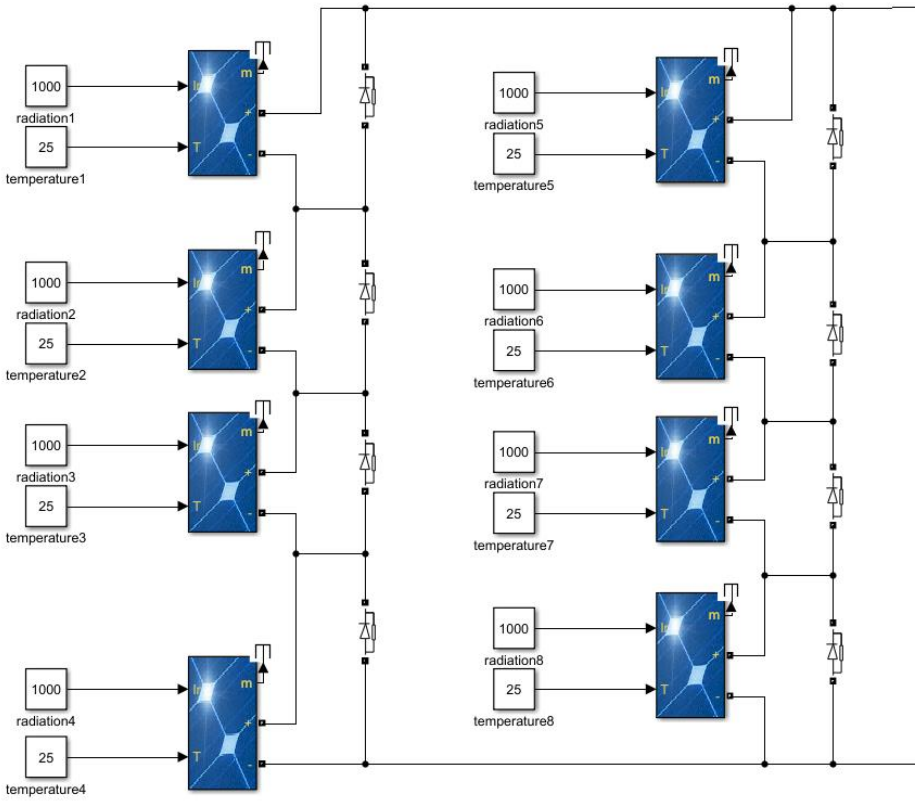


Figure II-10: Representing Series-Parallel association of 4 Series PV array & 2 parallel PV array

The current and voltage outputs of the solar-generator in the photovoltaic array are given by the following equations: [Bou12]

$$V_{Out} = \sum_1^n V_n = V_1 + V_2 + V_3 + \ldots\ldots + V_n \quad \text{(II.17)}$$

$$I_{Out} = \sum_1^m I_m = I_1 + I_2 + I_3 + \ldots\ldots + I_m \quad \text{(II.18)}$$

The power of the solar-generator ($P_{out}$) is written as: [Bou12]

$$P_{Out} = \sum_1^n V_n \sum_1^m I_m = (V_1 + V_2 + V_3 + \ldots\ldots + V_n)(I_1 + I_2 + I_3 + \ldots\ldots + I_m) \quad \text{(II.19)}$$

## II.4 Modeling the DC-DC Converter:

### II.4.1 DC-DC boost converter

The corresponding circuit of the DC/DC boost converter is depicted in Figure II-11, which is positioned between the photovoltaic arrays and the Voltage Source Inverter to amplify the voltage and optimize the panels power output. [Saa25]

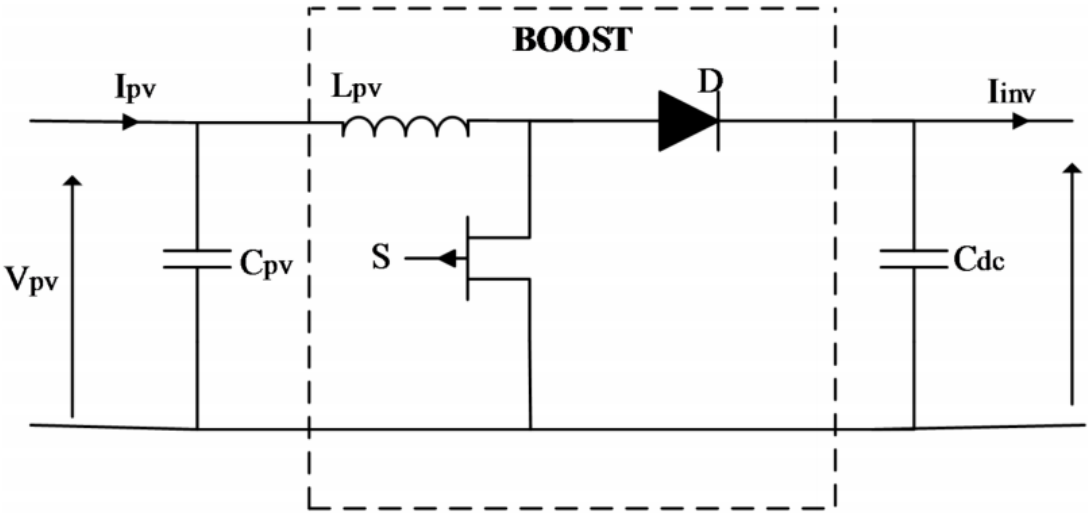


Figure II-11: Design of the DC/DC boost converter. [Saa25]

### II.4.2 Parameters of DC-DC boost converter

#### II.4.2.1 Duty cycle D

The boost dc-dc converters provide a voltage at the output greater than the input for supplying a PV solar water pump with sufficient voltage and maximum power extraction from the PV array under variable radiation conditions. The steady-state duty cycle of this converter can be expressed as [Har11].

$$D = \frac{V_{DC} - V_{PV}}{V_{DC}} \quad \text{(II.20)}$$

where, $V_{dc}$ is the inverter side voltage, $V_{pv}$ is the voltage at the PV side, and $D$ is the duty cycle of the boost converter.

#### II.4.2.2 Inductor and capacitor of the boost converter

The estimated values of the inductor and the capacitor of the boost converter under continuous conduction mode (CCM) operation can be given by the following equations [Has22]:

$$L_{Boost} = \frac{V_{pv}(V_{dc} - V_{pv})}{V_{dc} \Delta I_L f_{sw}} \quad \text{(II.21)}$$

$$C_{Boost} = \frac{I_{dc}(V_{dc}-V_{pv})}{V_{dc}\Delta V_0 f_{sw}} \quad \text{(II.22)}$$

The $f_{sw}$ is switching frequency, $\Delta I_L$ is the estimated maximum amplitude of the current ripple at the inductor terminals of (20%), $\Delta V_o$ is the peak voltage ripple at the output capacitor of (1%).

### II.4.2.3 The input capacitor $C_{in}$ ($C_{pv}$)

The input capacitor ensures that the DC-DC boost converter will operate efficiently at the max. power point and reduce ripple in the PV arrays voltage output. This capacitor can be calculated as [Ayo18]

$$C_{in} = \frac{D}{8L_{Boost}\Delta V_{pv} f_{sw}^2} \quad \text{(II.23)}$$

where, $\Delta V_{pv}$ is the ripple of the output voltage from the PV array measured at the PV capacitor side (1% typical value).

## II.5 Maximum Power Point Tracking Techniques (MPPT)

MPPT (Maximum Power Point Tracking) control is essential for the optimal operation of a photovoltaic system. The principle behind this control is based on automatically adjusting the duty cycle D (or α) to its optimal value in order to maximize the power output of the PV panel. [Bah20]

Figure II-12 shows the block diagram of a photovoltaic module equipped with a DC-DC conversion stage between the PV array and the output load. [Ben20]

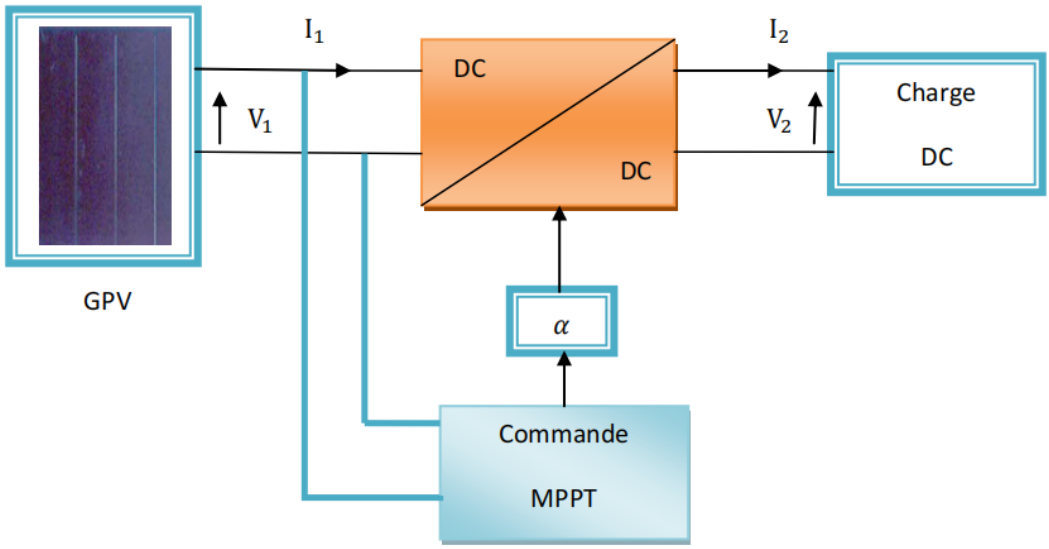


Figure II-12: Basic photovoltaic conversion system [Ben20]

### II.5.1 MPPT classification for PV systems

PV cells and modules generate varying levels of power based on changing environmental conditions, such as wind velocity, shading, and the solar insolation angle. Consequently, maximum power generation is not guaranteed across all electrical loads. MPPT techniques are equipped with proper controllers to extract maximum available power from PV configurations. There are various types of MPPT techniques used to run PV modules on maximum power. Nevertheless, the efficiency of the particular technique depends on its tracking ability in instantaneously changing weather conditions. So, depending on the tracking nature in PSC's, these techniques are classified. Discussion is done on all classified techniques and categorized into the following classification, as shown in Figure II-13. [Bol20]

- Classical MPPT
- Intelligence MPPT
- Optimization MPPT
- Hybrid MPPT

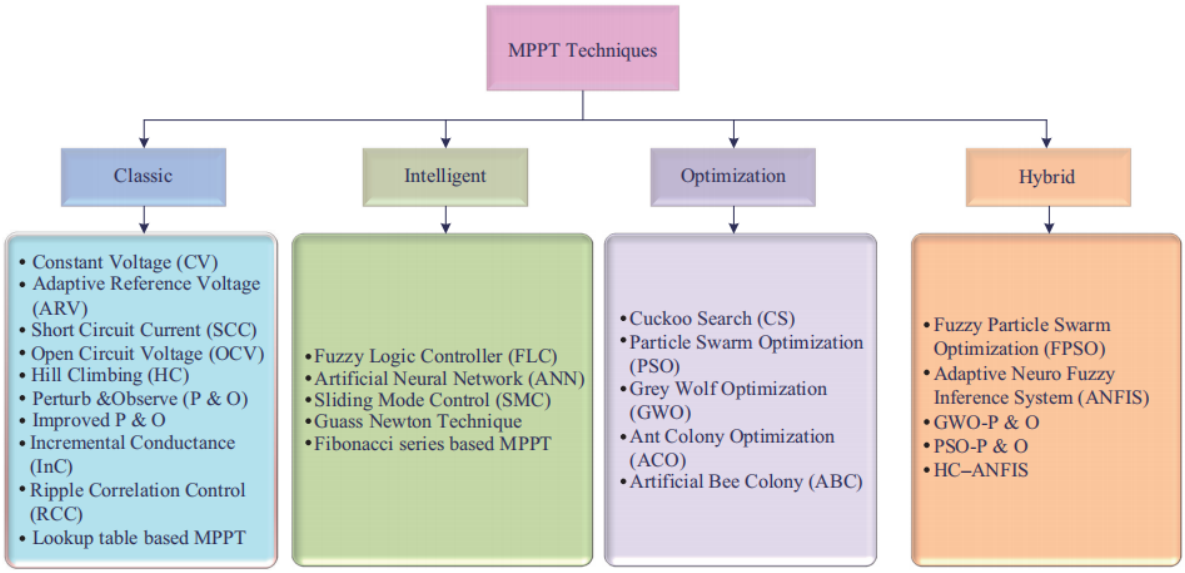


Figure II-13: Basic classification of tracking techniques [Bol21]

### II.5.2 Performance specifications of MPPT control algorithm

As noted earlier, the dynamic response, steady-state error and tracking efficiency should be considered for a successful design when evaluating the performance of a new or modified MPPT control algorithms [Xia04].

#### II.5.2.1 Dynamic response

The response of an MPPT control algorithm must be fast enough to track the MPP during rapid changes in atmospheric conditions (solar irradiation and temperature). The higher the tracking speed of the MPPT algorithm, the lower the solar energy losses in the system. [Aas15]

### II.5.2.2 Steady-state error

The MPPT control algorithm should stop tracking, once the MPP is located and should force the system to maintain operation at this optimal operating point as long as possible. However, this is impossible to achieve practically in an actual MPPT system because of the active perturbation process in MPPT algorithms with fixed tracking step-size and the continuous variation in solar insolation and temperature. This phenomenon has a negative impact on the PV system efficiency. [Aas15]

### II.5.2.3 Tracking efficiency

Defining the tracking efficiency is a very important step, to quantify how successfully an MPPT control algorithm tracks the MPP and to what extent it contributes to increase the overall performance of the PV system compared to other methods. The tracking efficiency is defined as the ratio between the actual power of the PV array and the theoretical power during the same time period as: [Taf08]

$$\eta_{mpp} = \frac{1}{n}\sum_{i}^{n}\frac{P_{actuel,i}}{P_{max,i}} \quad \text{(II.24)}$$

Where $P_{actual}$ is the *i*th sample of real measured power produced by the PV array while using the MPPT control, Pmax is the *i*th sample of true maximum power of the PV array could produce under the given solar insolation and temperature and n is the total number of samples.

### II.5.3 Examples of two most common methods of MPPT:

### II.5.3.1 Perturb and Observe (P&O) method of MPPT

The P&O tracking process is carried out by observing the array output power and determining the next action, either to increase or decrease the array operating voltage.. If the operating voltage of a PV array is perturbed in a given direction and if the power drawn from the PV array increases, this means that the operating point has moved towards the MPP and therefore, the operating voltage must be further perturbed in the same direction. Otherwise, if the power drawn from the PV array decreases, the operating point has moved away from the MPP and therefore, the direction of the operating voltage perturbation must be reversed. This is explained in the form of a flowchart below in Figure II-14. [Fin13]

The algorithm continuously "climbs" the power curve until it reaches the peak (MPP).

Let:

- $V(k)$: voltage at iteration $k$
- $I(k)$: current at iteration $k$
- $P(k) = V(k) \times I(k)$: power at iteration $k$
- $\Delta V(k) = V(k) - V(k-1)$: voltage change
- $\Delta P(k) = P(k) - P(k-1)$: power change

The P&O decision logic is [Pat20] :

**Case 1: Power Increases ($\Delta P > 0$)**

$$\begin{cases} \text{If } \Delta V > 0: & \text{Continue increasing voltage} \\ & V(k+1) = V(k) + \Delta V_{step} \end{cases} \quad (II.25)$$

$$\begin{cases} \text{If } \Delta V < 0: & \text{Continue decreasing voltage} \\ & V(k+1) = V(k) - \Delta V_{step} \end{cases} \quad (II.26)$$

**Case 2: Power Decreases ($\Delta P < 0$)**

$$\begin{cases} \text{If } \Delta V > 0: & \text{Reverse direction (decrease voltage)} \\ & V(k+1) = V(k) - \Delta V_{step} \end{cases} \quad (II.27)$$

$$\begin{cases} \text{If } \Delta V < 0: & \text{Reverse direction (increase voltage)} \\ & V(k+1) = V(k) + \Delta V_{step} \end{cases} \quad (II.28)$$

**Case 3: Power Unchanged ($\Delta P = 0$)**

$$V(k+1) = V(k) \text{ (Maintain voltage)} \quad (II.29)$$

**Duty Cycle Adjustment**

The duty cycle is updated based on the P&O decision:

$$D(k+1) = D(k) \pm \Delta D \quad (II.30)$$

where:

- $\Delta D$: step size for duty cycle (typically 0.001 to 0.01)
- **(+)** when voltage should increase
- **(-)** when voltage should decrease

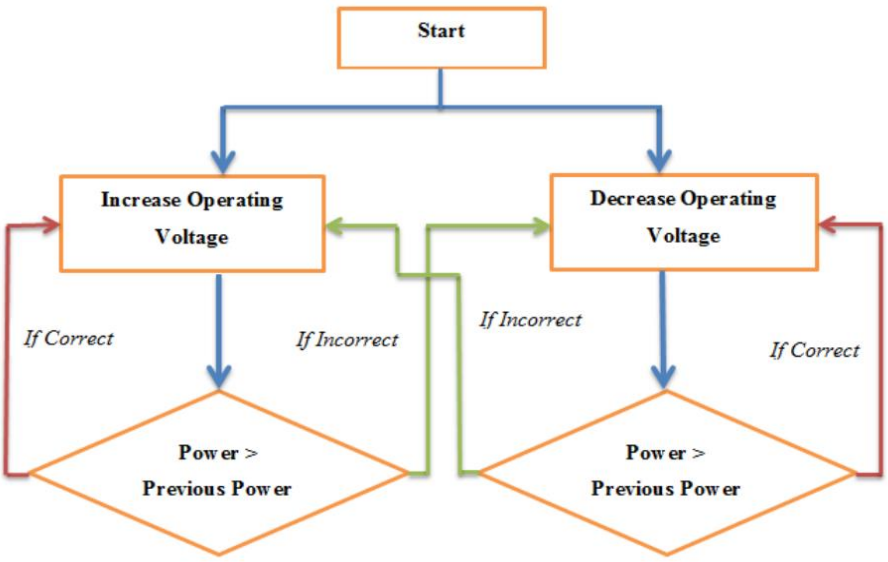


Figure II-14 : P&O Algorithm. [Fin13]

### II.5.3.1 Incremental Conductance method of MPPT

The method can track the maximum power points accurately at high speeds and greatly increase the power output of a solar array under Partially Shaded Conditions. Figure II-15 shows the IC MPPT algorithm in the form of a flow chart. [Fin13]

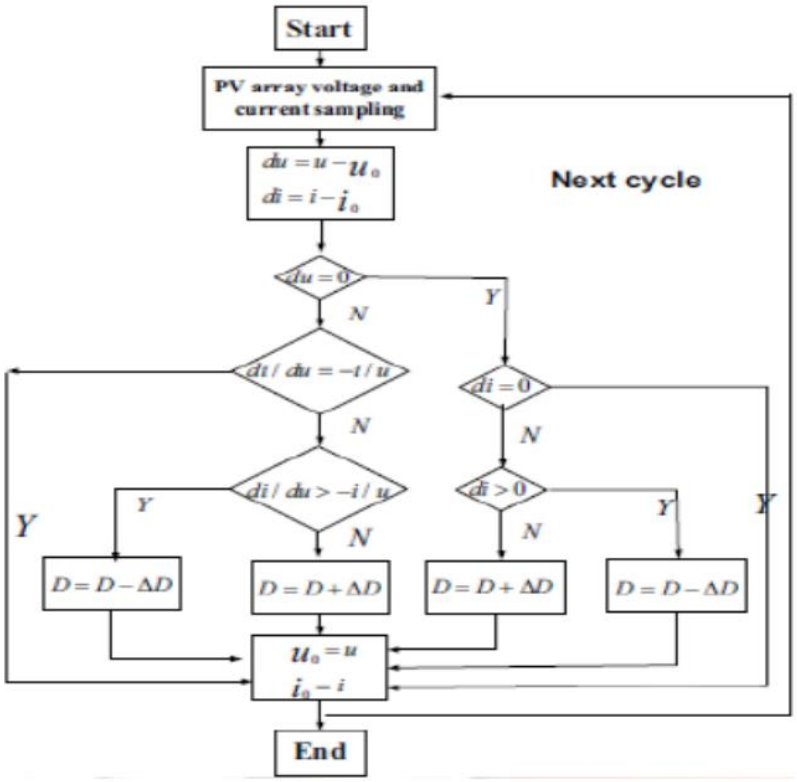


Figure II-15: Flow chart of IC method [Fin13]

The output power of a PV panel is the product of voltage and current:

$$P = V \times I \tag{II.31}$$

To find the maximum power point, we differentiate power with respect to voltage:

$$\frac{dP}{dV} = \frac{d(V \times I)}{dV} \tag{II.32}$$

Applying the product rule of differentiation:

$$\frac{dP}{dV} = I + V \times \frac{dI}{dV} \tag{II.33}$$

At the maximum power point, the derivative of power with respect to voltage equals zero:

$$\frac{dP}{dV} = 0 \tag{II.34}$$

Substituting Equation (33) into Equation (31):

$$I + V \times \frac{dI}{dV} = 0 \quad \text{(II. 35)}$$

Rearranging the terms:

$$\frac{dI}{dV} = -\frac{I}{V} \quad \text{(II. 36)}$$

This is the fundamental equation of the INC algorithm. It states that at the MPP, the incremental conductance ($\frac{dI}{dV}$) equals the negative of the instantaneous conductance ($-\frac{I}{V}$). [Kja12]

**Operating Regions**

Based on Equation (36), we can define three distinct operating regions:

**Region 1: Left of MPP (Below MPP Voltage)**

When the operating voltage is less than $V_{mpp}$:

$$\frac{dP}{dV} > 0 \implies I + V \times \frac{dI}{dV} > 0 \implies \frac{dI}{dV} > -\frac{I}{V} \quad \text{(II. 37)}$$

**Action:** Increase the voltage to reach MPP.

**Region 2: At MPP**

At the maximum power point:

$$\frac{dP}{dV} = 0 \implies \frac{dI}{dV} = -\frac{I}{V} \quad \text{(3II. 8)}$$

**Action:** Maintain the current voltage (no perturbation needed).

**Region 3: Right of MPP (Above MPP Voltage)**

When the operating voltage exceeds $V_{mpp}$:

$$\frac{dP}{dV} < 0 \implies I + V \times \frac{dI}{dV} < 0 \implies \frac{dI}{dV} < -\frac{I}{V} \quad \text{(II. 39)}$$

**Action:** Decrease the voltage to reach MPP.

**Duty Cycle Update Equation**

The INC algorithm updates the duty cycle as follows:

$$D(k+1) = D(k) + \Delta D \times \text{sign} \quad \text{(II. 40)}$$

where:

- sign $= +1$ when voltage should increase
- sign $= -1$ when voltage should decrease
- $\Delta D$: step size (fixed or variable)

## II.6 Modeling the voltage inverter (DC/AC)

The main function of the inverter is to convert the current produced by the solar generator into single-phase or three-phase alternating current. In this study, we consider the ideal case of a three-phase inverter with two voltage levels represented by perfect switches with instantaneous switching. The inverter, considered as a perfect voltage source, has a negligible internal impedance. [Amr16]

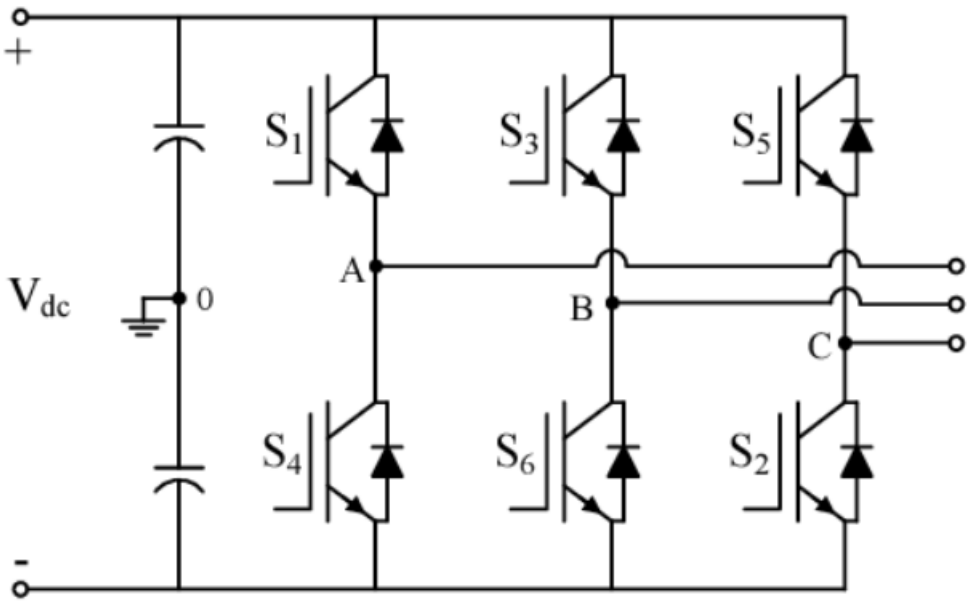


Figure II-16: Schematic diagram of a two-level three-phase inverter.

The composite voltages are derived from the inverter outputs, and the single-phase voltages of the load derived from the composite voltages have a sum of zero, so:

$$\begin{cases} U_{ab} = V_{an0} - V_{bn0} \\ U_{bc} = V_{bn0} - V_{cn0} \\ U_{ca} = V_{cn0} - V_{an0} \end{cases} \quad \text{(II.41)}$$

$$\begin{cases} V_{an} = \left(\frac{1}{3}\right)[U_{ab} - U_{ca}] \\ V_{bn} = \left(\frac{1}{3}\right)[U_{bc} - U_{ab}] \\ V_{cn} = \left(\frac{1}{3}\right)[U_{ca} - U_{bc}] \end{cases} \quad \text{(II.42)}$$

They can be expressed in terms of the inverter's output voltages by introducing the neutral voltage of the load relative to the reference point n0.

$$\begin{cases} V_{an} + V_{nn0} = V_{an0} \\ V_{bn} + V_{nn0} = V_{bn0} \\ V_{cn} + V_{nn0} = V_{cn0} \end{cases} \quad \text{(II.43)}$$

So, we can conclude that:

$$V_{nn} = \left(\frac{1}{3}\right)[V_{an0} + V_{bn0} + V_{cn0}] \quad \text{(II.44)}$$

Assuming ideal switches, the switching states for (i = a, b, c), we obtain:

$$\begin{cases} V_{an0} = (S_a - 0.5)U_0 \\ V_{bn0} = (S_b - 0.5)U_0 \\ V_{cn0} = (S_c - 0.5)U_0 \end{cases} \quad \text{(II.45)}$$

Substituting (48) into (50) gives:

$$\begin{cases} V_{an} = \left(\frac{2}{3}\right)V_{an0} - \left(\frac{1}{3}\right)V_{bn0} - \left(\frac{1}{3}\right)V_{cn0} \\ V_{bn} = \left(\frac{1}{3}\right)V_{an0} + \left(\frac{2}{3}\right)V_{bn0} - \left(\frac{1}{3}\right)V_{cn0} \\ V_{cn} = \left(\frac{1}{3}\right)V_{an0} - \left(\frac{1}{3}\right)V_{bn0} + \left(\frac{2}{3}\right)V_{cn0} \end{cases} \quad \text{(II.46)}$$

Substituting (49) into (50) gives:

$$\begin{bmatrix} V_{an} \\ V_{bn} \\ V_{cn} \end{bmatrix} = \frac{U_0}{3}\begin{bmatrix} 2 & -1 & -1 \\ -1 & 2 & -1 \\ -1 & -1 & 2 \end{bmatrix}\begin{bmatrix} S_a \\ S_b \\ V_c \end{bmatrix} \quad \text{(II.47)}$$

## II.7 Direct Torque Control (DTC)

The direct torque control (DTC) technique was proposed by Isao Takahashi in 1986. It consists of a pair of hysteresis controllers, flux and torque estimators, and a voltage vector selection table. The basic advantages of the DTC scheme are presented as follows:

- ❖ High dynamic
- ❖ Robustness
- ❖ Reduced response time
- ❖ Absence of park transformation

The DTC has also some disadvantages, namely, the control of the torque and the flux at low speed is difficult, the switching frequency is not constant. The last one produces higher current and torque ripple and, consequently, higher machine losses, more noises and mechanical stress, which may reduce the lifespan of the machine. It is well known that the direct torque control (DTC) of a PMSM machine is based on the" direct" determination of the sequence of the control signal applied to the switches of the used voltage source inverter. This choice is generally based

on the use of hysteresis regulators whose function is to control the amplitude of the stator flux and the electromagnetic torque. [Kha22]. Figure II-17 shows the block diagram of the DTC system for a PMSM.

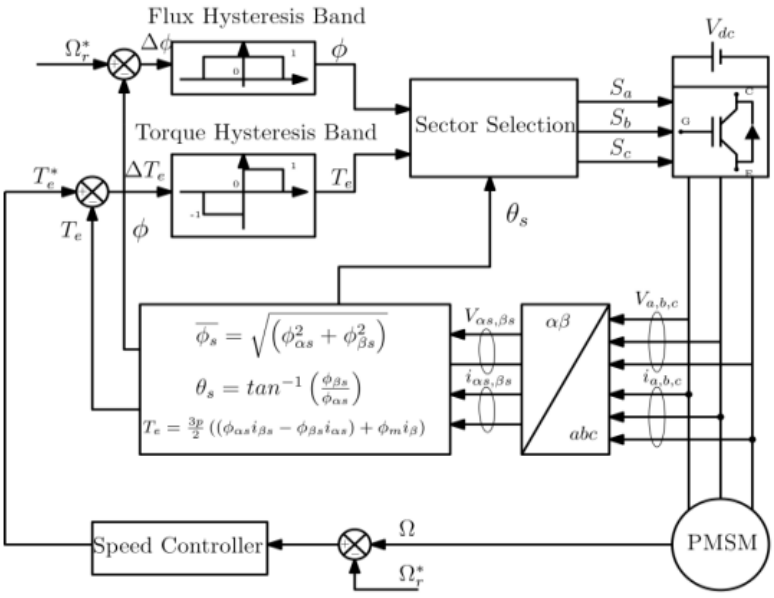


Figure II-17: Block diagram of the DTC. [Hac19]

According to the operating principles of DTC, there are six active voltage vectors and two zero voltage vectors. The selection of these voltage vectors is made to maintain the torque and stator flux within the limits of their respective hysteresis bands (Figure II-18).

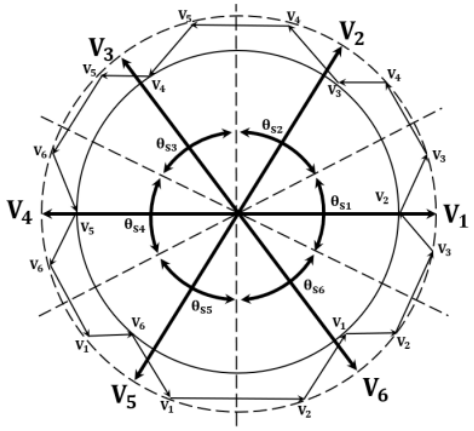


Figure II-18: Stator flux trajectory according to the voltage vector command under DTC using LUT (lookup table). [Son23]

### II.7.1 Principle of DTC Control

The DTC scheme is based on three fundamental principles [Khe18]:

- Real-time estimation of electromagnetic torque $T_e$ and stator flux $|\psi_s|$.
- Comparison with their references using hysteresis comparators.

- Selection of an optimal voltage vector via a switching table (Look-Up Table) to keep $T_e$ and $|\psi_s|$ within their hysteresis bands.

### II.7.1.1 Stator Flux Estimation

In the stationary $\alpha\beta$ reference frame, the stator flux is estimated using the voltage model [Pan14]:

$$\psi_\alpha = \int (v_\alpha - R_s i_\alpha) dt \quad \text{(II. 48)}$$

$$\psi_\beta = \int (v_\beta - R_s i_\beta) dt \quad \text{(II. 49)}$$

The flux magnitude and electrical angle are then:

$$|\psi_s| = \sqrt{\psi_\alpha^2 + \psi_\beta^2} \quad \text{(II. 50)}$$

$$\theta_s = \tan^{-1}\left(\frac{\psi_\beta}{\psi_\alpha}\right) \quad \text{(II. 51)}$$

### II.7.1.2 Torque Calculation

The electromagnetic torque is calculated directly from the $\alpha\beta$ quantities [Pan14] :

$$T_e = \frac{3}{2} p_n (\psi_\alpha i_\beta - \psi_\beta i_\alpha) \quad \text{(II. 52)}$$

### II.7.1.3 Hysteresis Comparators

The outputs of the flux and torque hysteresis comparators can be defined as follows:

- Flux comparator: 2 levels (↑/↓) → output $\phi \in \{+1, -1\}$
- Torque comparator: 3 levels (↑/hold/↓) → output $T \in \{+1, 0, -1\}$

These outputs determine whether flux or torque should be increased, maintained, or decreased.

### II.7.1.4 Switching Table (Look-Up Table)

The switching table selects the optimal voltage vector V_k (k=0…7) based on:

- The stator flux sector (6 sectors of 60°)
- The flux comparator output ϕ
- The torque comparator output T

The switching selection table for voltage is shown in Table II -2. [Hac19]

| Flux | Torque | Stator Flux Section | | | | | |
|---|---|---|---|---|---|---|---|
| | | $\theta_{s1}$ | $\theta_{s2}$ | $\theta_{s3}$ | $\theta_{s4}$ | $\theta_{s5}$ | $\theta_{s6}$ |
| 1 | 1 | $V_2$ | $V_3$ | $V_4$ | $V_5$ | $V_6$ | $V_1$ |
| | 0 | $V_7$ | $V_0$ | $V_7$ | $V_0$ | $V_7$ | $V_0$ |
| | −1 | $V_6$ | $V_1$ | $V_2$ | $V_3$ | $V_4$ | $V_5$ |
| −1 | 1 | $V_3$ | $V_4$ | $V_5$ | $V_6$ | $V_1$ | $V_2$ |
| | 0 | $V_0$ | $V_7$ | $V_0$ | $V_7$ | $V_0$ | $V_7$ |
| | −1 | $V_5$ | $V_6$ | $V_1$ | $V_2$ | $V_3$ | $V_4$ |

Table II -1: LUT (lookup table) used for conventional DTC control. [Son23]

## II.8 Permanent Magnet Synchronous Motor (PMSM)

The stator of a three-phase synchronous machine consists of three identical windings spaced 120° apart, housed in the slots of the fixed magnetic circuit. The latter is laminated to reduce eddy currents and limit iron losses. It is generally constructed of iron-silicon alloy sheet metal, which allows for high induction [Bou23].

In the rotor, the windings carrying direct current (in the case of a wound-rotor machine) are replaced by permanent magnets with alternating north and south poles. The inducing flux sweeps across the stator windings and induces alternating electromotive forces (e.m.f.) in them. The interaction of the stator and rotor fields generates a torque on the motor shaft and drives the motor at synchronous rotational speed. The following figure shows a surface-mounted permanent magnet synchronous machine.

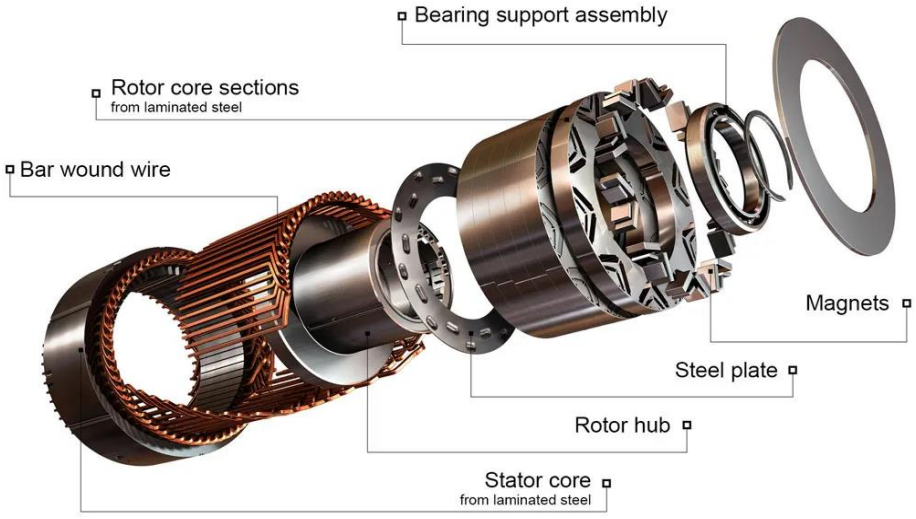


Figure II-19: Exploded view diagram of PMSM [Bou23]

### II.8.1 Modeling of a permanent-magnet synchronous motor in the park plane

Figure II-20 shows the exploded view of a permanent magnet synchronous motor. By applying the Park transformation to the system of equations in the abc reference frame, all vectors can be expressed in a rotor-fixed coordinate system [Bou05].

$$\begin{bmatrix} V_d \\ V_q \\ V_0 \end{bmatrix} = \frac{2}{3}\begin{bmatrix} \cos(\theta) & \cos\left(\theta - \frac{2\pi}{3}\right) & \cos\left(\theta + \frac{2\pi}{3}\right) \\ -\sin(\theta) & -\sin\left(\theta - \frac{2\pi}{3}\right) & -\sin\left(\theta + \frac{2\pi}{3}\right) \\ \frac{1}{2} & \frac{1}{2} & \frac{1}{2} \end{bmatrix} \cdot \begin{bmatrix} V_a \\ V_b \\ V_c \end{bmatrix} \quad \text{(II.53)}$$

Figure II-20 illustrates the equivalent circuit of a PMSM.

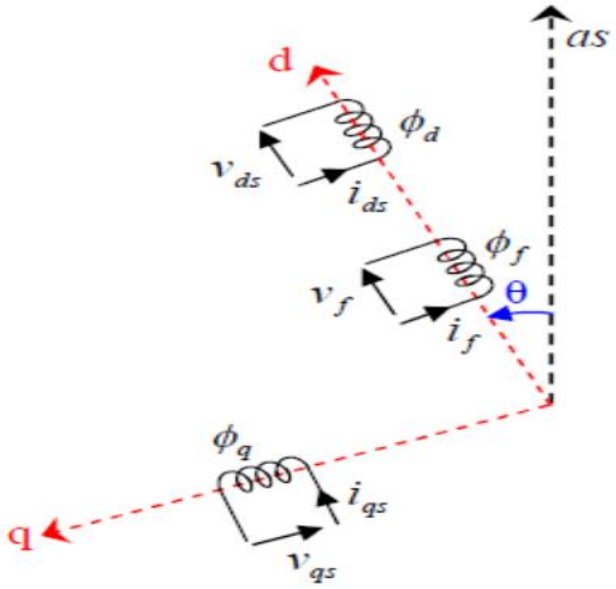


Figure II-20: Equivalent circuit of a PMSM in the (d,q) coordinate system [Bou05].

After expanding the equations, we obtain the electrical equations as:

$$\begin{cases} V_d = R_s I_d + \frac{d}{dt}\varphi_d - \Omega\varphi_q \\ V_q = R_s I_q + \frac{d}{dt}\varphi_q - \Omega\varphi_d \end{cases} \quad \text{(II.54)}$$

The fluxes can be expressed by the magnetic equations:

$$\begin{cases} \varphi_d = L_d I_d + \varphi_{sf} \\ \varphi_q = L_q I_q \end{cases} \quad \text{(II.55)}$$

So, The PMSM model can be written in the following form:

$$\begin{cases} V_d = R_s I_d + L_d \frac{d}{dt} I_d - \Omega L_q I_q \\ V_q = R_s I_q + L_q \frac{d}{dt} I_q - \Omega \left( L_d I_d + \varphi_{sf} \right) \end{cases} \quad \text{(II.56)}$$

$$\begin{cases} \frac{d}{dt} I_d = -\frac{R_s}{L_{d_s}} I_d - \Omega \frac{L_q}{L_d} I_q + \frac{V_d}{L_d} \\ \frac{d}{dt} I_q = -\frac{R_s}{L_q} I_q - \Omega \frac{L_d}{L_q} I_d - \frac{1}{L_q} \Omega \varphi_{sf} + \frac{V_q}{L_q} \end{cases} \quad \text{(II.57)}$$

**Expression of the electromagnetic torque**

The electromechanical torque is generated by the interaction between the poles formed by the magnets on the rotor and the poles generated by the FMMs in the air gap created by the stator currents. [Ami17]

$$T_e = \frac{3}{2} P \left( \varphi_d I_q - \varphi_q I_d \right) \quad \text{(II.58)}$$

After performing the necessary operations, we can write:

$$T_e = \frac{3}{2} P \left[ \left( L_d - L_q \right) I_d I_q - \varphi_{sf} I_q \right] \quad \text{(II.59)}$$

If the rotor is smooth ($L_d = L_q$), this equation simplifies to:

$$T_e = \frac{3}{2} P \left[ \varphi_{sf} I_q \right] \quad \text{(II.60)}$$

**Mechanical equations**

The dynamics of the machine are described by the following equation:

$$T_e - T_R - f\Omega = J \frac{d\Omega}{dt} \quad \text{(II.61)}$$

## II.9 Centrifugal Pump Performance and Characteristics

### II-9.1 Definition

A centrifugal pump is a dynamic turbomachine designed to transport fluids by converting rotational kinetic energy, typically from an electric motor or engine, into hydrodynamic energy. The fluid enters the pump casing axially along the rotating shaft, is accelerated radially outward by the vanes of the rapidly spinning impeller, and exits through a volute casing where its high velocity is efficiently converted into static pressure.

Figure II-21 shows the cross-sectional view of the primary mechanical and hydraulic components of a centrifugal pump.

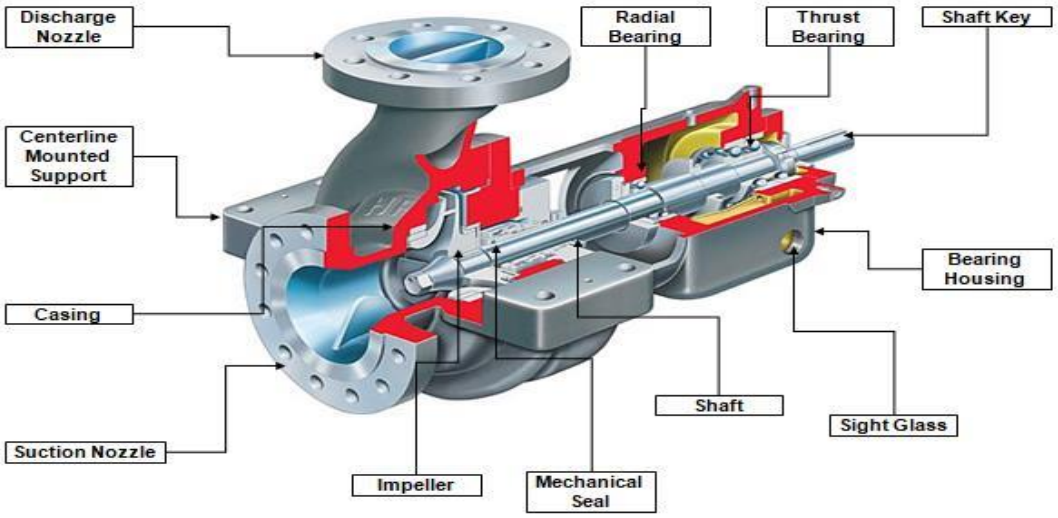


Figure II-21: Centrifugal pump components [Ben23]

The essential parameters and operating curves that dictate the hydraulic behavior, energy transfer, and overall efficiency of a centrifugal pump are:

### II.9.2 Flow Rate (Q)

The flow rate is the volume of fluid pumped per unit time.

$$Q = \frac{V}{t} \tag{II.62}$$

Where: Q is the volumetric flow rate ($m^3/s$). V is the total volume of fluid ($m^3$). *t* is the pumping duration (s).

### II.9.3 Head (H)

The head is the height that the pump can lift the fluid. It represents the pressure increase across the pump, expressed in meters of fluid column.

$$H = \frac{P_{out} - P_{in}}{\rho g} \tag{II.63}$$

where:

$P_{out}$: Discharge pressure (Pa),
$P_{in}$: Suction pressure (Pa),
$\rho$: Fluid density ($kg/m^3$) - for water,
$\rho = 1000\ kg/m^3$,
$g$: Gravitational acceleration (9.81 $m/s^2$)

Table II-2 shows the types of head [Zhi25]:

Table II -2Types of head

| Type | Description |
|---|---|
| **Static Head** | Vertical height the fluid must be lifted |
| **Friction Head** | Loss due to pipe friction |
| **Total Head** | Static + Friction + Pressure head |

The operation of a centrifugal pump involves three parameters: head, flow rate, and speed, which are related by the following equation [Pet08]

$$f(H, Q, \omega) = 0 \tag{II.64}$$

To solve this system of equations, we treat one of the three parameters like a constant; generally, it is the speed that is constant.

The total head is the sum of static head and dynamic head.

$$H = H_S + H_D \tag{II.65}$$

Where:

H: Total head.

$H_S$: Static head, which is the distance between the static water level in the well and the highest point to which the water must be pumped.

$H_D$: The sum of linear and specific losses.

### II.9.4 Performance Curves

Pump performance is described using three main curves provided by the manufacturer [Zhi25].

#### II.9.4.1 The pump's flow-head Q(H) characteristic:

The relationship between the head H and the pump flow rate Q is given by the "PELEIDER PETERMANN" model as: [Seg20]

$$H = a_0\omega^2 - a_1\omega Q - a_2 Q^2 \tag{II.66}$$

Where: $a_0$, $a_1$, and $a_2$ are constants for the pump specified by the manufacturer.

The figure below illustrates the flow-head characteristic curve of the centrifugal pump:

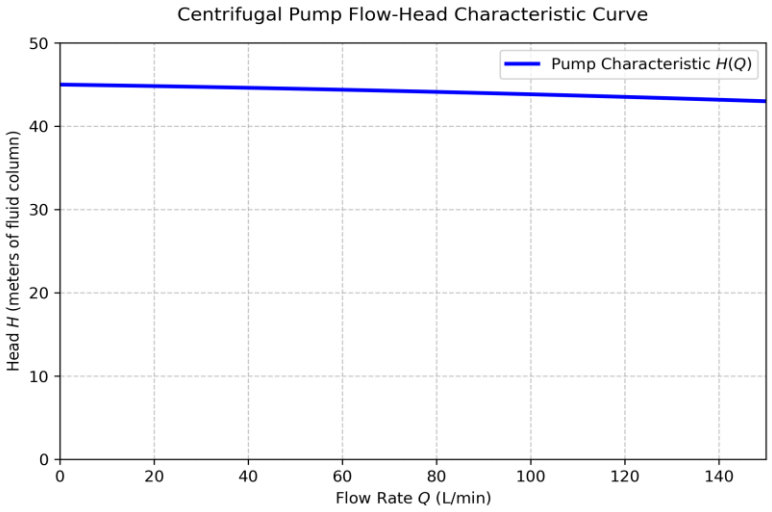


Figure II-22: Pump characteristic curve H(Q)

### II.9.4.2 Efficiency-Flow Curve ($\eta$-Q)

The $\eta$-Q curve shows how efficiency varies with flow rate (Fig. II-23).

- Efficiency is zero at shut-off (Q = 0)
- Efficiency peaks at the BEP
- Efficiency decreases at high flow rates

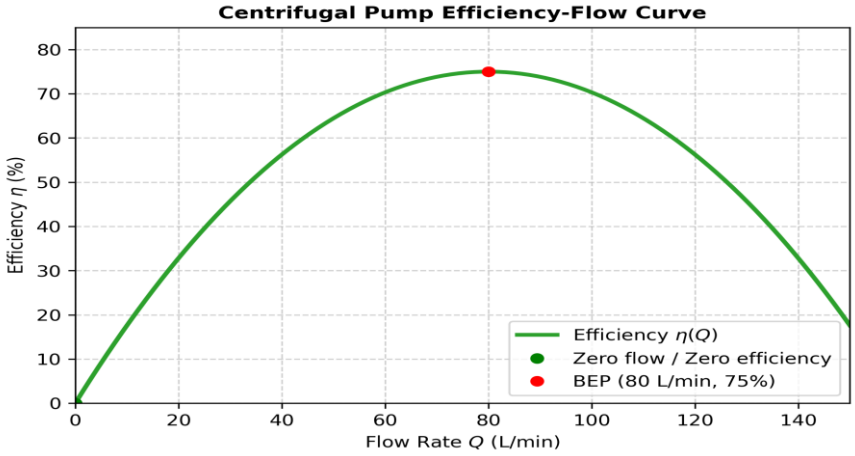


Figure II-23: Pump Efficiency

### II.9.4.3 Power-Flow Curve (P-Q)

The P-Q curve shows how power consumption increases with flow rate (Fig. II-24).

- Power is minimum at shut-off
- Power increases with flow
- Maximum power at run-out point

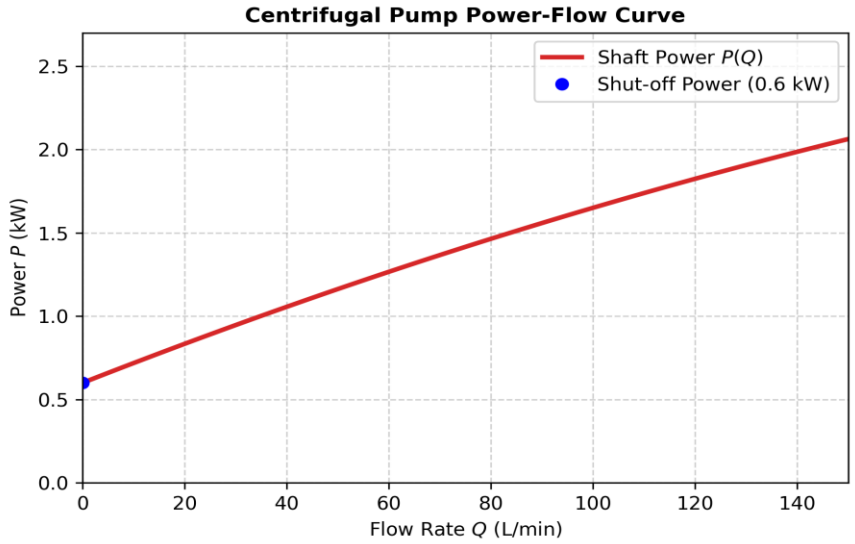


Figure II-24: Pump Shaft Power curve

### II.9.5 Power calculation:

A centrifugal pump is a machine that transfers energy to a fluid in order to move it from one point to another point. The general expression for hydraulic power is given as follows:

$$P_H = \rho g Q H \tag{II.67}$$

the power required for its mechanical drive, which is expressed by the following equation:

$$P_M = \frac{\rho g Q H}{\eta_P} \tag{II.68}$$

Where:

$\eta_p$: The pump's efficiency.

$P_M$: The motor's mechanical power.

### II.9.6 The pump's torque-speed characteristic (ω):

The centrifugal pump is primarily characterized by a resistant torque that takes the following form:

$$T_R = k_p \omega^2 \tag{II.69}$$

where: $k_p$: is a constant specific to the geometric and design characteristics of the pump.

### II.9.7 efficiency calculation:

For pump-motor units, manufacturers generally provide the overall efficiency with the following equation:

$$\eta_{mp} = \frac{P_H}{P_M} \tag{II.70}$$

## II.10 Conclusion

This chapter presented a comprehensive model for the simulation of a standalone photovoltaic (PV) pumping system, analyzing each stage of energy conversion. First, the PV generator was modeled alongside a Boost chopper to optimize power extraction. Two classic algorithms for maximum power point tracking under varying solar irradiance conditions, namely Perturb and Observe (P&O) and Incremental Conductance (INC), were detailed. Furthermore, emphasis was placed on the electromechanical drive system by coupling a three-phase inverter to a permanent magnet synchronous motor (PMSM) managed by a Direct Torque Control (DTC) strategy. Finally, a brief overview of the centrifugal pump characteristics was provided

# Chapter III

Simulation of PSA-based MPPT for a solar PV water pumping system

## III.1 Introduction

Traditional MPPT algorithms, including Perturb and Observe (P&O) and Incremental Conductance (INC), are widely used because of their simplicity and low implementation cost. However, these methods often suffer from limitations such as oscillations around the MPP, slow convergence speed, and reduced tracking accuracy under rapidly changing atmospheric conditions. To overcome these drawbacks, modern optimization-based techniques inspired by natural and mathematical phenomena have gained increasing attention in recent years. Among these advanced methods, the Projectile Search Algorithm (PSA) represents a promising optimization strategy due to its strong exploration capability, fast convergence behavior, and adaptability to nonlinear optimization problems. This chapter presents the design and implementation of an MPPT control strategy based on the Projectile Search Algorithm (PSA). It provides a detailed simulation study of the PSA-based MPPT and compares its performance with the Perturb and Observe (P&O) method under various shading patterns for a solar water pumping system. Evaluate the impact on electrical, mechanical and hydraulic variables: pump power, torque, stator currents $I_{abc}$, rotor speed, pump head and flow rate Q, plus performance metrics (Tracking Response Time, Total Harmonic Distortion of the stator current THD, Steady-State Power RMSE, Electromagnetic Torque Ripple System Efficiencies, Average Centrifugal Pump Power.

## III.2 Projectile model:

The projectile is defined to be launched from a ground level (h = 0), with an initial velocity v, and at an angle of inclination θ measured with respect to the horizontal as shown in Figure III-1. The path function of the projectile (y) as a function of horizontal distance (x) is specified as follows: [Hie19]

$$y(x) = x\,tan(\theta) - \frac{g.x^2}{2v^2}sec^2(\theta) \qquad \text{(III.1)}$$

where: g = 9.81 m/s$^2$

As illustrated in Figure III-2, the geometry and dimensions of flight paths are governed by the launch angles relative to the horizontal, assuming a constant initial velocity *v*.

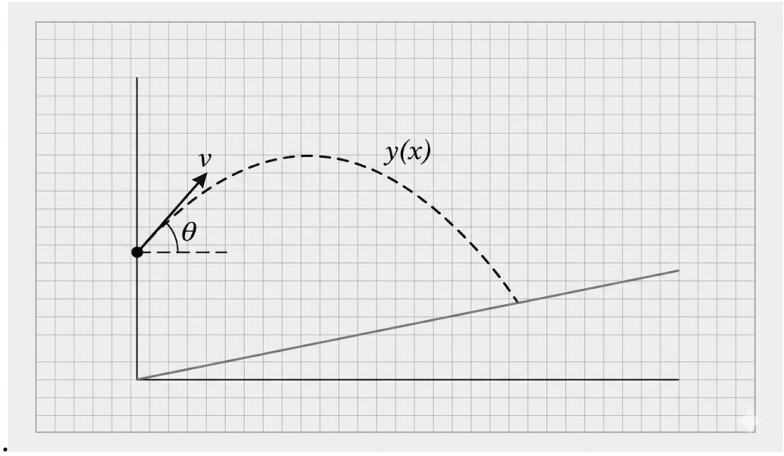


Figure III-1: The projectile moving path

Collectively, these flight paths are bounded by a limiting curve known as the trajectory envelope. Mathematically, this envelope $\varphi$ defines the boundary path that encloses and intersects every individual projectile function ψ [Hie19]

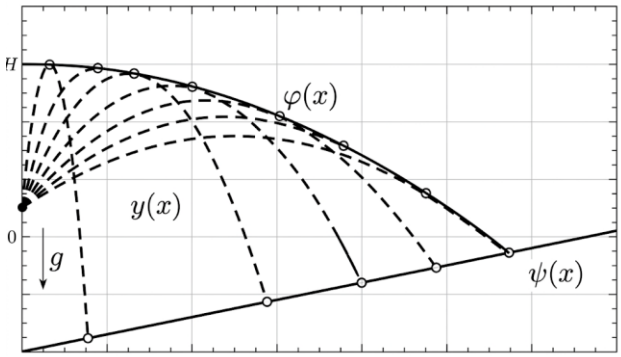


Figure III-2: The enveloping parabola path

The equation for the envelope of projectile trajectory [Hie19] is determined by:

$$\varphi(x) = \frac{v^2}{2g} - \frac{g}{2v^2}x^2 \tag{III.2}$$

For a continuous impact function $\psi(x)$ on $0 \leq x < \infty$ with $\psi(0) = 0$, the surface of $\psi$ and the path of $\varphi$ have exactly one point of intersection. It is noted that there exists a unique target for which $\psi(x) = \varphi(x)$. The main goal of the proposed PTS algorithm is to minimize the difference between ψ and φ in order to ensure a projectile reach the target precisely. A function $\gamma(x)$ is then implemented to search the target on the impact surface and it is given by: [Hie19]

$$\gamma(x) = \psi(x) - \varphi(x) \tag{III.3}$$

**III.3 Modeling of Projectile search algorithm PSA** [Hus25]

Inspired by the motion principles of projectiles in physics, the PSA employs trajectory-based search mechanisms to identify optimal solutions efficiently. When integrated into MPPT control, this algorithm can enhance the tracking performance of photovoltaic systems by reducing steady-state oscillations and improving response under partial shading and dynamic environmental conditions.

The PSA technique starts with the population size (Np), number of variables (D), lower limit ($X_{min}$) upper limit ($X_{max}$), and maximum iteration $T_{max}$ [Hus25]. The variables lower and upper boundaries are stated in equation (4) as:

$$X_{minj} = [X_{min1}X_{min2} \dots X_{minD}],\ X_{maxj} = [X_{max1}X_{max2} \dots X_{maxD}] \tag{III.4}$$

To create the initial population of projectiles as potential solutions, random values $\boldsymbol{rand_j}$ from the range [0, 1] are assigned to each border as follows in equation (III.5):

$$X_{i,j}^{I=1} = X_{minj} + rand_j, \left(X_{maxj} - X_{minj}\right),\ i = 1,2,\dots,N\ ;\ j = 1,2,\dots,D \tag{III.5}$$

The target population is formed at random by disturbing one randomly selected projectile with the differential between the other two randomly selected projectiles. The intended population is produced by using equation (III.6).

$$t_{k,j}{}^{(I)} = X_{a1,j}{}^{(I)} + 0.5\left(X_{a2,j}{}^{(I)} - X_{a3,j}{}^{(I)}\right), k = 1,2,\ldots,N\ ;\ j = 1,2,\ldots,D \quad \text{(III.6)}$$

where: the indices such as $a_1$, $a_2$, and $a_3$ belongs to {1, 2, ..., N} randomly selected numbers that must be distinct from one another and from the base index. Using (III.7) and (III.8), the following criteria are used to evaluate the targets and projectiles fitness values [Hus25]:

$$f_i{}^{(I)} = f\left(x_{i,j}{}^{(I)}\right) \quad \text{(III.7)}$$

$$f_k{}^{(I)} = f\left(t_{k,j}{}^{(I)}\right) \quad \text{(III.8)}$$

Then, by contrasting the fitness values of each $X_{i,j}{}^{(I)}$ and $t_{k,j}{}^{(I)}$, the best projectile $X_{best}{}^{(I)}$ and its best value $f_{best}{}^{(I)}$ are chosen using equation (III.9) and (III.10) logic:

$$X_{bestj}{}^{(I)} = \begin{cases} X_{i,j}{}^{(I)} \ \ if\ min\left(f\left(X_{i,j}^{(I)}\right)\right) \le min\left(f\left(t_{k,j}^{(I)}\right)\right) \\ t_{k,j}{}^{(I)}\ otherwise \end{cases} \quad \text{(III.9)}$$

$$f_{best}{}^{(I)} = f\left(X_{bestj}{}^{(I)}\right) \quad \text{(III.10)}$$

where $I$ is the succeeding generation produced by each iteration and consists of 1, 2,..., $I_{max}$. Iterating the projectile until it has the greatest fitness value is the primary PSA optimization method. The following equation (III.11) and (III.12) describes the projectile search paradigm for focusing on the target [Hus25]

$$for\ i\ =\ 1:\ N$$
$$for\ j\ =\ 1:\ D$$
$$If\ rand\ <\ 0.5$$
$$X_{i,j}{}^{(I+1)} = X_{best1,j}{}^{(I)} - \alpha\left(\frac{\gamma\left(d_{i,j}{}^{(I)}\right)}{\acute{\gamma}\left(d_{i,j}{}^{(I)}\right)}\right) \quad \text{(III.11)}$$
$$else$$
$$X_{i,j}{}^{(I+1)} = X_{i,1}{}^{(I)} - \alpha\left(\frac{\gamma\left(d_{i,j}{}^{(I)}\right)}{\acute{\gamma}\left(d_{i,j}{}^{(I)}\right)}\right) \quad \text{(III.12)}$$
$$end$$
$$end$$
$$end$$

With a slope of $m$ and a linear shape, the impact function in PSA optimization is represented by a hill in equation (III.13). The function of impact is:

$$\psi(X) = m.X \quad \text{(III.13)}$$

Given the function of impact specification [Bac02], the function(X) might be defined as shown in equation (III.14) and (III.15):

$$\gamma(X) = m.X - \frac{v^2}{2g} + \frac{g}{2v^2}x^2 \tag{III.14}$$

$$\left(\frac{\gamma\left(d_{i,j}{}^{(I)}\right)}{\dot{\gamma}\left(d_{i,j}{}^{(I)}\right)}\right) = \left(\frac{m.d_{i,j}{}^{(I)} - \frac{v^2}{2g} + \frac{g}{2v^2}.\left(d_{i,j}{}^{(I)}\right)^2}{m + \frac{g}{v^2}.d_{i,j}{}^{(I)}}\right) \tag{III.15}$$

At the present iteration, the equation (III.16) formula is used to determine the distance between projectile and target [Hus25]

$$d_{i,j}{}^{(I)} = \left[abs\left(\left(t_{i,j}{}^{(I)}\right)^r - \left(X_{i,j}{}^{(I)}\right)^r\right)\right]^{1/s} \tag{III.16}$$

The parameters *r* and *s*, where (*r*, *s*) > 0, are used to adjust the distance (*d*). The definition of another control parameter for (III.11) and (III.12) is shown below in equation (III.17).

$$\alpha = p^q, p = \left(1 - \frac{I}{I_{max}}\right), q > 0 \tag{III.17}$$

Here, the new target population is additionally built as $t_{k,j}^{(I+1)}$. The ideal projectile for the next iteration is calculated by using equations (18) and (19).

$$X_{bestj}{}^{(I+1)} = \begin{cases} X_{i,j}{}^{(I+1)} \ \ if\ min\left(f\left(X_{i,j}^{(I+1)}\right)\right) \le min\left(f\left(t_{k,j}^{(I+1)}\right)\right) \\ t_{k,j}{}^{(I+1)}\ otherwise \end{cases} \tag{III.18}$$

$$f_{best}{}^{(I+1)} = f\left(X_{bestj}{}^{(I+1)}\right) \tag{III.19}$$

Until $f_{best}{}^{(I+1)}$ achieves the necessary accuracy level (ε) or the iteration reaches $I_{max}$, the operations are repeated, with the end outcome being ($X_{bestj}{}^{(I+1)}$) as the pleased projectile touching down on the target [Hus25].

## III.4 Simulation of solar water pumping system based on PSA-MPPT control

### III.4.1 Description of the Simulink Model

The developed Simulink model represents a standalone photovoltaic water pumping system controlled by a Maximum Power Point Tracking strategy (PSA-MPPT). The purpose of the system is to ensure efficient conversion of solar energy into hydraulic energy for water pumping applications. The photovoltaic array is the primary energy source of the system. It converts solar irradiation into DC electrical power. Its output characteristics are influenced by solar irradiance and temperature variations, which affect both the generated voltage and current.
To maximize the extracted energy, the PV voltage and current are measured continuously and used as inputs for the PSA-MPPT controller. The controller calculates the optimal operating point of the photovoltaic generator used projectile search algorithm and produces the control signal required for converter switching (Duty cycle).

The generated command is applied to a boost DC–DC converter. This converter increases and regulates the DC voltage supplied by the photovoltaic array. It also ensures impedance adaptation between the PV generator and the load, which improves energy transfer efficiency. The output of the converter supplies the motor-pump subsystem via a three-phase inverter that converts the DC voltage Vdc into AC voltage. The electric motor converts electrical power into mechanical rotation, which drives the centrifugal pump. The pump then transforms mechanical power into hydraulic power for water transport.
The model also includes measurement and monitoring blocks used to evaluate the system behavior under variable operating conditions. Parameters such as PV voltage, PV current, output power, motor speed, torque, flow rate, and hydraulic head are observed during simulation. The simulation results allow analysis of both the electrical and hydraulic performance of the installation, as well as the effectiveness of the MPPT strategy under changing environmental conditions.

Figure III-3 shows the block diagram of the proposed PSA-MPPT control for a solar PV water pumping system.

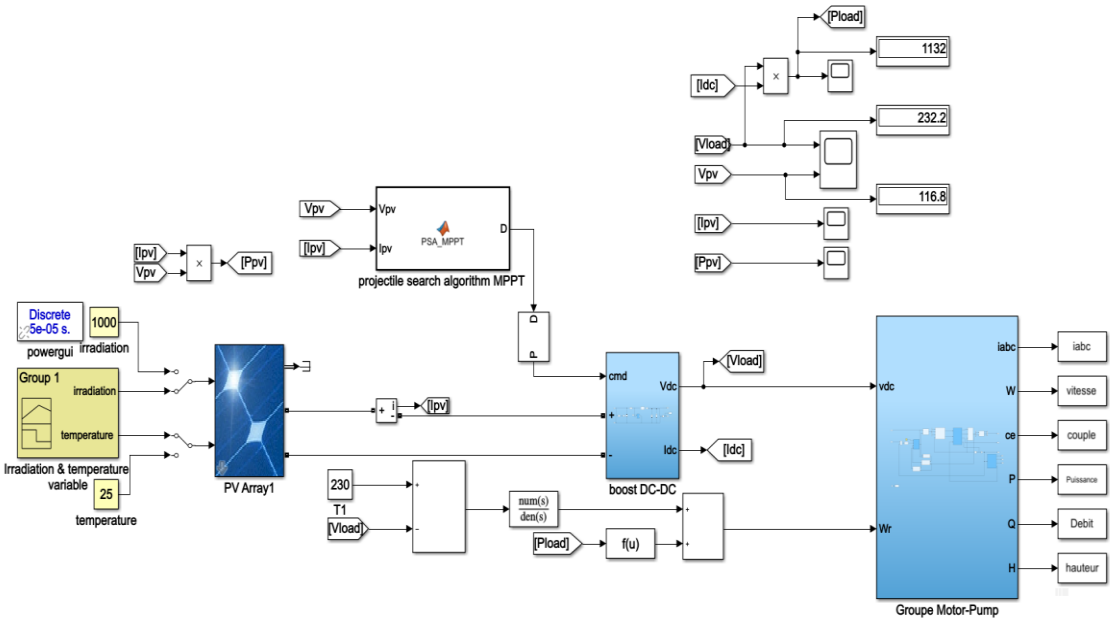


Figure III-3: Model of a solar pumping system based on projectile search algorithm-MPPT on MATLAB-Simulink

### III.4.2 Parameters of Photovoltaic Panel and Boost Converter used in Simulation

In this model, the BP Solar SX3190 photovoltaic panel is utilized, configured with four modules connected in series and two in parallel. The parameters of this panel are indicated in Table III-1.

Table III -1: Technical Specifications of BP Solar SX3190 Solar Panel

| Parameter | Value | Unit |
|---|---|---|
| **Maximum Power ($P_{max}$)** | 190.2567 | W |
| **Number of Cells ($N_{cell}$)** | 50 | |
| **Open-Circuit Voltage ($V_{oc}$)** | 30.6021 | V |
| **Short-Circuit Current ($I_{sc}$)** | 8.5103 | A |
| **Voltage at Maximum Power ($V_{mp}$)** | 24.3003 | V |
| **Current at Maximum Power ($I_{mp}$)** | 7.8294 | A |

The Boost converter was employed to increase the photovoltaic system's output voltage. A switching frequency of 10,000 Hz was chosen for this model. The key parameters of the Boost converter are listed in the table below.

Table III -2: Technical Parameters of the Boost Converter Implemented

| Component | Value | Unit |
|---|---|---|
| **Inductor (L)** | 4.15 | mH |
| **Capacitor (Cout)** | 1150 | µF |
| **DC link (Cin)** | 470 | µF |
| **Load Resistance (Rload)** | 100 | Ω |

Table III-3 illustrates the Projectile search algorithm parameters used for PSA-MPPT control.

### III.4.3 Analysis of environmental impacts

Environmental factors such as partial shading, rapid irradiance fluctuations, and temperature-induced non-linearities present significant challenges to the photovoltaic system.

#### III.4.3.1 Partial Shading

Under partial shading conditions, classical MPPT algorithms like P&O and Incremental Conductance (IncCond) are prone to track local maxima, resulting in significant power loss. In contrast, global optimization techniques such as PSA, PSO, GA, and hybrid fuzzy-PSO methods have been shown in literature to successfully identify the global peak, thereby improving energy yield in shaded environments [Gua25] Partial shading occurs when the entire array does not receive uniform isolation. An example of this is shown in Figure III-4 .

Table III -3: Technical Parameters of the Projectile search algorithm

| Parameter | Value | Description | Effect on Performance |
|---|---|---|---|
| **Population Size (N)** | 3 projectiles | Number of search agents exploring the duty-cycle space. | Larger population improves exploration but increases computation time. |
| **Search Space Lower Bound ($X_{min}$)** | 0.05 | Minimum duty cycle allowed. | Prevents operation in invalid regions. |
| **Search Space Upper Bound ($X_{max}$)** | 0.85 | Maximum duty cycle allowed. | Limits the search to feasible operating points. |
| **Maximum Iterations ($I_{max}$)** | 12 | Maximum number of PSA iterations before convergence. | Controls convergence speed and computational effort. |
| **Projectile Mass (m)** | 0.25 | Represents the projectile mass in the ballistic motion model. | Influences the exploration step size. |
| **Initial Velocity (v)** | 3.5 | Initial projectile velocity. | Higher values increase exploration capability. |
| **Gravity Constant (g)** | 9.81 | Gravitational acceleration used in trajectory calculations. | Determines the projectile trajectory shape. |
| **Distance Exponent (r)** | 1.0 | Controls distance calculation between current and target positions. | Affects search dynamics. |
| **Convergence Factor (q)** | 5.0 | Controls the decay rate of the exploration coefficient α. | Higher values promote faster convergence. |



Figure III-4: Partially shaded Solar panel [Fin13]

Figures III-5 and II-6 show the P–V and I-V characteristics of a partially shaded solar array under different shadow patterns. Local maximum points can be seen clearly in the power-versus-voltage graph. These peaks occur due to sudden drops in current on the current-versus-voltage graph. These local maximum power points result directly from partial shading and do not represent the absolute Global Maximum Power Point (GMPP). The global peak is the correct maximum power point that tracking systems must locate and maintain. [Fin13]

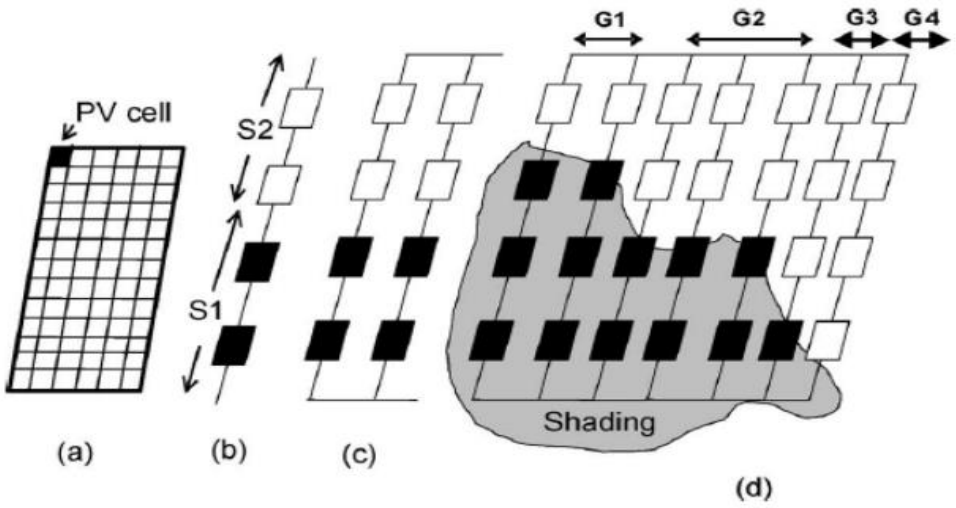


Figure III-5: Partial shading of a PV module [Fin13]

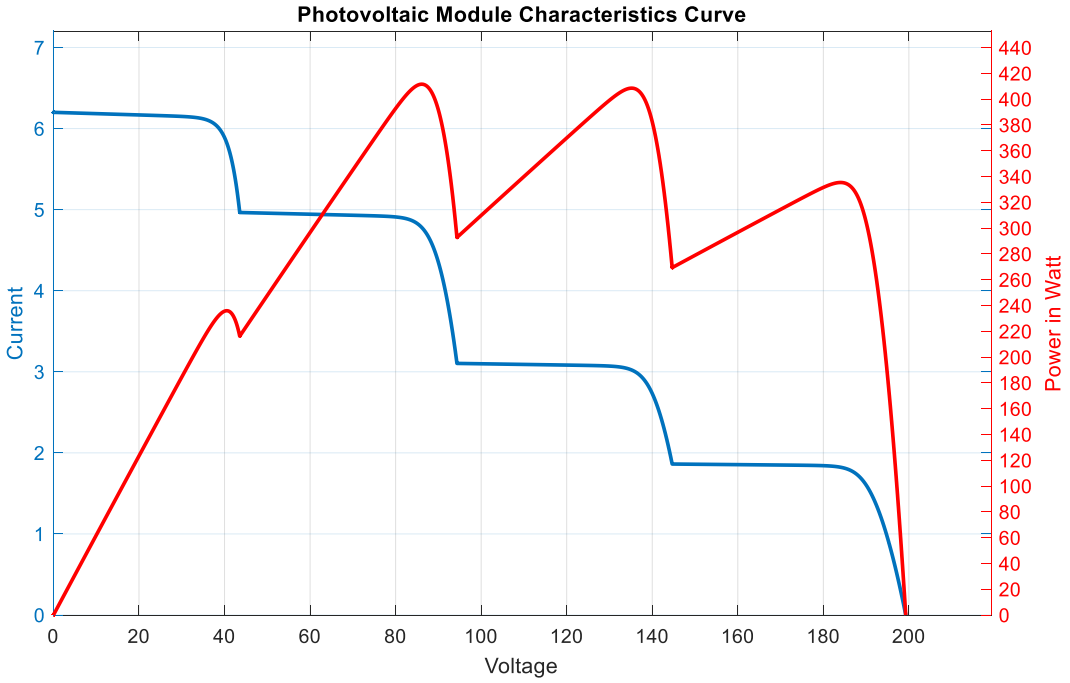


Figure III-6: P–V & I-V Characteristics Under different partial shadow patterns

### III.4.3.2 Rapid irradiance fluctuation

During fast-changing solar irradiance, especially in cloudy or transient conditions, intelligent controllers such as ANN and reinforcement learning models outperform traditional techniques. These methods offer quicker dynamic response and smoother power tracking by learning system behavior and adapting in real-time. [Gua25]

### III.4.3.3 Temperature-induced non-linearities

Temperature variations induce nonlinear shifts in PV output characteristics. Adaptive techniques such as fuzzy logic controllers and MPC-based MPPT adjust their rule bases or prediction models accordingly to maintain optimal performance. Their robustness under thermal nonlinearity makes them suitable for outdoor and high-temperature applications. [Gua25]

### III.4.4 Performance indicators

The performance of the proposed PSA-MPPT solar pumping system is evaluated based on the following six performance indicators:

- Tracking Response Time (s)
- Total Harmonic Distortion of the stator current THD (%)
- Steady-State Power RMSE (W)
- Electromagnetic Torque Ripple $\sigma_{Ce}$ (N.m)
- System Efficiency $\eta_{system}$ (%)
- Average Centrifugal Pump Power $P_p$ (W)

### III.4.4.1 Tracking Response Time

In a solar water pumping system, the MPPT Tracking Response Time defines how quickly the system's controller detects and adjusts to changing environmental conditions (like passing clouds or shifting sun angles) to continuously pull maximum power from the PV array and drive the pump at peak efficiency [Loz25]

### III.4.4.2 Electromagnetic Torque Ripple $\sigma_{Te}$

the torque ripple, including cogging torque, is calculated from peak-to-peak electromagnetic torque. The percentage of torque ripple is calculated using the following formula:

$$\sigma_{Te} = \frac{T_{pp}}{T_{av}} \times 100\% = \frac{T_{max} - T_{min}}{T_{av}} \times 100\% \qquad \text{(III.20)}$$

Where $T_{pp}$, $T_{max}$, $T_{min}$, $T_{av}$ are peak to peak torque, maximum torque, minimum torque, and average torque, respectively. [Bde21]

### III.4.4.3 Total Harmonic Distortion THD (%)

Total Harmonic Distortion (THD) is a measure of the level of harmonic distortion in electrical power systems, expressed as a function of frequency. This expression allows for the calculation of the influence of harmonics on the current/voltage waveform.

$$(THD)_{\%} = 100 \times \frac{\sqrt{\sum_{i=2}^{n} x_i^2}}{x_1} \quad \text{(III.21)}$$

$x_i$: the RMS values of the various harmonics of the current and voltage.
$x_1$: the value of the current and voltage.

### III.4.4.4 Steady-State Power RMSE

The RMSE is defined with the following equation:

$$\text{RMSE} = \sqrt{\frac{1}{n}\sum_{i=1}^{n}(X_i - Y_i)^2)} \quad \text{(III.22)}$$

The RMSE for a solar pumping system's steady-state power is calculated as:

$$\text{RMSE} = \sqrt{\frac{1}{n}\sum_{i=1}^{n}\left(P_{\text{pred},i} - P_{\text{meas},i}\right)^2)} \quad \text{(III.23)}$$

### III.4.4.5 System Efficiency

The global efficiency of the proposed solar pumping system, denoted as $\eta_{system}$, is defined as the ratio of the useful hydraulic power delivered by the pump to the total solar power incident on the photovoltaic array. It is mathematically expressed as follows:

$$\eta_{system}(\%) = \left(\frac{P_{hyd}}{P_{sun}}\right) \times 100 \quad \text{(III.24)}$$

Where $P_{hyd}$ represents the hydraulic power (W) and $P_{sun}$ is the incident solar power (W). The hydraulic power depends on the fluid properties and pumping head, given by:

$$P_{hyd} = \rho \cdot g \cdot Q \cdot H \quad \text{(III.25)}$$

Where $\rho$ is the water density (Kg/m$^3$), g is the acceleration due to gravity (m/s$^2$), Q is the volumetric flow rate (m$^3$/s), and H is the total manometric head (m).

The total solar power received by the photovoltaic array is determined by:

$$P_{sun} = G \cdot A \quad \text{(III.26)}$$

Where G is the solar irradiance (W/m$^2$) and A is the total surface area of the PV array (m$^2$).

Alternatively, considering the cascaded stages of energy conversion within the PSA-MPPT system, the global efficiency can be expressed as the product of the individual efficiencies of each component:

$$\eta_{system} = \eta_{pv} \cdot \eta_{mppt} \cdot \eta_{motor} \cdot \eta_{pump} \quad \text{(III.27)}$$

where $\eta_{pv}$, $\eta_{mppt}$, $\eta_{motor}$, $\eta_{pump}$ represent the efficiencies of the PV array, the MPPT-controlled converter, the electric motor, and the centrifugal pump, respectively.

## III.5 Simulation Results and Discussion

### III.5.1 Simulation Environment and Scenarios

To evaluate the performance of the PSA-based MPPT under shading conditions, its results are compared with the conventional Perturb and Observe (P&O) optimization method. The simulations are carried out under the MATLAB/Simulink environment using the parameters of the PSA-MPPT listed in Table 3 for a total simulation time of $t$ = 3s. To thoroughly assess the PSA-MPPT controller, the following joint irradiance-temperature scenario as shown on Figure III-7: is applied.

The irradiation and temperature profiles used to evaluate the MPPT controller. The solar irradiance varies from 1000 W/m² to 700 W/m², then to 500 W/m², before increasing to 800 W/m² and finally returning to 1000 W/m². Simultaneously, the cell temperature is maintained at 25°C during the first second, increased to 35°C between 1 s and 2.5 s, and then restored to 25°C.

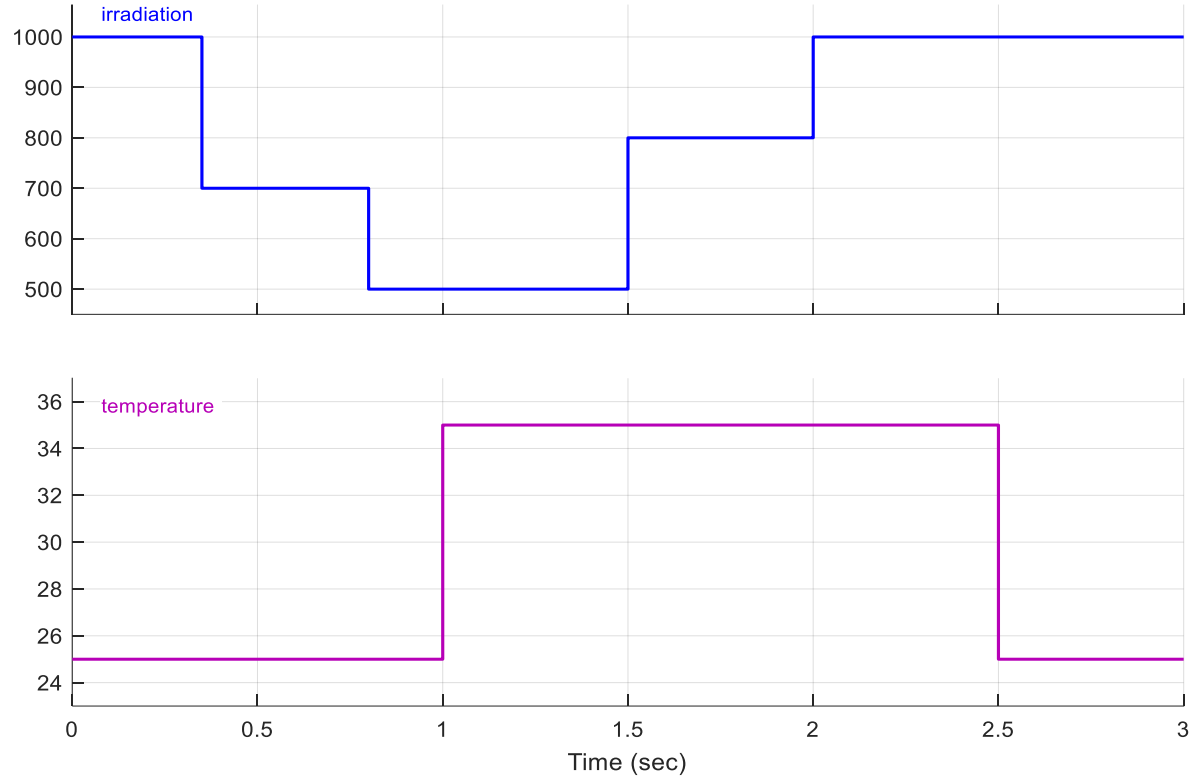


Figure III-7: The irradiation and temperature profiles used in simulation

- **Electromagnetic torque and rotor speed**

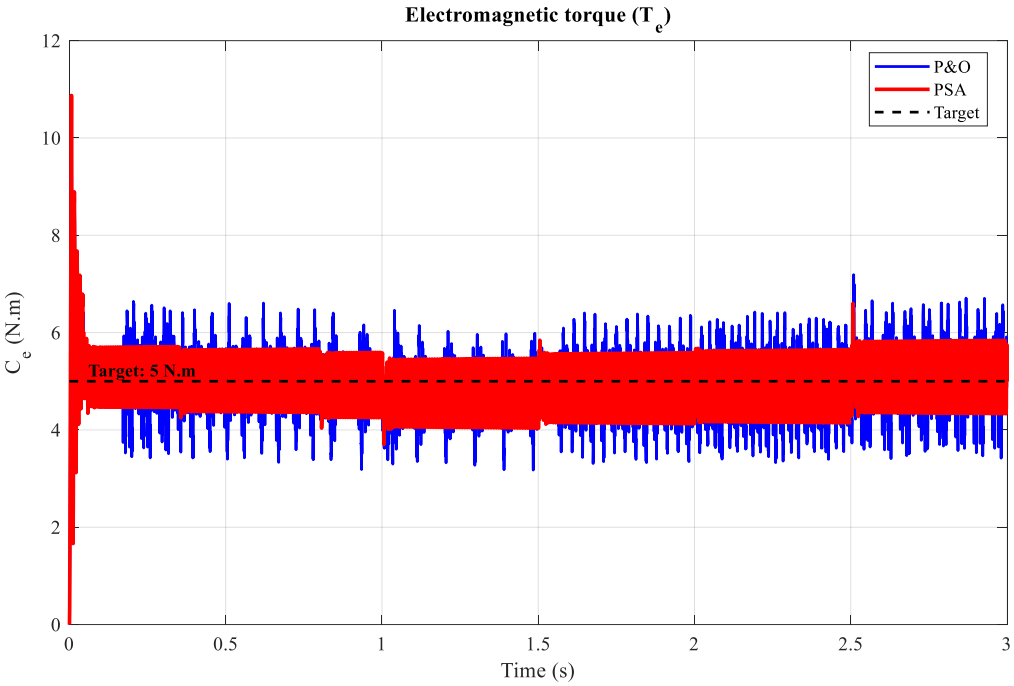


Figure III-8: Electromagnetic torque responses using P&O and PSA techniques.

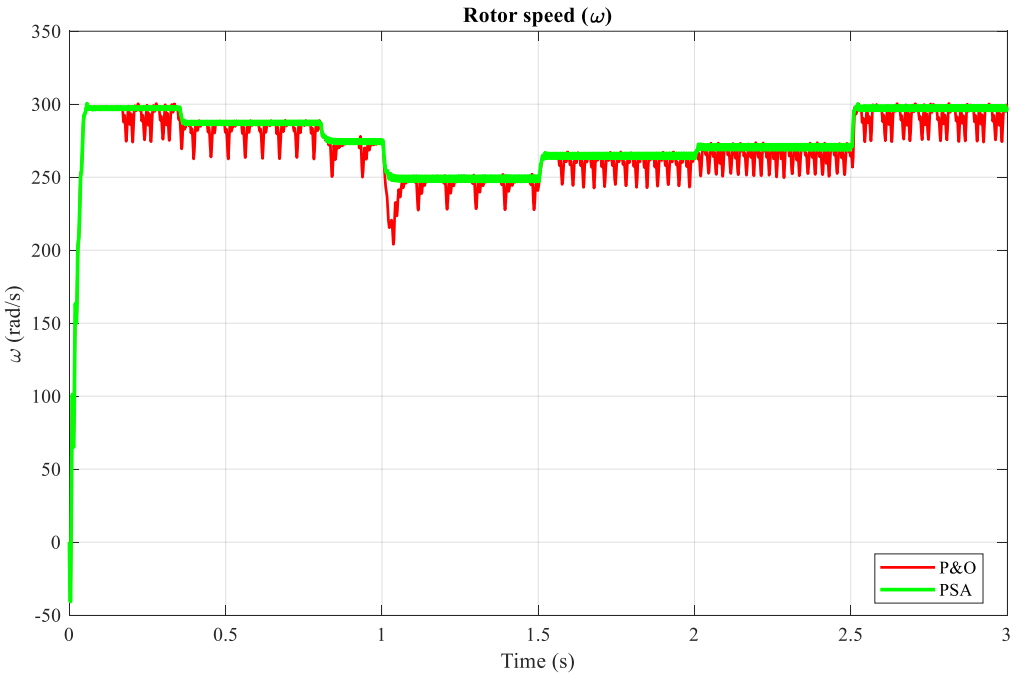


Figure III-9: Rotor speed responses using P&O and PSA techniques

- **Stator currents $I_{abc}$**

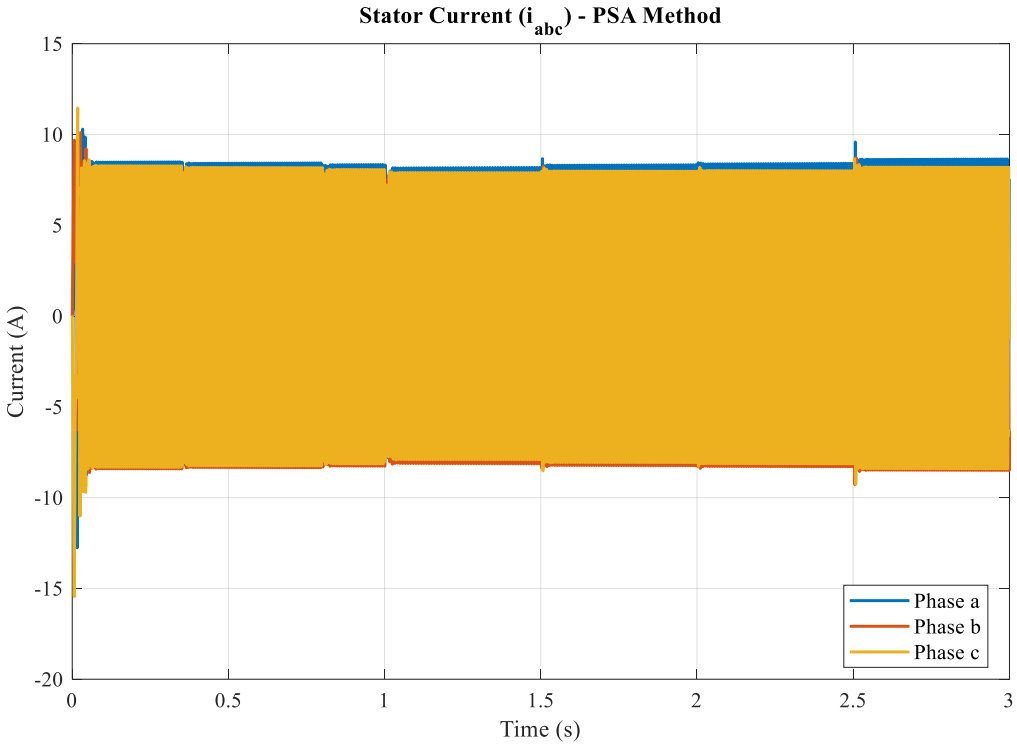


(1)

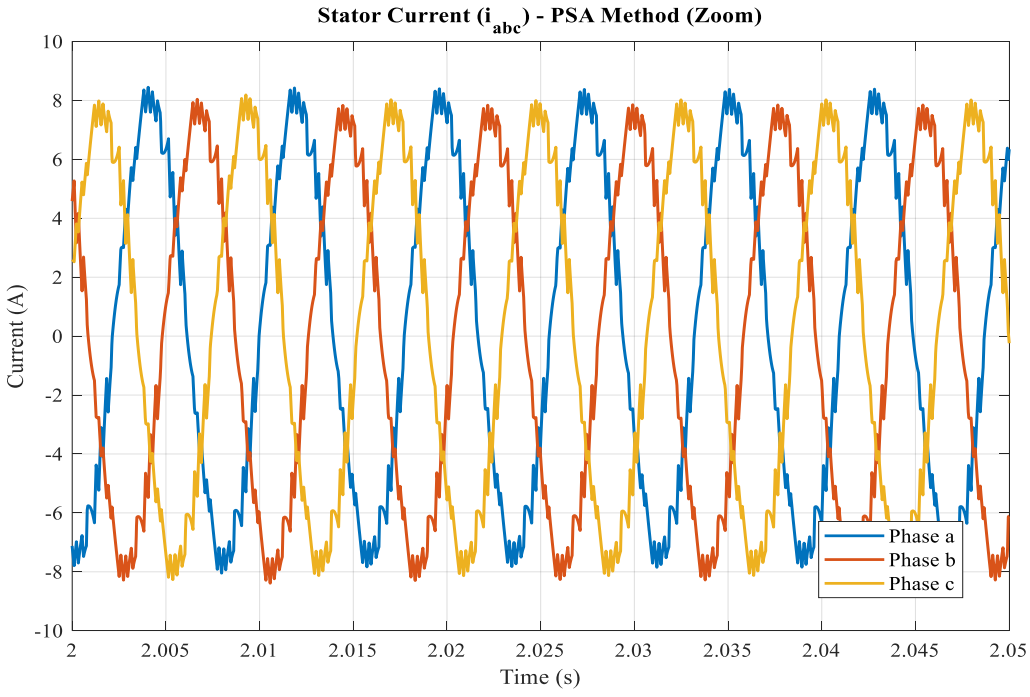


(2)

Figure III-10: (1) Stator currents $I_{abc}$ response using PSA method (2) Zoomed Output current.

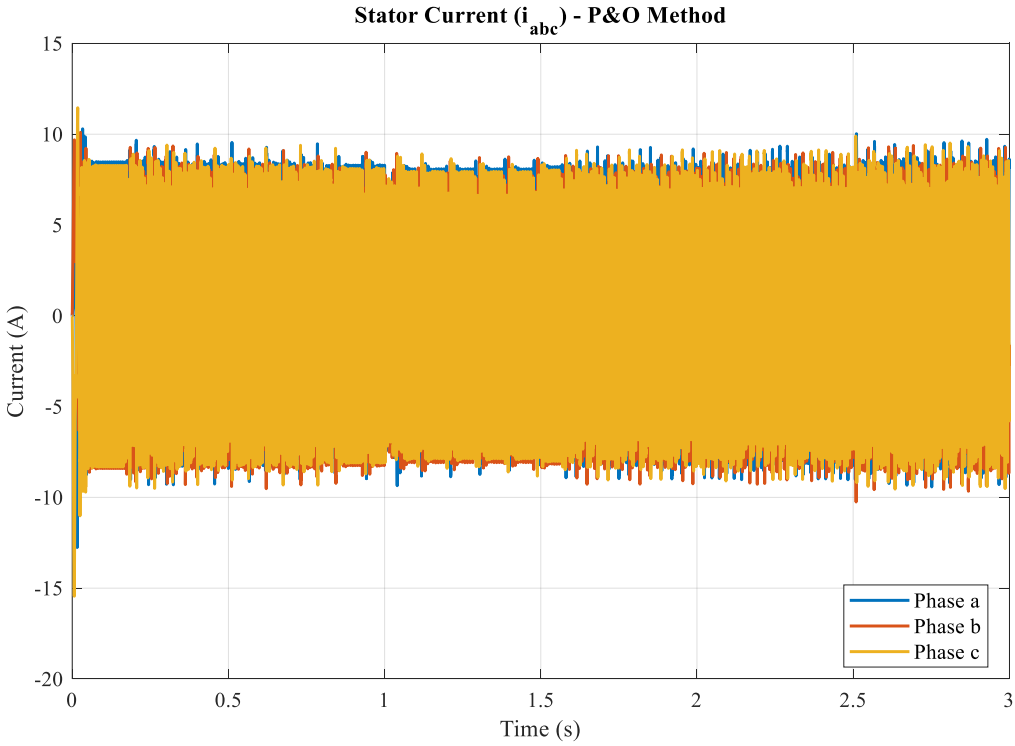


(1)

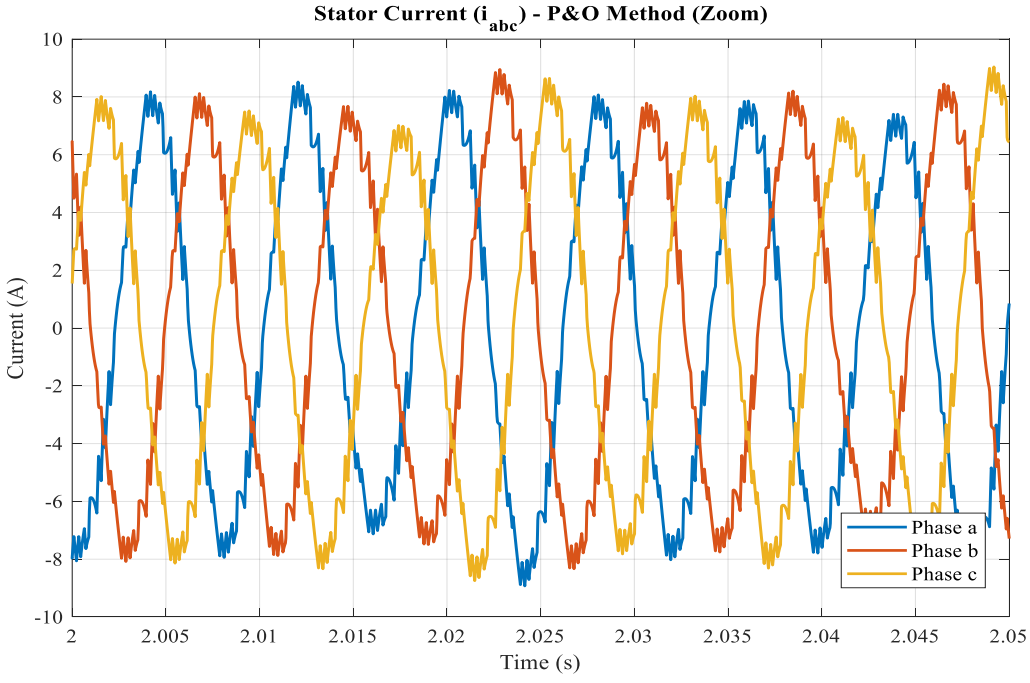


(2)

Figure III-11: (1) Stator currents $I_{abc}$ response using P&O method (2) Zoomed Output current.

- **Pump Head (H), Volumetric Flow Rate (Q), and Power (P)**

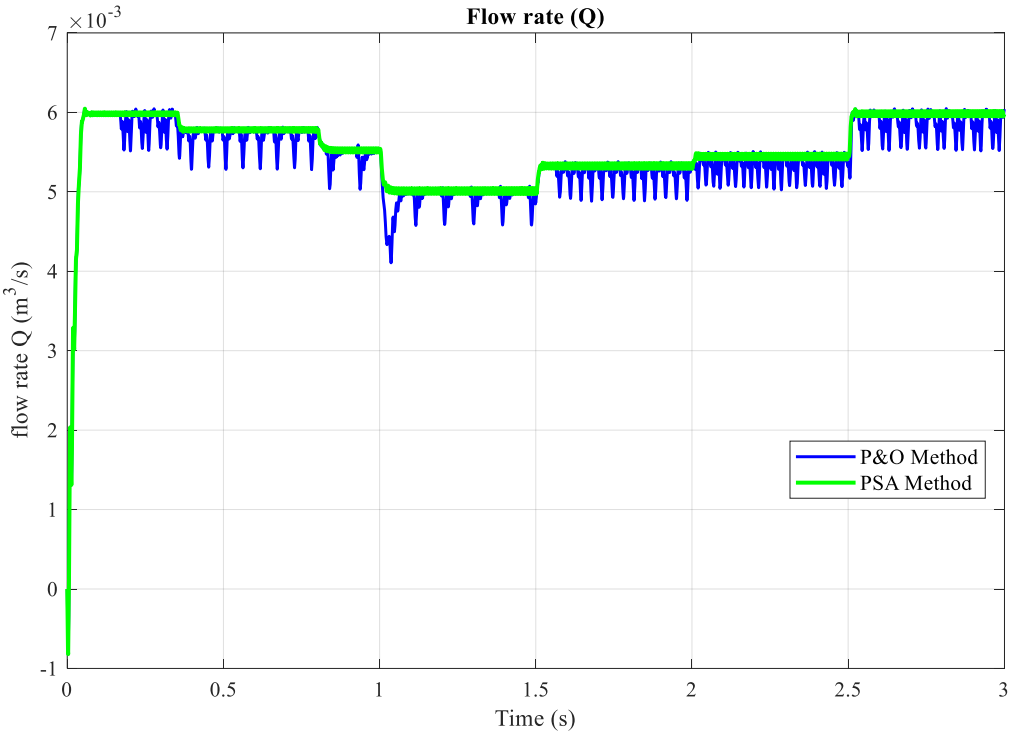


Figure III-12: Pump flow rate Q responses using P&O and PSA techniques

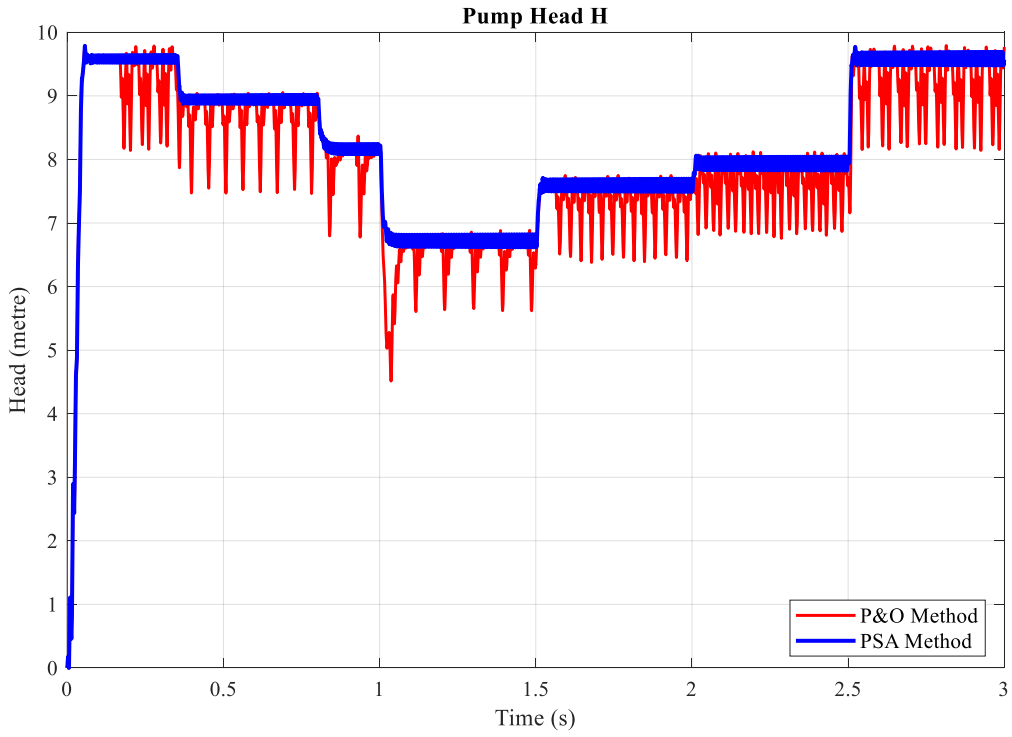


Figure III-13: Pump Head H responses using P&O and PSA techniques

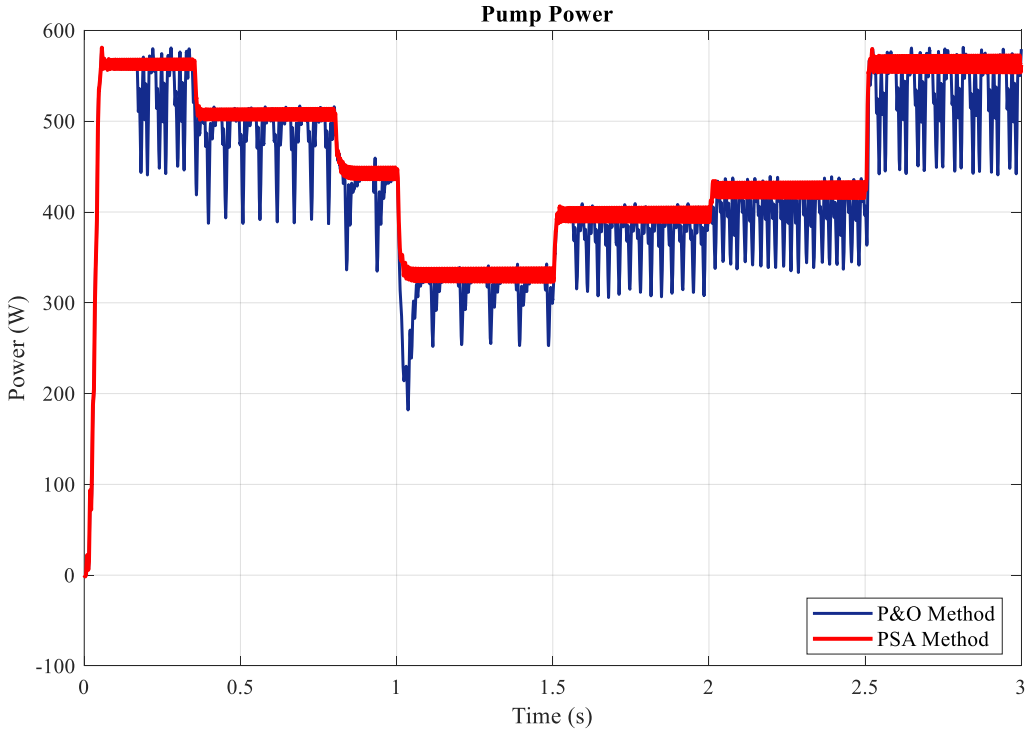


Figure III-14: Pump Power $P_{pump}$ responses using P&O and PSA techniques

### III.5.2 Discussion of Simulation Results:

#### III.5.2.1 Electromagnetic Torque

Figure III-8 shows the electromagnetic torque responses obtained using the PSA-MPPT and P&O-MPPT methods under a partial shading scenario with varying irradiance and temperature conditions. The results indicate that both of PSA and P&O are capable of regulating the PMSM torque around the reference value of 5 N·m (Resistant torque produced). However, the PSA algorithm method reaches the max power point desired (MPP) faster and exhibits significantly lower oscillations during both transient, steady-state periods and during irradiance transitions too. In contrast, the P&O method produces larger torque fluctuations, especially during irradiance transitions.

These oscillations are caused by the continuous perturbation mechanism of the P&O algorithm, which inherently generates power and torque ripple around the maximum power point. In contrast, The PSA algorithm thanks to its global search capability with its Principe of searching with projectiles, converges more smoothly toward the max power point and reduces electromagnetic torque ripple. Consequently, PSA method is more robust than P&O to reduce torque ripples.

#### III.5.2.2 Rotor Speed

As shown in Figure III-9, the rotor speed responses are presented for both the PSA-MPPT and P&O-MPPT methods under a partial shading scenario with varying irradiance and temperature conditions. The rotor speed follows the variations of irradiations and temperatures

of the simulation scenario. During irradiance reductions, the speed decreases, whereas it increases when irradiations increases and the temperature becomes close to the ideal temperature 25°C.

We can observe that the PSA method give us a faster dynamic response and smoother speed evolution compared with P&O. The speed fluctuations are noticeably reduced, and the PMSM rotor speed curve reaches its steady-state value more rapidly after each environmental change of irradiations and temperature, in contrast, with P&O method the rotor speed curve had a lot of fluctuation on its steady-states value.

### III.5.2.3 Stator Currents $I_{abc}$

Figure III-10 and Figure III-11 illustrate the three-phase stator currents output generated by PSA and P&O methods under varying irradiance and temperature conditions (shading scenario).

For both methods, the currents remain balanced and take the sinusoidal form, confirming the proper operation of the PMSM.

However, the zoomed curve reveal that the PSA method produces smoother current outputs signals with lower distortion and reduced high-frequency oscillations. In contrast P&O method introduces additional current ripple due to the continuous perturbation of the searching for the maximum power point MPP.

The reduced current distortion obtained with PSA implies:

- ✓ Lower Total Harmonic Distortion (THD)
- ✓ Reduced losses
- ✓ Improved electrical efficiency

### III.5.2.4 Pump Flow Rate Q

As shown in Figure III-12, the pump flow rate *Q* responses are presented for both the PSA-MPPT and P&O-MPPT methods under a partial shading scenario with varying irradiance and temperature conditions. Consistent with the rotor speed results, the flow rate closely follows the environmental variations of the simulation scenario. During irradiance reductions and high temperatures above 25 °C (which is the Standard Test Condition (STC) temperature), the flow rate decreases. Conversely, it increases when irradiance increases and the temperature approaches the nominal 25 °C threshold. The PSA method consistently achieves slightly higher flow rates value than the P&O method throughout the simulation period. This improvement results from the ability of PSA to extract more photovoltaic power to our pumping system.

The smoother flow-rate curve obtained with PSA also indicates better hydraulic stability and reduced possibility of cavitation problems.

### III.5.2.5 Pump Head H

As shown in Figure III-13, the pump head H responses are presented for both the PSA-MPPT and P&O-MPPT methods under a partial shading scenario with varying irradiance and temperature conditions. Consistent with the rotor speed and flow rate results, to which it is proportional, the pump head closely follows the environmental variations of the simulation scenario. During irradiance reductions and high temperatures above 25 °C, the pump head decreases. Conversely, it increases when irradiance increases and the temperature approaches the nominal 25 °C threshold.

The results show that the PSA maintains a higher pump head compared with the P&O method during most operating conditions on the simulation scenario. This improvement is attributed to the superior tracking capability of PSA, which enables the solar photovoltaic system to operate closer to its global maximum power point and therefore deliver more energy to the PMSM-pump system.

### III.5.2.6 Pump Power $P_{pump}$

As shown in Figure III-14, the pump power responses are obtained using the PSA-MPPT and P&O-MPPT methods. The pump power closely follows the irradiance and temperature variations of the simulation scenario. It can be observed that the PSA method consistently achieves higher pump power than the P&O method throughout the simulation period. This superior performance is attributed to the ability of the PSA algorithm to accurately track the Global Maximum Power Point (GMPP) and rapidly adapt to environmental changes. As a result, more photovoltaic energy is extracted and delivered to the PMSM-pump system.

### III.5.3 Overall Comparison Between PSA and P&O

The simulation results demonstrate that the Projectile Search Algorithm (PSA) outperforms the conventional Perturb and Observe (P&O) method. Specifically, the PSA provides:

- ✓ Reduced electromagnetic torque ripple
- ✓ Lower stator current THD
- ✓ More stable rotor speed
- ✓ Higher pump power
- ✓ Higher pump head
- ✓ Higher water flow rate

### III.5.3.1 performances metrics

Performances metrics of this system are: Tracking Response Time, Total Harmonic Distortion of the stator current THD, Steady-State Power RMSE, Electromagnetic Torque Ripple System Efficiencies, Average Centrifugal Pump Power as shown in Figs. III-15 to III-20.

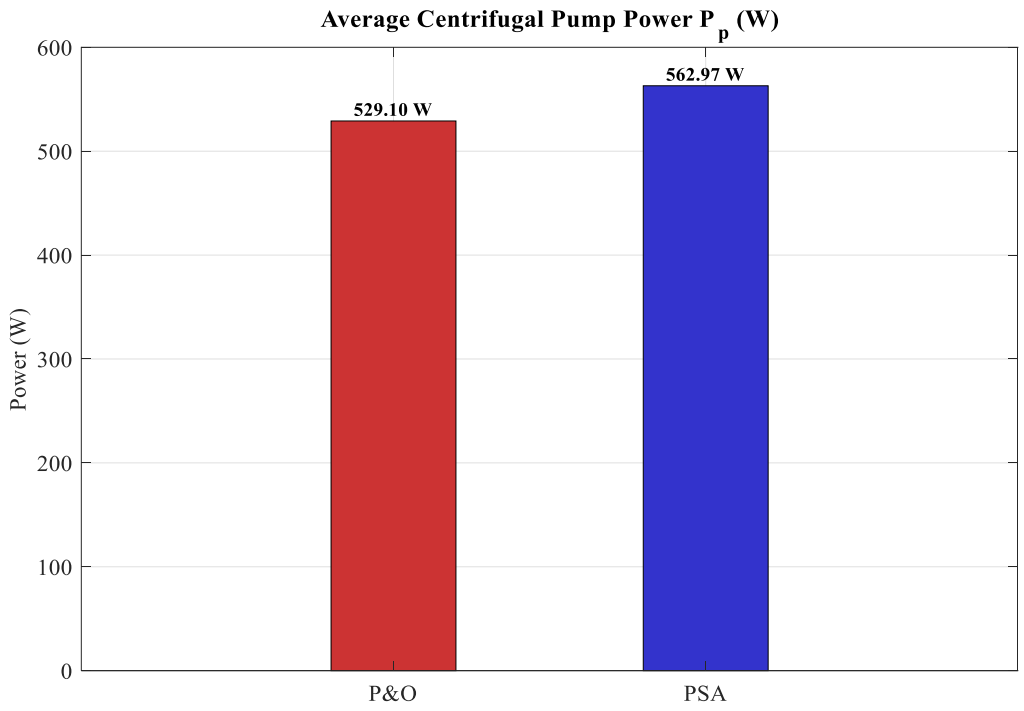


Figure III-15: Average centrifugal pump power using PSA and P&O Methods

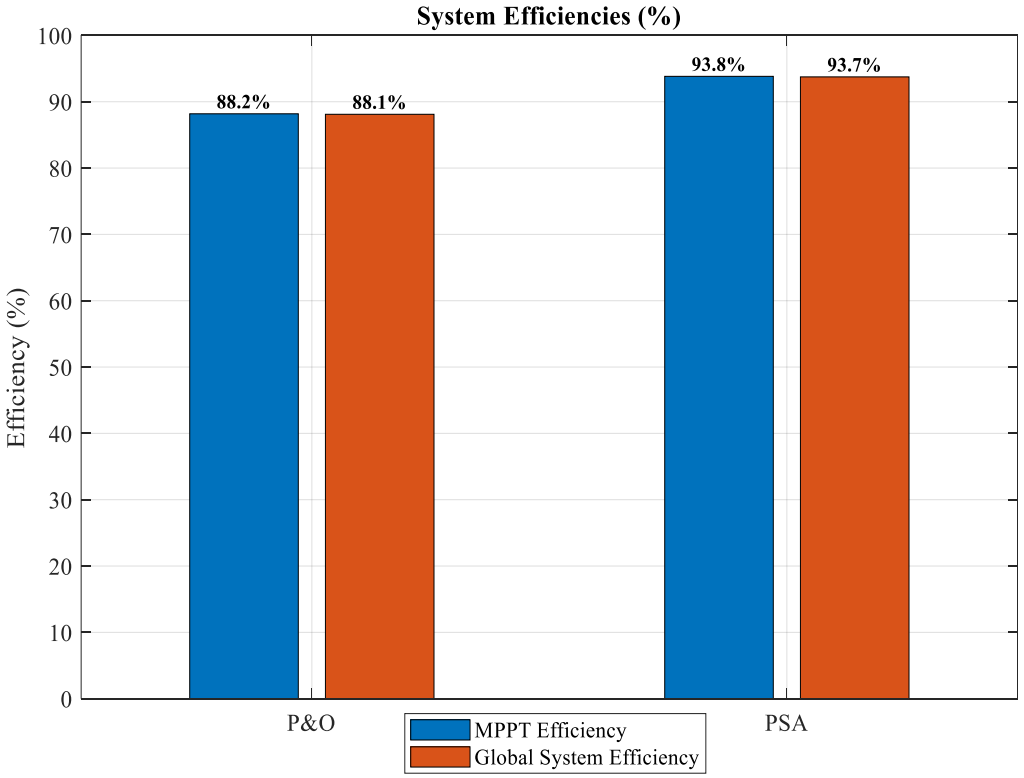


Figure III-16: Global system efficiencies and MPPT efficiencies using PSA and P&O Methods

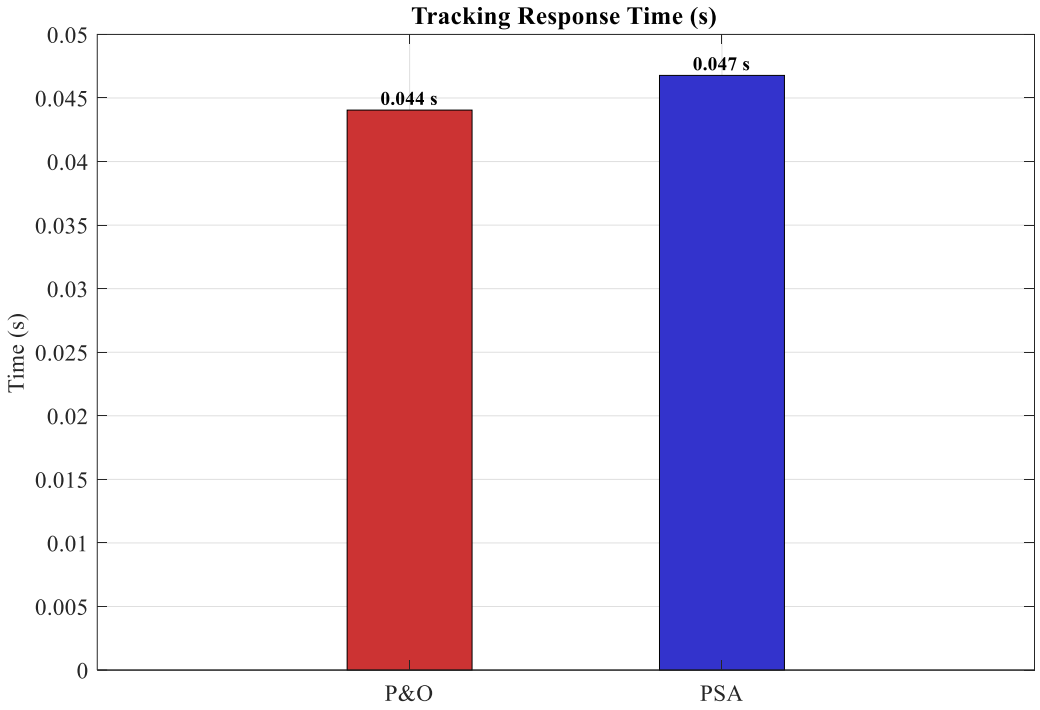


Figure III-17: Tracking response time using PSA and P&O Methods

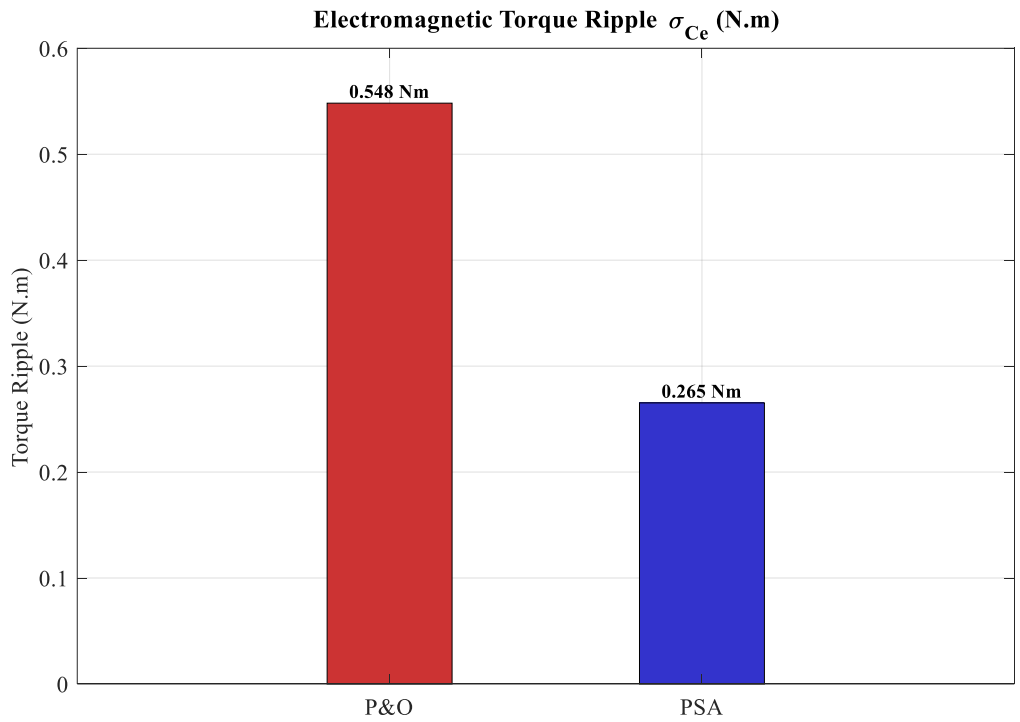


Figure III-18: Electromagnetic Torque Ripple $\sigma_{ce}$ (N.m) using PSA and P&O Methods

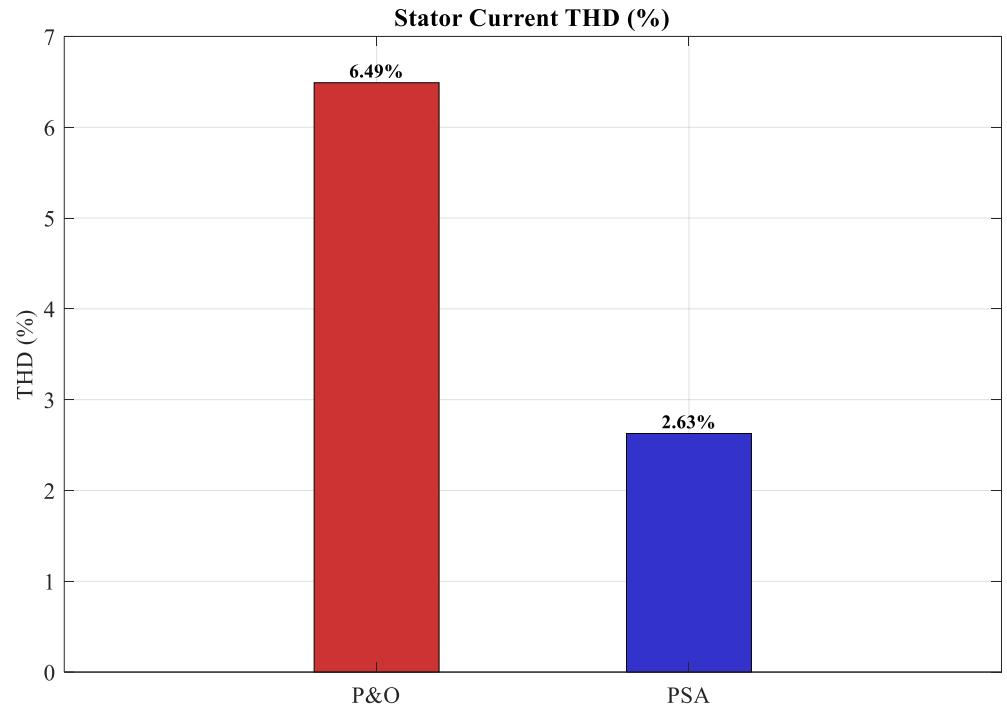


Figure III-19: Stator Current Total Harmonic Distortion THD using PSA and P&O Methods

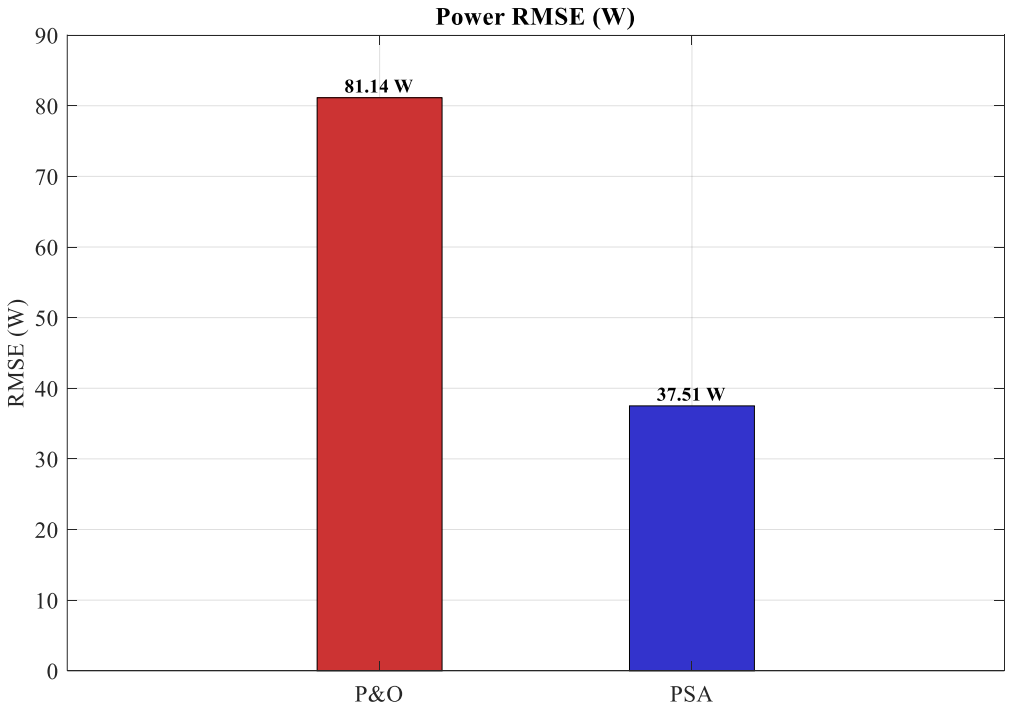


Figure III-20: Steady-State Power RMSE using PSA and P&O Methods

Table III -4: comparison table between PSA and P&O Performances metrics

| Performance Metric | P&O | PSA | Best method |
|---|---|---|---|
| **Tracking Response Time (s)** | 0.044 | 0.047 | P&O |
| **Electromagnetic Torque Ripple** | 0.548 | 0.265 | PSA |
| **Stator Current THD (%)** | 6.49 | 2.63 | PSA |
| **Steady-State Power RMSE** | 81.14 | 37.51 | PSA |
| **Average Pump Power (W)** | 529.10 | 562.97 | PSA |
| **MPPT Efficiency (%)** | 88.2 | 93.8 | PSA |
| **Global System Efficiency (%)** | 88.1 | 93.7 | PSA |

### III.5.4 Discussion of performances metric results

The comparative performance metrics demonstrate the robustness of the Projectile Search Algorithm (PSA) over the conventional Perturb and Observe (P&O) method for MPPT-controlled solar pumping systems. Although the P&O algorithm exhibits a slightly faster tracking response time (0.044s compared to 0.047s), this marginal difference does not affect the overall system performance. The most advantage of PSA is the ability to reduce system oscillations and perturbation. We notice the electromagnetic torque ripple decreases from 0.548 with P&O method to 0.265 with PSA, as result we can say that PSA is more robust to reduce torque ripples on our pumping system based on MPPT methods. Similarly, the PSA achieves a significant reduction in stator current harmonic distortion, lowering the THD from 6.49% with the P&O method to 2.63% with the PSA. This improvement reflects cleaner sinusoidal three-phase stator current $I_{abc}$ waveforms and better power quality, as the power characteristics are directly linked to the current waveform quality as the power characteristics are directly linked to the current waveform quality. In terms of MPPT accuracy, the steady-state power RMSE decreases from 81.14 W for P&O method to 37.51 W for PSA. As result, the lower error demonstrates that PSA maintains system closer to the maximum power point MPP, thereby minimizing tracking losses. As a direct consequence of the improved tracking accuracy, the average pump power increases from 529.10 W for P&O method to 562.97 W for PSA. This performance result confirms that the PSA extracts more energy from the solar array and transfers it effectively to the pumping system, achieving a power output improvement of 33.87W. As result of efficiency of MPPT and global system efficiency, we notice that MPPT

efficiency increase from 88.2% for P&O method to 93.8% for PSA method, and in the overall system efficiency, which increases from 88.1% for P&O to 93.7% for PSA. These results demonstrate that PSA give as a better efficiency for our solar pumping system under shading then P&O.

### III.5.5 Simulation of the 4S × 2P PV Array under Partial Shading

In this section, the 4S×2P PV array configuration is split into four identical branches, where each branch is configured with two panels connected in series, as shown in Figure III-21.

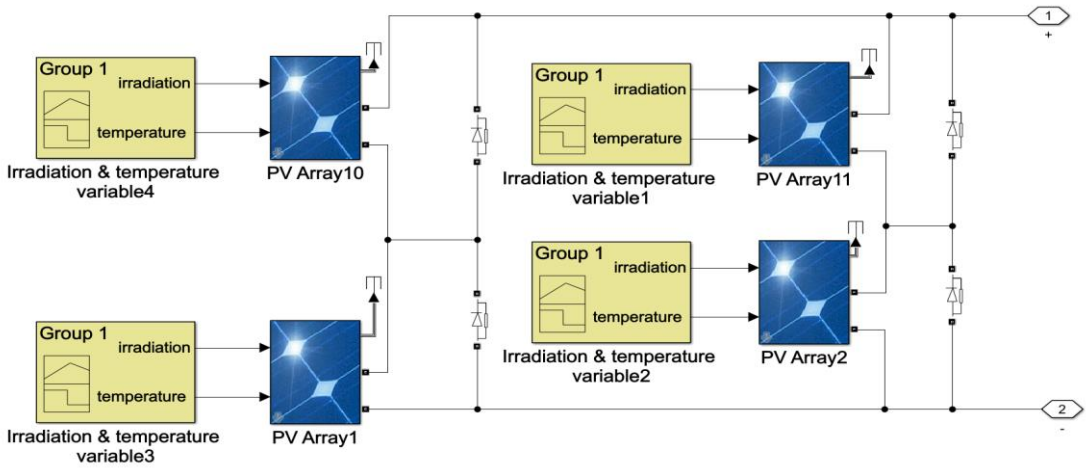


Figure III-21: Representing Series-Parallel association of 2 Series PV array & 2 parallel PV array (Every PV array is configured with 2 series panels)

To evaluate the system under various operating conditions, different partial shading configurations are defined. Table III-5 details the specific shading patterns applied to each of the four photovoltaic modules

Table III -5: Different patterns of shading on each of the four solar panels modules.

| **Operating Conditions** | **Irradiation Values (W/m2)** | | | |
|---|---|---|---|---|
| | **Panel 1** | **Panel 2** | **Panel 3** | **Panel 4** |
| t=0s à t=0.35s | 1000 | 650 | 300 | 100 |
| t=0.35s à t=0.8 | 1000 | 900 | 500 | 400 |
| t=0.8s à t=1.5s | 1000 | 1000 | 1000 | 500 |
| t=1.5s à t=2s | 1000 | 950 | 800 | 600 |
| t=2s à t=3s | 1000 | 900 | 700 | 700 |

- **Presentation of simulation performance results**

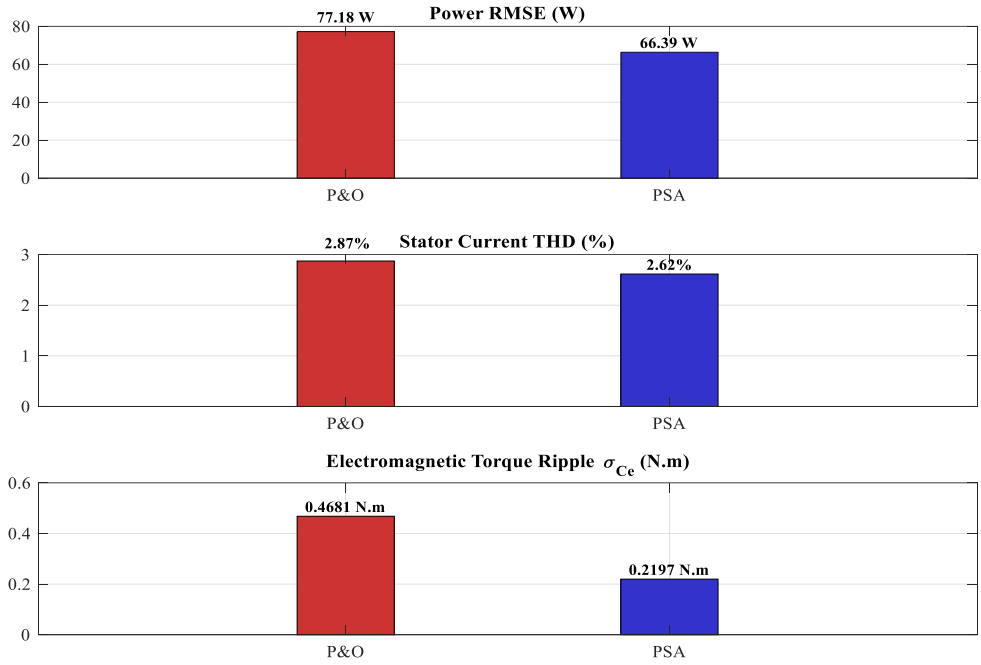


(1)

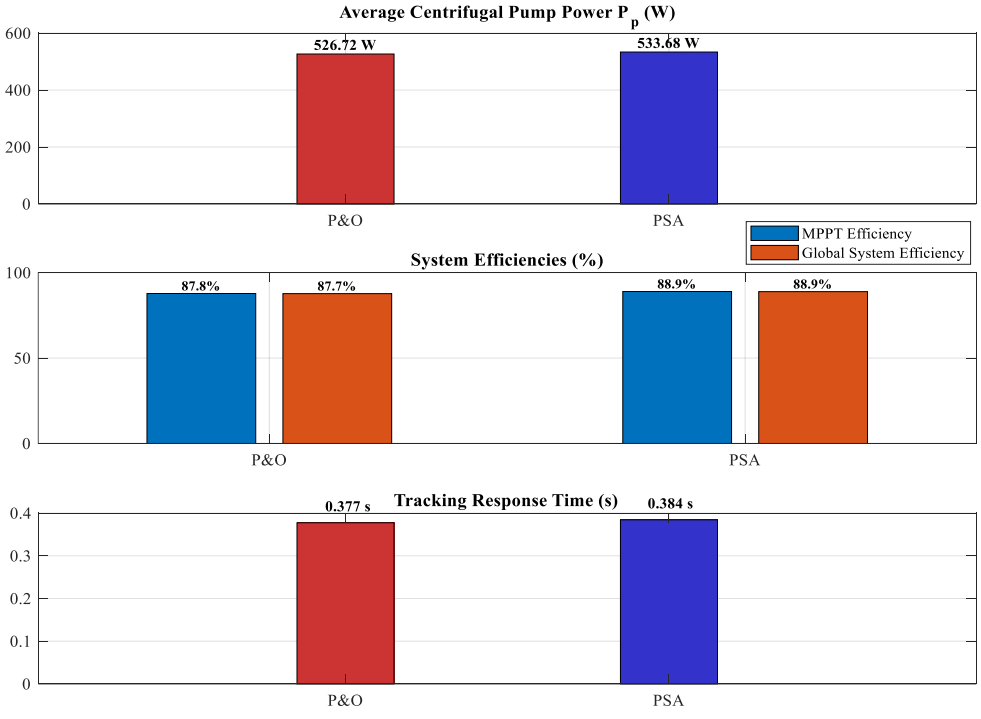


(2)

Figure III-22 Performance metrics under a partial shading condition. (1): RMSE, THD & $\sigma_{Ce}$ . (2) : $P_p$, η & $t_r$

### III. III.5.5.1 Comparative Performance Results between PSA and P&O

To provide a comprehensive evaluation, the quantitative results for all analyzed indicators are compiled. Table III-6 presents a detailed comparison of the performance metrics between the PSA and P&O methods under partial shading conditions.

Table III -6: comparison table between PSA and P&O Performances metrics for Scenario of simulation under a partial shading condition

| Performances Metrics | P&O | PSA | Best method |
|---|---|---|---|
| **Tracking Response Time (s)** | 0.377 | 0.384 | P&O |
| **Electromagnetic Torque Ripple** | 0.4681 | 0.2197 | PSA |
| **Stator Current THD (%)** | 2.87 | 2.62 | PSA |
| **Steady-State Power RMSE** | 77.18 | 66.39 | PSA |
| **Average Pump Power (W)** | 526.72 | 533.68 | PSA |
| **MPPT Efficiency (%)** | 87.8 | 88.9 | PSA |
| **Global System Efficiency (%)** | 87.7 | 88.9 | PSA |

## III.6 Conclusion

In this chapter, a comprehensive comparative study was conducted between two MPPT methods—the Projectile Search Algorithm (PSA) and the conventional Perturb and Observe (P&O) method—under partial shading conditions. All system performance indicators were analyzed and evaluated, including stator current, pump power, pump head, electromagnetic torque, rotor speed, and volumetric flow rate. The results demonstrate that the PSA outperforms the P&O method across almost all performance parameters, with the sole exception of a slightly slower tracking response time. Consequently, it can be concluded that the PSA delivers significantly better overall performance than the P&O method, thereby confirming the robustness and high efficiency of the PSA-MPPT technique for solar water pumping systems operating under challenging shading conditions.

# General conclusion

# General Conclusion

Conventional algorithms such as perturb and observe (P&O) and Incremental conductance (INC) prove most effective under consistent irradiation situations since the PV system only produces a single MPP in such conditions, but can become stuck at local maxima under partial shading (PS) conditions. Metaheuristic-based optimization algorithms, such as the Projectile Search Algorithm (PSA), which use envelope of the projectile trajectory as the basis for their search criteria, were employed for MPPT to overcome these limitations.

In this project, our work focuses on improving the performance of a solar photovoltaic pumping system by applying the PSA optimization technique to extract the maximum available power from the PV module under non-uniform environmental conditions.

The first chapter was devoted to a comprehensive overview of the key principles of solar photovoltaic PV technology.

In the second chapter, we modeled the entire solar photovoltaic pumping system, including the PV generator, the DC-DC boost converter, the three-phase inverter, the Direct Torque Control (DTC) block, the Permanent Magnet Synchronous Motor (PMSM), and the centrifugal pump. After that, we studied the conventional maximum power point tracking (MPPT) techniques: (P&O) and (INC).

In the third chapter, we discussed the underlying mechanics of projectile motion and modeled the projectile search algorithm used for extracting power from the solar PV system. Following this, we presented our complete MATLAB/Simulink simulation model with every technical parameter and described the environmental impact of partial shading conditions.

The simulation results were presented and compared in the last chapter, according to performance metrics such as Tracking Response Time (s), Steady-State Power RMSE (W), Total Harmonic Distortion of the stator current THD (%), Electromagnetic Torque Ripple (N·m), Overall System Efficiency (%), and Average Centrifugal Pump Power (W). When the irradiance and shading patterns change rapidly, the results showed that the PSA-based MPPT method maintains very low power oscillations, successfully avoids local traps, and minimizes electromagnetic torque ripples and harmonic distortion. Consequently, the controller achieves significantly higher accuracy in tracking the global optimal operating point, resulting in increased energy harvesting and superior hydraulic pumping efficiency.

In summary, this innovative approach, based on metaheuristic optimization, offers promising perspectives for the development of maximum power point tracking techniques based on the Projectile Search Algorithm and provides a robust framework for future hybridization with other advanced soft-computing methods.

# *Bibliography*

[Abi23] Abidet, N. E. H., Haouam, A., *Etude et optimisation d'un système de pompage photovoltaïque au fil soleil*. Master's thesis, Département de Génie Électrique, Faculté des Sciences et de la Technologie, Université Échahid Cheikh Larbi Tebessi - Tébessa, Algérie, 2023.

[Aas15] Aashoor, F. A. O., *Maximum power point tracking techniques for photovoltaic water pumping system*. Doctoral dissertation. University of Bath, Department of Electronic and Electrical Engineering, 2015. Available: Bath's Research Portal.

[Alm20] Al-Majidi, S. D. A. *Efficient Maximum Power Point Tracking Techniques for a Grid-connected Photovoltaic System using Artificial Intelligence*, thesis of doctorate, Brunel University London, Royaume-Uni, 2020.

[Ami17] Amiri, M., Ali Dahmane, O., *Commande vectorielle en vitesse du moteur synchrone à aimants permanents dotée d'un observateur mode glissant*. Master's thesis. Département d'Électrotechnique, Spécialité : Commande des machines électriques, Université Aboubakr Belkaïd - Tlemcen, Algérie, 2017.

[Amr16] Amrouche, R., Bedjou, S., *Contrôle d'un système de pompage photovoltaïque.* Master's thesis. Option : Énergies Renouvelables, Université Abderrahmane Mira de Bejaia, Algérie, 2016

[Ayo18] Ayop, R., Tan, C.W., *Design of boost converter based on maximum power point resistance for photovoltaic applications*, Solar Energy, 2018, vol. 160, pp. 322-335.

[Bab25] Babaoumoussa, A., Lassakeur, A., *Système de Pompage d'Eau Photovoltaïque pour l'Irrigation Agricole: Dimensionnement Optimal et Validation Expérimentale sur le Site de Ghardaïa*. Master's thesis. Université de Ghardaïa, Algérie, 2025.

[Bah20] Bahri, A., Abdelkrim, T., Mordjaoui, M., Becar, B., Bouraghda, S, *Environment, Plasma and Materials. In The National Conference on Energy Systems ESEPM*, MESTEL Laboratory, Université de Ghardaïa, Algérie, 2020.

[Bac02] Baće, M., Ilijić, S., Narančić, Z., Bistričić, L., *The envelope of projectile trajectories, European Journal of Physics*, 2002, vol. 23, no. 6, pp. 637–642.

[Bde21] Bdewi, M. Y., Mohammed, A. M., Ezzaldean, *M. M., Design and performance analysis of permanent magnet synchronous motor for electric vehicles application, Engineering and Technology Journal*, 2021, vol. 39, no. 03, pp. 394–406.

[Bel25] Belmezouar, A., Belmiloud, A., *Commande MPPT Photovoltaïque Via Un Observateur Par Mode Glissant*. Master's thesis. Université Mohamed El-Bachir El-Ibrahimi - Bordj Bou Arreridj, Algérie, 2025.

[Ben11] Benkhelil, E., Gherbi, A., *Modélisation et simulation d'un générateur photovoltaïque avec un étage d'adaptation DC/DC*, *Revue des Énergies Renouvelables*, 2011, (ICESD'11 Adrar), pp. 41-48.

[Ben14] Bendjoudi, F., *Etude et simulation d'un système de pompage photovoltaïque avec batteries*. Master's thesis. Département de Génie Électrique, Université Abderrahmane Mira de Béjaïa, Algérie, 2014.

[Ben17] Ben Tria, M. R., *Etude d'un système de pompage photovoltaïque pour des puits de parcours (cas de la région de Taïbet-Ouargla)*. Master's thesis. Université Kasdi Merbah Ouargla, Algérie, 2017.

[Ben20] Benzait, B., Touahria, D. E., *Etude comparative des algorithmes P&O et INC pour l'optimisation de l'énergie photovoltaïque*. Master's thesis. Université de Ghardaïa, Algérie, 2020.

[Ben23] Ben Mahmoud, M., Messaoud, O. et Ouacherine, D. *Étude conceptuelle d'une pompe centrifuge à 11 étages Pourgazoil (MC 80-260/11)*. Master thesis, faculté de technologie département de mécanique Université Blida 1, Algérie ,2023.

[Bol20] Bollipo, R. B., Mikkili, S., Bonthagorla, P. K*., Critical review on PV MPPT techniques: Classical, intelligent and optimisation*, *IET Renewable Power Generation*, 2020, vol. 14, no. 9, pp. 1433–1452.

[Bol21] Bollipo, R. B., Mikkili, S., Bonthagorla, P. K., *Hybrid, optimal, intelligent and classical PV MPPT techniques: A review, CSEE Journal of Power and Energy Systems*, 2021, vol. 7, no. 1, pp. 9-41.

[Bou05] Bouchereb, C*., Contrôle direct du couple des machines synchrones*. Magister's thesis. Université de Batna, Algérie, 2005.

[Bou12] Boutelhig, A., *Study and sizing of a stand-alone Photovoltaic Water Pumping System (PVPS) optimal design for typical installation in Ghardaia region*. Master's thesis. Université Saad Dahlab de Blida, Algérie, 2012.

[Bou23] Bouhadjar, A. et Amriou, W. *Commande Vectorielle de la Machine Synchrone à Aimants Permanents*. Master thesis, Faculté des Sciences et de la Technologie Département d'Electrotechnique Université Belhadj Bouchaib d'Aïn Témouchent, Algérie, 2023.

[Bou25] Bouksaim, M., Mekhfioui, M., Srifi, M. N., A *Comprehensive Decade-Long Review of Advanced MPPT Algorithms for Enhanced Photovoltaic Efficiency*, *Solar*, 2025, vol. 5, no. 3, pp. 44.

[Bra11] Branker, K., Pathak, M. J. M., Pearce, J. M., *A review of solar photovoltaic levelized cost of electricity, Renewable and Sustainable Energy Reviews*, 2011, vol. 15, no. 9, pp. 4470–4482.

[Bul22] Bulmez, A. M., Ciofoaia, V., Năstase, G., Dragomir, G., Brezeanu, A. I., Şerban, A., *An experimental work on the performance of a solar-assisted ground-coupled heat pump using a horizontal ground heat exchanger, Renewable Energy*, 2022, vol. 183, pp. 849-865.

[Bur01] Burton, T., Jenkins, N., Sharpe, D., Bossanyi, E., *Wind energy handbook*, John Wiley & Sons, 2001.

[Car11] Carrasco, F., *Introduction to hydropower*, The English Press, 2011.

[Dee24] Deepak, G., Aggarwal, K., Dineshbabu, N., Sowndharya, R., Manimaran, B., Job Karuna Sagar, B. J., *Thermodynamic analysis of a novel concentrated solar power plant with integrated thermal energy storage, Thermal Science and Engineering Progress*, 2024, vol. 56, Article 103055.

[Deh14] Dehouche, K., *Étude et conception d'un système de pompage photovoltaïque avec stockage électrochimique.* Master's thesis. Département de Génie Électrique, Faculté de Technologie, Université de Béjaïa, Algérie, 2014.

[Dem22] Demmouche, F. J*., Simulation et commande d'une liaison photovoltaïque en régime du défaut.* Master's thesis. Département Electrotechnique faculté de science et technologie Université-Ain-Temouchent- Belhadj Bouchaib , 2022.

[Ela24] El Alami, Y., Zohal, B., Nasrin, R., Benhmida, M., Faize, A., Baghaz, E., *Solar thermal, photovoltaic, photovoltaic thermal, and photovoltaic thermal phase change material systems: A comprehensive reference guide*, *International Communications in Heat and Mass Transfer*, 2024, vol. 159, Part B, Article 108335.

[Elt10] Eltawil, M. A., Zhao, Z., *Grid-connected photovoltaic power systems: Technical and potential problems—A review*, *Renewable and Sustainable Energy Reviews*, 2010, vol. 14, no. 1, pp. 112–129.

[Fin13] Finan, B. G., *Maximum power point tracking for solar power applications with partial shading*. Bachelor's thesis. National University of Ireland, Galway, Irlande, 2013.

[Goe05] Goetzberger, A., Hoffmann, V. U., *Photovoltaic solar energy generation*, Vol. 112, Springer Science & Business Media, 2005.

[Gua25] Guanghua, L., Soomar, A. M., Shah, S. H. H., Shaikh, S., Musznicki, P*., Maximupower point tracking strategies for solar PV systems: A review of current methods and future innovations*, *Results in Engineering*, 2025, vol. 28, Article 107227.

[Hac19] Hachelfi, W., Rahem, D., Meddour, S., Djouambi, A. E., *Fractional Order Direct Torque Control of Permanent Magnet Synchronous Machine, European Journal of Electrical Engineering*, 2019, vol. 21, no. 5, pp. 431-438.

[Hai11] Haillant, O., *Accelerated weathering testing principles to estimate the service life of organic PV modules*, *Solar Energy Materials and Solar Cells*, 2011, vol. 95, no. 5, pp. 1284–1292.

[Ham25] Hamouda, M., Elsherbiny, H., Zaky, A. A., Odinaev, I., Bureš, V., Menaem, A. A., *Improved Efficiency and Reliability of a Single-Stage Solar Water Pumping System*, *IEEE Access*, 2025, vol. 13, pp. 26991-27006.

[Har11] Hart, D. W., *Power Electronics*, Vol. 166, pp. 211-218, New York: McGraw-Hill, 2011.

[Has22] Hasabelrasul, H., Cai, Z., Sun, L., Suo, X., Matraji, I., *Two-stage converter standalone PV-battery system based on VSG control*, *IEEE Access*, 2022, vol. 10, pp. 39825-39832.

[Hie19] Hiendro, A., *Projectile-target search algorithm: a stochastic metaheuristic optimization technique, International Journal of Electrical and Computer Engineering (IJECE)*, 2019, vol. 9, no. 5, pp. 3772-3778.

[Ibe26] Iberdrola, *Solar radiation: what is its impact on the planet and on humans?* [en ligne], disponible sur: https://www.iberdrola.com/sustainability/solar-radiation-impact (consulté le 01 juin 2026).

[Ish13] Ishaque, K., Salam, Z., A *deterministic particle swarm optimization maximum power point tracker for photovoltaic system under partial shading condition*, *IEEE Transactions on Industrial Electronics*, 2013, vol. 60, no. 8, pp. 3195–3206.

[Kal13] Kalogirou, S. A., *Solar energy engineering: Processes and systems*, Academic Press, 2013.

[Kha22] Khaldi, A., Berkouk, E. M., Mahmoudi, M. O., Kouzou, A., *Direct Torque Control of Three-Phase Induction Motor Powered by Three-Level Indirect Matrix Converter*, *Nonlinear Dynamics and Systems Theory*, 2022, vol. 22, no. 2, pp. 178-196.

[Khe18] Khelif, I., Meghni, B., *La commande directe du couple (DTC) d'une machine synchrone à aimant permanent "MSAP"*. Master thesis , Université Kasdi Merbah Ouargla, Algérie, 2018.

[Khe25] Khettache, L., Rezoug, M. R., Saadi, A., Sahraoui, L., *A novel design of a photovoltaic system based on a linear induction motor and reciprocating pump*, *Revue Roumaine des Sciences Techniques–Série Électrotechnique et Énergétique*, 2025, vol. 70, no. 1, pp. 3-8.

[Kja12] Kjaer, S. B., *Evaluation of the "Hill Climbing" and the "Incremental Conductance" Maximum Power Point Trackers for Photovoltaic Power Systems*, *IEEE Transactions on Energy Conversion*, 2012, vol. 27, no. 4, pp. 922–929.

[Lou08] Louazane, M. L., *Étude technico-économique d'un système de pompage photovoltaïque sur le site de Ouargla*. Magister thesis , Université El Hadj Lakhdar - Batna, Algérie, 2008.

[Loz25] Lozanova, S., *What Is MPPT? The Key to Optimizing Solar Output*, GreenLancer, 12 février 2025, https://www.greenlancer.com/post/maximum-power-point-tracking-mppt (consulté le 4 mai 2026).

[Mis21] Mishu, M. K., Rokonuzzaman, M., Pasupuleti, J., Shakeri, M., Rahman, K. S., Binzaid, S., Tiong, S. K., Amin, N., *An adaptive TE-PV hybrid energy harvesting system for self-powered IoT sensor applications*, *Sensors*, 2021, vol. 21, no. 8, art. no. 2604.

[Man24] Manglik, R., *Renewable Energy Sources and Their Applications*, EduGorilla Prep Experts, 2024.

[Moh07] Mohan, N., Undeland, T. M., *Power electronics: Converters, applications, and design*, Wiley-India, 2007.

[Pan14] Panda, A., *Direct torque control of permanent magnet synchronous motor*. University bachelor's thesis, National Institute of Technology, Rourkela, Inde, 2014.

[Pet08] Petrova-Koch, V., Hezel, R., Goetzberger, A. (Eds.), *High-efficient low-cost photovoltaics: Recent developments*, Vol. 140, Springer, 2008.

[Res25] ResearchGate, *The Algerian Solar Map*, [en ligne], disponible sur: https://www.researchgate.net (consulté le 25 juin 2025).

[Rod15] Rodríguez Gallegos, C. D., *Analysis of the Stationary and Transient Behavior of a Photovoltaic Solar Array: Modeling and Simulation, International Journal of Computer Applications*, 2015, vol. 127, no. 4, pp. 1-6.

[Roy21] Roy, R. B., Rokonuzzaman, M., Amin, N., Mishu, M. K., Alahakoon, S., Rahman, S., Mithulananthan, N., Rahman, K. S., Shakeri, M., Pasupuleti, J., *A comparative performance analysis of ANN algorithms for MPPT energy harvesting in solar PV system, IEEE Access*, 2021, vol. 9, pp. 102137-102152.

[Roy98] Royer, J., *Le pompage photovoltaïque : Manuel de cours à l'intention des ingénieurs et des techniciens*, Institut de l'Énergie des Pays ayant en commun l'usage du Français (IEPF), Université d'Ottawa, École Inter-États d'Ingénieurs de l'Équipement Rural (EIER) & Centre Régional pour l'Eau Potable et l'Assainissement à faible coût (CREPA), 1998.

[Saa25] Saady, I., Majout, B., El Kafazi, I., Karim, M., Bossoufi, B., El Ouanjli, N., Mahfoud, S., Althobaiti, A., Alghamdi, T. A. H., Alenezi, M., *Improving photovoltaic water pumping system performance with ANN-based direct torque control using real-time simulation, Scientific Reports*, 2025, vol. 15, art. no. 4024.

[Sah25] Sahi, W., Beggah, R. N. E. Y., *Etude et simulation d'un système de pompage solaire pour l'irrigation d'une ferme agricole dans la région d'Ain Sefra.* Master thesis, École Supérieure en Sciences Appliquées - Tlemcen, Algérie, 2025.

[Sas17] Sasi, M. A., *Fuzzy Logic Control of MPPT Controller for PV Systems.* Master's thesis, Faculty of Engineering and Applied Science, Memorial University of Newfoundland, St. John's, Newfoundland, Canada, 2017.

[Seg20] Seghiri, A., Kadri, N., *Étude d'un système de pompage photovoltaïque à base d'une MSAP commandé par une nouvelle technique MPPT GSS*. Academic Master's Thesis, Option: Commandes électriques, Université Mohamed Boudiaf - M'Sila, Algérie, 2020.

[Sol26] Solar Energy Industries Association, *Solar Energy*, [en ligne], disponible sur: https://www.seia.org/initiatives/about-solar-energy/ (consulté en 26 Mars 2026).

[Son23] Son, D. I., Han, J. S., Park, J. S., Lim, H. S., Lee, G. H., *Performance Improvement of DTC-SVM of PMSM with Compensation for the Dead Time Effect and Power Switch Loss Based on Extended Kalman Filter, Electronics*, 2023, vol. 12, no. 4, art. no. 966.

[Spi98] Spiers, D., Royer, J., *Guidelines for the use of batteries in photovoltaic systems*, NESTE Advanced Power Systems & CANMET Energy Diversification Research Laboratory, 1998.

[Taf08] Tafticht, T., Agbossou, K., Chériti, A., Doumbia, M. L., *An improved maximum power point tracking method for photovoltaic systems, Renewable Energy*, 2008, vol. 33, no. 7, pp. 1508-1516.

[Tan20Tang, F., Nowamooz, H., *Outlet temperatures of a slinky-type horizontal ground heat exchanger with the atmosphere–soil interaction, Renewable Energy*, 2020, vol. 146, pp. 705–718.

[Xia04] Xiao, W., Dunford, W. G., *A modified adaptive hill climbing MPPT method for photovoltaic power systems, Dans PESC 04. 2004 IEEE 35th Annual Power Electronics Specialists Conference*, IEEE, 2004, vol. 3, pp. 1957-1963.

[Zer25] Zerguine, A., Rahabi, B., *Rayonnement solaire et système photovoltaïque : simulation et modélisation*. Master thesis, Université 8 Mai 1945 - Guelma, Algérie, 2025. Disponible sur : Archive universitaire.

[Zhi25] Zhilong, *Centrifugal pump curve equation*, [en ligne], disponible sur : https://www.zhilong-pump.com/article/Industry-Knowledge/729.html (consulté en 7 Mai 2026).

**Abstract:**

This master's thesis models, simulates, and evaluates a standalone, PV-powered water pumping system designed to provide clean water to isolated regions. To overcome the limitations of traditional algorithms under PSC, a novel metaheuristic MPPT technique based on the Projectile Search Algorithm (PSA) is proposed. Inspired by projectile dynamics, the PSA utilizes parabolic trajectories to dynamically explore the search space, allowing it to "leap" over local maxima and isolate the true Global Maximum Power Point (GMPP). The integrated system—comprising a PV array, DC-DC boost converter, inverter, and a centrifugal pump driven by a Permanent Magnet Synchronous Motor (PMSM) under Direct Torque Control (DTC)—was developed and simulated using MATLAB/Simulink across various dynamic shading profiles. The performance of the proposed PSA-MPPT was compared against conventional P&O method using metrics. The simulation results demonstrate that the PSA-MPPT method achieves Robust and performant tracking efficiency significantly minimizes steady-state power RMSE, while simultaneously reducing the electromagnetic torque ripple of the motor and improving the stator current Total Harmonic Distortion THD offering a highly resilient, stable, and sustainable solution for remote water supply infrastructure.

**Résumé :**

Ce mémoire de master modélise, simule et évalue un système autonome de pompage d'eau alimenté par énergie photovoltaïque, conçu pour fournir de l'eau potable à des régions isolées. Pour surmonter les limites des algorithmes traditionnels en conditions de PSC, une nouvelle technique MPPT métaheuristique basée sur l'algorithme de recherche par projectile (PSA) est proposée. Inspiré de la dynamique des projectiles, le PSA utilise des trajectoires paraboliques pour explorer dynamiquement l'espace de recherche, ce qui lui permet de « sauter » par-dessus les maximas locaux et d'identifier le véritable point de puissance maximale global (GMPP). Le système intégré — comprenant un générateur photovoltaïque, un convertisseur élévateur CC-CC, un onduleur et une pompe centrifuge entraînée par un moteur synchrone à aimants permanents (PMSM) sous commande directe du couple (DTC) — a été développé et simulé à l'aide de MATLAB/Simulink pour divers profils d'ombrage dynamiques. Les performances de la méthode PSA-MPPT proposée ont été comparées à celles de P&O-MPPT à l'aide d'indicateurs . Les résultats de la simulation démontrent que la méthode PSA-MPPT permet d'obtenir un suivi robuste et performant, qui minimise considérablement l'erreur quadratique moyenne (RMSE) de la puissance en régime permanent, tout en réduisant simultanément l'ondulation du couple électromagnétique du moteur et en améliorant la distorsion harmonique totale (THD) du courant statorique, offrant ainsi une solution hautement résiliente, stable et durable pour les infrastructures d'approvisionnement en eau en milieu isolé.

**الملخص:**

تقوم أطروحة الماستر هذه بنمذجة ومحاكاة وتقييم نظام مستقل لضخ المياه يعمل بالطاقة الكهروضوئية، مصمم لتوفير المياه النظيفة للمناطق المعزولة. وللتغلب على قيود الخوارزميات التقليدية في ظل ظروف التظليل الجزئي(PSC) ، يُقترح أسلوب جديد لتتبع نقطة الطاقة القصوى (MPPT)قائم على الخوارزمية الاستكشافية للمقذوفات .(PSA) مستوحاة من ديناميكيات المقذوفات، تستخدم خوارزمية PSA مسارات مكافئة لاستكشاف مساحة البحث ديناميكيًا، مما يسمح لها بـ«القفز» فوق القيم القصوى المحلية وعزل نقطة الطاقة القصوى العالمية الحقيقية .(GMPP) تم تطوير النظام المتكامل — الذي يتألف من مصفوفة كهروضوئية، ومحول رفع تيار مستمر إلى تيار مستمر(DC-DC) ، وعاكس، ومضخة طرد مركزي مدفوعة بمحرك متزامن مغناطيسي دائم (PMSM) تحت التحكم المباشر في العزم — (DTC) ومحاكاته باستخدام MATLAB/Simulinkعبر مختلف أنماط التظليل الديناميكية. تمت مقارنة أداء تقنية PSA-MPPT المقترحة بشكل دقيق مع الطرق التقليدية باستخدام مقاييس هندسية .تُظهر نتائج المحاكاة أن طريقة PSA-MPPT تحقق كفاءة تتبع قوية وعالية الأداء، وتقلل بشكل كبير من الخطأ المربع المتوسط (RMSE) للطاقة في حالة الاستقرار، مع تقليل تموج العزم الكهرومغناطيسي للمحرك في الوقت نفسه، وتحسين التشوه التوافقي الكلي (THD)لتيار الجزء الثابت، مما يوفر حلاً عالي المرونة والاستقرار والاستدامة للبنية التحتية لإمدادات المياه في المناطق النائية.